International Journal of Polymer Science

Natural Polymer: Oriental Lacquer

Guest Editors: Rong Lu, Michel Sablier, Yoshida Takashi, and Michael Schilling

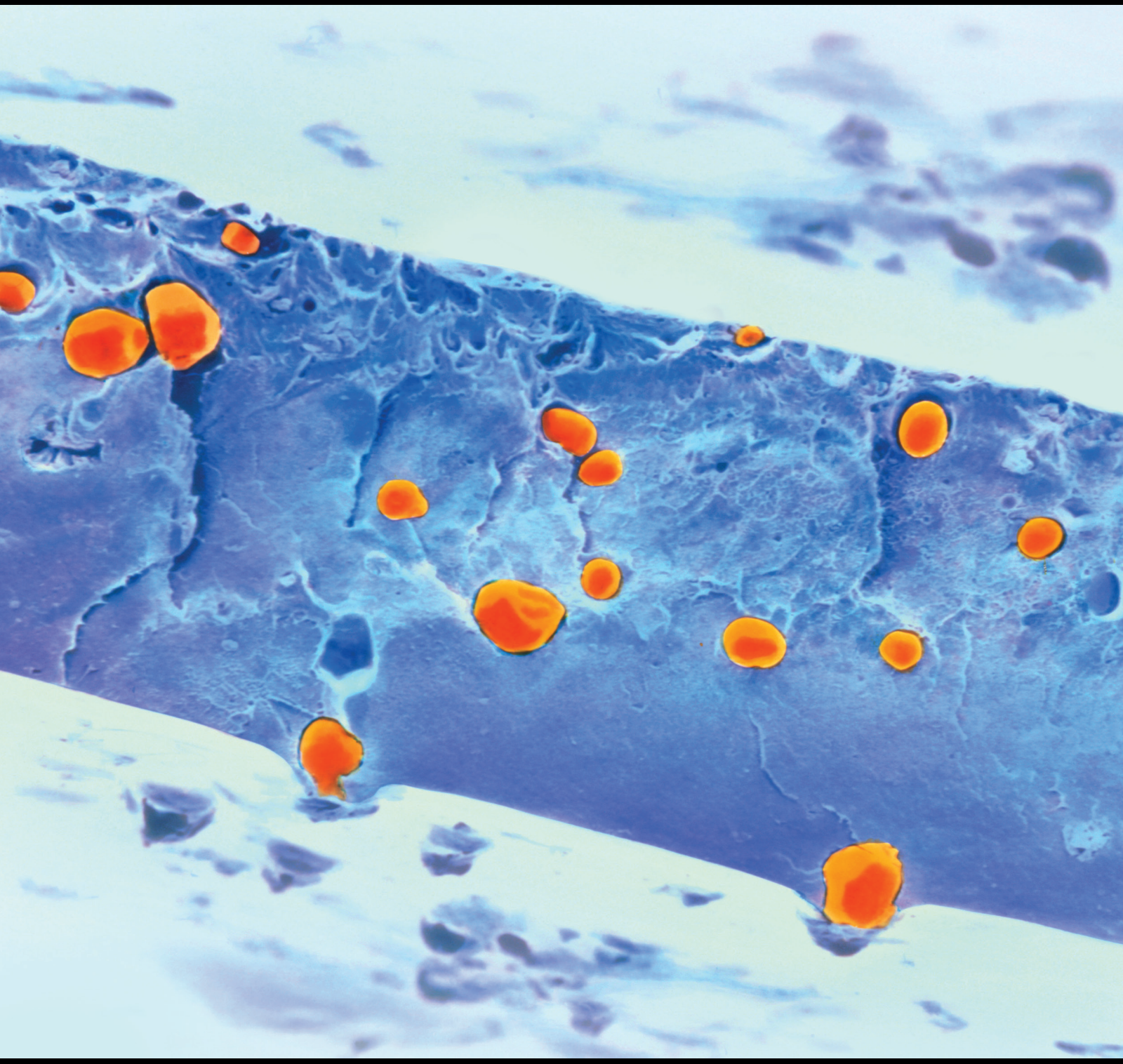

Natural Polymer: Oriental Lacquer

International Journal of Polymer Science

Natural Polymer: Oriental Lacquer

Guest Editors: Rong Lu, Michel Sablier, Yoshida Takashi, and Michael Schilling

Editorial Board

Contents

Hindawi Publishing Corporation
International Journal of Polymer Science
Volume 2015, Article ID 132809, 8 pages
http://dx.doi.org/10.1155/2015/132809

Research Article

Modification of Urushiol Derivatives by Liquid Crystal Epoxy Resin

Gongwen Tang, Zhishan Yan, Linrong Ma, and Xin Huang

The Institute of Seawater Desalination and Multipurpose Utilization, SOA, Tianjin 300192, China

Correspondence should be addressed to Gongwen Tang; 13752134728@163.com

Received 2 December 2014; Revised 26 January 2015; Accepted 26 January 2015

Academic Editor: Rong Lu

Urushiol derivatives have vast potentials for using as coating materials. However, the cured coatings are quite brittle, limiting their applications. In this study, urushiol-furfural (UFUR) was chosen as an example of urushiol derivatives and a liquid crystal (LC) epoxy resin, tetramethylbiphenyl diglycidyl ether (TMBPDE), was for the first time utilized to modify UFUR. Fourier transform infrared spectroscopy and solid-state ^{13}C nuclear magnetic resonance showed the reactions between TMBPDE and UFUR after the UFUR/TMBPDE composite resin was cured. Differential scanning calorimetry analysis showed that the T_g significantly increased after the addition of TMBPDE. Thermogravimetry analysis indicated that the cured UFUR/TMBPDE composite resin exhibited increasing thermodecomposition temperature as the TMBPDE concentration increased, indicating its great potential for high temperature applications. Moreover, the presence of TMBPDE enhanced the toughness of UFUR as observed by impact test and reflected in the morphologies observed from SEM images of fracture surfaces. It would also be novel and effective to modify urushiol derivatives by the LC polymer.

1. Introduction

Oriental lacquer, known as the king of paints, has been used as coating materials for several thousand years in China [1]. It is a unique invention of uninterrupted civilization with 7000 years and becomes one of the most important sources of the chemistry in China [2]. Oriental lacquer is cut from phloem of the lacquer tree, an important economic tree of China [3]. The dried lacquer coatings possess a beautiful surface and high durability. Therefore, it has been used as decorative coatings to make life more beautiful and has become the symbol of wealth and status in ancient China [2, 4]. Lacquer has been also widely used in chemical, textile, industry, ship-building, mechanical, and electrical products [5]. However, the limited production causes the high price of natural lacquer, which limits its application [6]. Lacquer paint dries by enzymatic oxidation of laccase and autoxidation of urushiol unsaturated side chains [7]. The curing progress is really slow and is strongly affected by the environmental conditions such as humidity and temperature [8]. Moreover, lacquer has poor flexibility, adhesion, alkali resistance, and ultraviolet degradation resistance. Therefore, modification of original lacquer is essential to expand its application fields [9]. Takahisa et al. [10] developed hybrid lacquers composed of natural lacquer and amine-functionalized organic silane compounds that showed good drying property at low relative humidity. Kanehashi et al. [11] reported hybrid microwave-adsorption materials prepared from natural lacquer, epoxy, and organic silane compounds. The results suggested that the chemical reactions among natural lacquer, epoxy, and organic silane improved the hybrid properties such as drying, hardness, and molding.

In general, urushiol, which was the main component of lacquer, was extracted from lacquer and chemically modified to obtain the urushiol derivatives. The urushiol derivatives exhibited superior properties and were used in various fields. In 1960, urushiol formaldehyde resin was synthesized by condensation reaction of urushiol and formaldehyde, which was a significant progress for lacquer modification in China [12]. Zhang and He [13] used inorganic boron to modify the urushiol formaldehyde polymer. Compared with urushiol formaldehyde resin, urushiol organic boron product has a higher antioxidant capacity, heat resistance, and transient high temperature performance. In addition,

Liu [14] synthesized urushiol-furfural resin (UFUR) which could be formulated to a varnish with excellent abrasion-resistance. However, the varnish was very brittle. Therefore, they modified the UFUR by epoxy E-12. The modified varnish showed excellent mechanical properties, especially the abrasion-resistance, corrosion protection, and alkali resistance. UFUR could be cured by heating and it own some superior properties. Therefore, it is quite necessary to find new ways to modify UFUR.

Liquid crystal (LC) epoxy resins have been investigated because of their unique properties, for example, low shrinkage upon curing, good thermal stability, and excellent thermomechanical properties [15]. They combine the advantages of both LCs and epoxy resins. Compared to ordinary epoxy resins, crosslinked LC epoxy resins have higher fracture toughness [16]. Traditional epoxy resins can be improved by introducing LC domains into the amorphous matrix [17]. Unlike other toughening methods such as incorporating rubber particles, the presence of LC domains will not lead to a decrease in the glass transition temperature (T_g) or moduli of the material. These desirable properties make LC epoxy resins good candidates for a wide range of potential applications, such as optical switches, electronic packaging, and matrices for high performance composites [15]. Many efforts were directed towards the increase of toughness by introduction of LC epoxy resins in epoxy resins [18–21]. For example, Punchaipetch et al. [18, 19] copolymerized diglycidyl ether of 4,4-dihydroxybiphenol (DGE-DHBP) with diglycidyl ether of bisphenol F networks and cured it with an anhydride curing agent as the matrix resins. DGE-DHBP enhances the toughness of the blended epoxy samples without decreasing the modulus of samples. However, to the best of our knowledge there are few researches on modification of UFUR with LC polymers.

In the current study, UFUR was chosen as an example of urushiol derivatives and an effective modification method was proposed. A LC epoxy resin, tetramethylbiphenyl diglycidyl ether (TMBPDE), was utilized to modify UFUR for the first time. The LC property of TMBPDE was investigated by polarized optical microscope (POM). The effects of TMBPDE on the T_g, thermal stability, and impact strength of the UFUR/TMBPDE composite resin were analyzed. The fracture surfaces of UFUR/TMBPDE composite resins were investigated by scanning electron microscope (SEM).

2. Materials and Methods

2.1. Materials. TMBPDE was supplied from Gansu Research Institute of Chemical Industry with an epoxy equivalent weight of 192. UFUR was purchased from Wuhan GuoQi Co., Ltd., China. Dimethylbenzene, acetone, and other chemicals were supplied by Tianjin Kemiou Chemical Reagent Co., Ltd., China, and used as received. The chemical structures of TMBPDE and UFUR are shown in Figure 1.

2.2. Sample Preparation. A certain amount of TMBPDE was dissolved in acetone to obtain a solution with the concentration of 25 wt%. Dimethylbenzene solution of UFUR was taken in a beaker. Then, a given ratio of TMBPDE was added and mixed for 10 min at room temperature. The mixture was placed in fume hood to volatilize most solvents at room temperature. For preparation of samples for impact strength test, the above mixture was heated at 80°C for 0.5 h and immediately poured into a preheated mold (inside size: 80 mm × 10 mm × 4 mm) at room temperature. The samples in the molds were cured at 80°C for 4 h, 110°C for 4 h, and 160°C for 4 h in an air-circulating oven. All samples prepared for other characterizations were cured as follows. The mixture was coated onto the treated galvanized iron sheets, dried at room temperature for 1–3 h, and cured at 110°C for 2 h and 160°C for 2 h in an air-circulating oven.

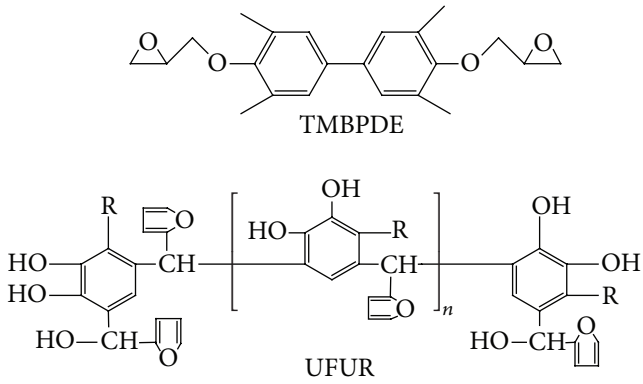

Figure 1: The chemical structures of TMBPDE and UFUR.

2.3. Characterization and Test. In order to study the effects of TMBPDE on the properties of UFUR, different contents of TMBPDE were added. Samples with the TMBPDE contents of 0%, 5%, 15%, and 30% with respect to UFUR were marked as TMBPDE-0, TMBPDE-5, TMBPDE-15, and TMBPDE-30, respectively.

LC property of TMBPDE was investigated using a polarized optical microscope (POM) from Leica (model DM 4500P equipped with a Linkam LTS-350 hot stage and TMS-94 temperature controller). A small amount of TMBPDE was placed on a microscope slide and then covered with a piece of cover glass. The formation and development of the LC phase were examined under polarized light. The sample was heated and cooled repeatedly from room temperature to 140°C at a rate of 10°C/min to investigate the change of birefringence.

The structure analyses of UFUR/TMBPDE composite resin upon curing were conducted via FTIR spectra and solid-state nuclear magnetic resonance (NMR) spectra. FTIR spectra was recorded in a spectrum 100 FTIR spectrometer (FTS3000, BIORAD, USA) in the range from 4000 cm^{-1} to 400 cm^{-1}. A potassium bromide pellet was used to support the IR sample. The sample was spread thinly on the potassium bromide pellet with a spatula, and the potassium bromide pellet was used as a blank. The solid-state ^{13}C NMR spectra were recorded on a JNM-ECA400 (JEOL Co. Ltd., 100 MHz) using zirconium sample tubes with the CP/MAS method.

The effects of TMBPDE on the T_g and thermal stability of the composite resin were investigated by differential scanning

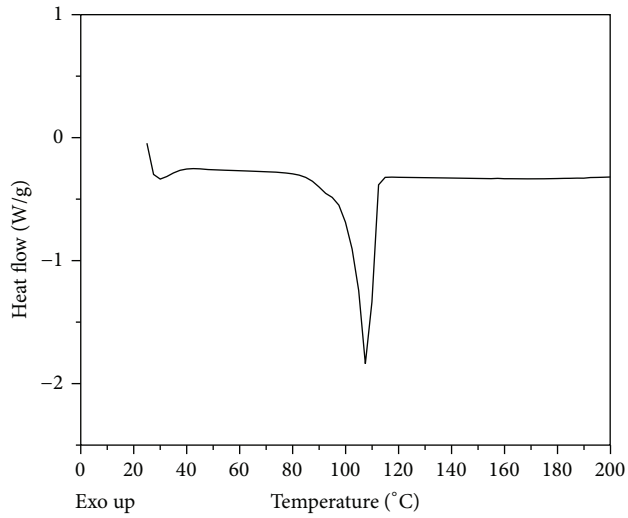

Figure 2: DSC thermogram of TMBPDE.

calorimetry (DSC) and thermogravimetry (TG) analysis with a simultaneous thermal analysis (DSC/DTA-TG, NETZSCH, STA 409 PC Luxx, Germany) under the nitrogen atmosphere at a heating rate of 10°C/min from 30°C to 500°C.

Impact strength was measured by an impact testing machine according to the GB/T1843-2008 standard. The samples were tested by the cantilever beam impact testing machine (Chengde Precision Tester XC-22, China). The sample was placed into the sample well and the pendulum bob fell through a vertical height on the surface. The morphologies of the fracture surfaces after impact tests were coated with gold and observed using SEM (Philips XL30, Dutch).

3. Results and Discussion

3.1. The UFUR/TMBPDE Composite Resin. It was generally believed that the ordered structure that was formed during cured process improved the toughness of the modified resins. If the composite resin was cured during the LC temperature range, more ordered mesogenic domains would be formed. Therefore, it is necessary to determine the LC temperature range. To investigate mesomorphic phase transition of TMBPDE, DSC and POM studies were carried out. The DSC thermogram of TMBPDE is shown in Figure 2. Only one endothermic peak was observed at about 107°C in the heating scan, which was the melting of TMBPDE. However, the clearing point of LC was not found. The thermal behavior of some liquid crystal monomer is not well understood. For example, Liu et al. [22] found two phase transition peaks in the heating scan of DSC. Li and coworkers [15] were not able to detect any LC phase of 4,4′-diglycidyloxybiphenyl (BP) upon heating or observed a LC phase by POM. However, upon reacting with sulfanilamide, a smectic LC phase started forming after 20 min of the curing reaction. The TMBPDE had similar structure as BP. We were also not able to detect any LC phase of TMBPDE upon heating by DSC.

As we know, POM is a powerful tool for characterization of liquid phases. In order to clarify the mesophases of TMBPDE under POM, the samples were prepared by sandwiching a tiny power between two glass plates. Figure 3 shows the POM images of TMBPDE taken at different temperatures (200x magnification). TMBPDE started to melt at 107°C, which is in good agreement with the DSC data. At the same time, LC birefringence was formed, which presents highly birefringent and nematic liquid crystal behavior. The texture color changed with increasing temperature. When the temperature was higher than 117°C, the POM image turned to be completely dark due to the disappearance of the LC phase.

In order to examine the reaction between UFUR and TMBPDE in the composite resin during the curing process, the FTIR spectrums of UFUR and UFUR with 15% TMBPDE before and after being cured were carried out. The results are shown in Figure 4. After the addition of TMBPDE, the peak at 910 cm^{-1} due to the absorption of the epoxy group appeared. After the UFUR/TMBPDE composite resin was cured, the peak at 910 cm^{-1} disappeared and the peak at 3400 cm^{-1} due to the hydroxyl groups decreased, suggesting that polymerization between the epoxy group and the hydroxyl groups had occurred. A decrease in the hydroxyl group peak also promoted the autoxidation of UFUR.

The solid-state ^{13}C NMR spectra of TMBPDE, UFUR, and cured TMBPDE/UFUR composite resin are shown in Figure 5. The peak at ca. 17 ppm belonging to carbon of methyl on the urushiol aromatic ring of TMBPDE was detected in the spectrum of TMBPDE/UFUR composite resin. For TMBPDE, the oxygen atom substituted carbons on the epoxy group were detected at ca. 45 ppm and 52 ppm (Figure 5(a)). After the TMBPDE/UFUR composite resin was cured, the peaks of these carbons disappeared (Figure 5(c)), indicating that polymerization between TMBPDE and UFUR had occurred during curing.

In conclusion, although the LC phase of TMBPDE could not be detected by DSC, it could be observed by POM. The LC temperature range was from 107°C to 117°C. During curing, UFUR/TMBPDE composite resin was cured at 110°C for 2 h and then 160°C for 2 h. At 110°C, TMBPDE presented a LC phase and it had enough time for the mesogenic segments to form LC domains during the curing process [15]. Figure 6 shows POM images of UFUR/TMBPDE composite resin taken at different temperatures (100x). The LC phase starts to appear above 100°C. As the temperature increased, the LC phase did not disappear. After being further cured at 160°C for 2 h, the LC domains would be "locked" in the network of the composite resin.

3.2. Thermal Properties. The cured thermosets are in glass state at room temperature. When the temperature was above its T_g, the uncured molecules could move in the micro-Brownian motion, which decreased the rigidity and strength. Therefore, the T_g is an important index to measure the heat resistance and available range of thermosetting resins. Therefore, it is necessary to study the effect of TMBPDE on the T_g of the composite resins. The relationship between the T_g and the TMBPDE content of the composite sample was valuated by DSC. As shown in Figure 7, T_g of UFUR was about 187.2°C. For UFUR/TMBPDE composite resins,

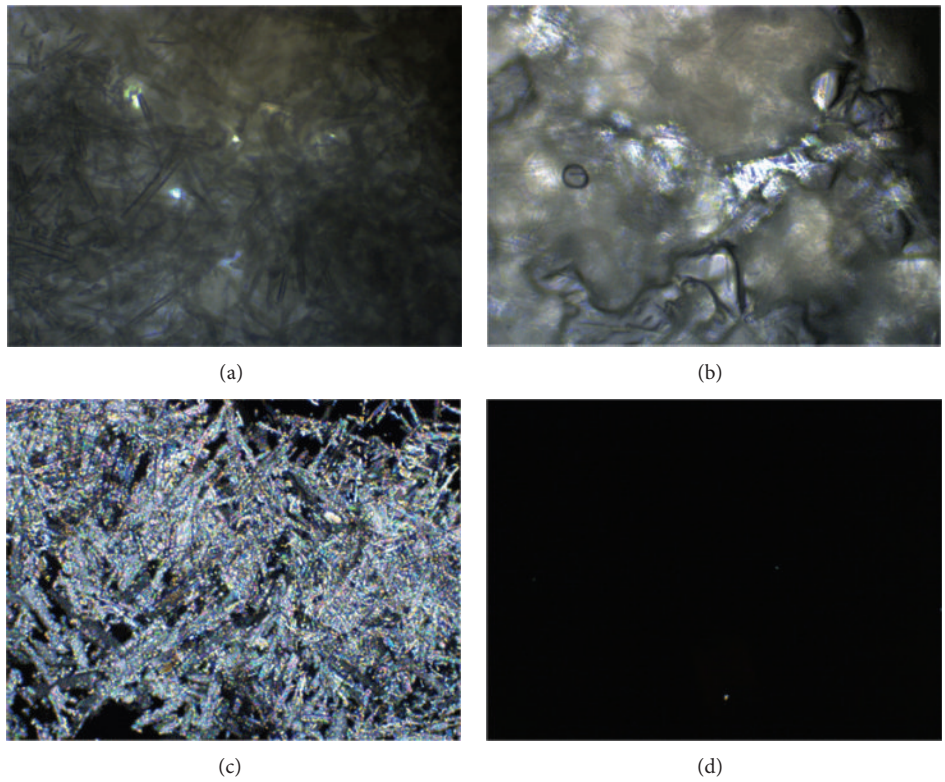

Figure 3: POM images of TMBPDE at different temperatures (200x): (a) 100°C; (b) 107°C; (c) 110°C; (d) 118°C.

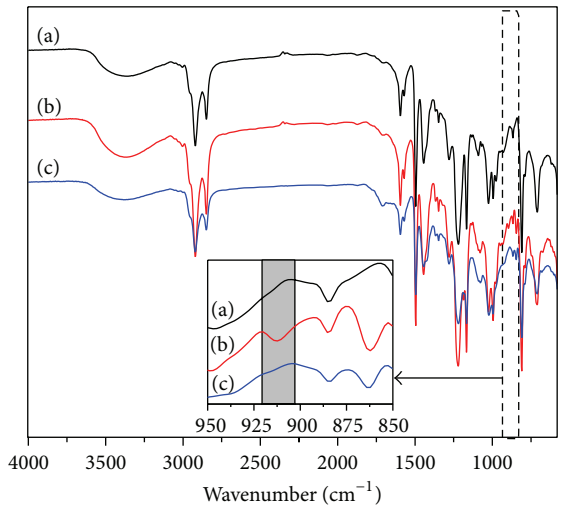

Figure 4: FTIR spectra of samples ((a) UFUR; (b) TMBPDE-15 (uncured); (c) TMBPDE-15 (cured)).

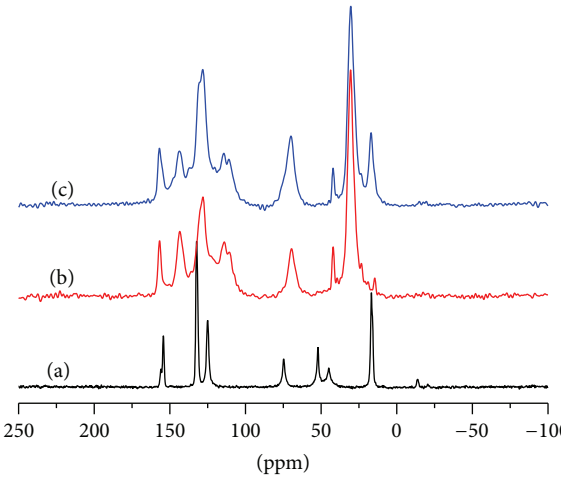

Figure 5: ^{13}C CP/MAS NMR spectra of samples ((a) TMBPDE; (b) UFUR; (c) TMBPDE-15 (cured)).

when TMBPDE content was less than 15%, T_g of the composite resin increased as the TMBPDE content increased. When 15% TMBPDE was added, the T_g of the composite resin increased from 187.2°C to 232°C. However, when the TMBPDE content reached 30%, the T_g of the composite resin decreased to 224.1°C. Huang et al. [23] found that the novel liquid crystalline polymers, polydiethyleneglycol bis(4-hydroxybenzoate) terephthaloyl and block copolymer, could enhance the T_g of the o-cresol formaldehyde epoxy resin remarkably due to the rigid segments in the liquid crystalline polymers. Therefore, in this study, it is also proposed that the rigid segments in TMBPDE are the main reason why TMBPDE can improve T_g of the composite resins. However, when the TMBPDE content was improved to 30%, T_g was

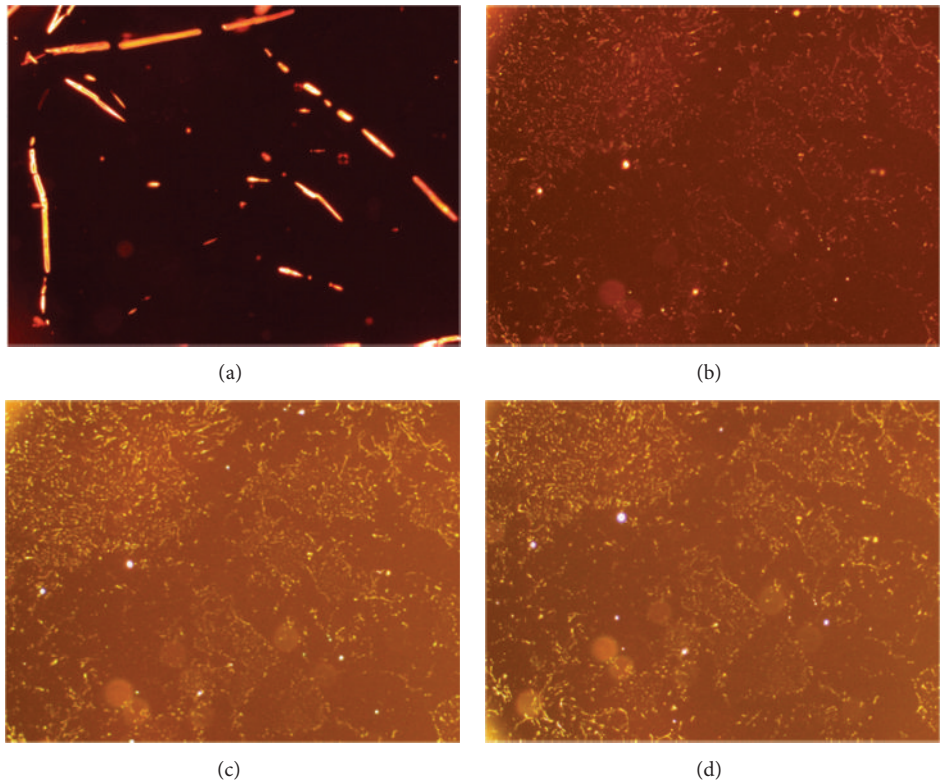

Figure 6: POM images of UFUR/TMBPDE composite resin at different temperatures (100x): (a) 90°C; (b) 100°C; (c) 110°C; (d) 160°C.

Table 1: Thermodata obtained from DSC (T_g) and TG (T_d).

Remarks	T_g (°C)	T_d (°C)
TMBPDE-0	187	330
TMBPDE-5	195	335
TMBPDE-15	232	345
TMBPDE-30	224	352

lower than the former but much higher than that of UFUR. We found similar phenomenon to Huang et al. [23], who found that T_g of the blends first increased and then decreased as the content of the liquid crystalline polymers is increasing. It was proposed that the molecular weight of TMBPDE was small. Therefore, when 30 wt% of TMBPDE was added, the structure density of the curing network would decrease, leading to the slight decrease of T_g of TMBPDE-30. However, this problem will need to be further gone into.

Effects of TMBPDE on thermal stability of the composite resins were also investigated. Figure 8 shows the TGA curves for UFUR/TMBPDE composite resins with different TMBPDE contents. The thermal degradation temperature (T_d) was defined as the temperature when the samples lost 5% of their initial weight, and the results were summarized in Table 1. It can be seen that the T_ds of all UFUR/TMBPDE composite resins were higher than that of pure UFUR, indicating that the addition of TMBPDE enhanced thermal stability of UFUR. For the composite resins, the T_ds increased with the TMBPDE contents. When the content of TMBPDE was 15%, the T_d of the composite resin increased to 352°C. The high value of the decomposition temperature can be ascribed to the presence of the biphenyl as rigid block. Therefore, TMBPDE strongly enhances the thermal stability of the UFUR/TMBPDE composite resin.

3.3. Impact Strength. Figure 9 shows the comparison of impact strength as a function of the TMBPDE contents. There was an increase in the impact strength of the composite resin on addition of the TMBPDE. When 30% TMBPDE was added, the UFUR/TMBPDE composite resin showed a four-fold increase in impact strength compared to pure UFUR. Punchaipetch [19] also has reported that the incorporation of a relatively small amount of the LC epoxy (diglycidyl ether of 4,4′-dihydroxybiphenol) could significantly enhance the toughness and T_g of the blended epoxy samples.

The impact surfaces were investigated by SEM, as shown in Figure 10. The cured UFUR exhibited a brittle type of fracture behavior. For the cured composite resin with 5% TMBPDE, the fracture surface was very sharp with no plastic deformation. The crack grew in one direction because of the minimum resistance. When the addition of TMBPDE was increased to 15%, the rigid segments which were crosslinked in the UFUR matrix could absorb some impact energy,

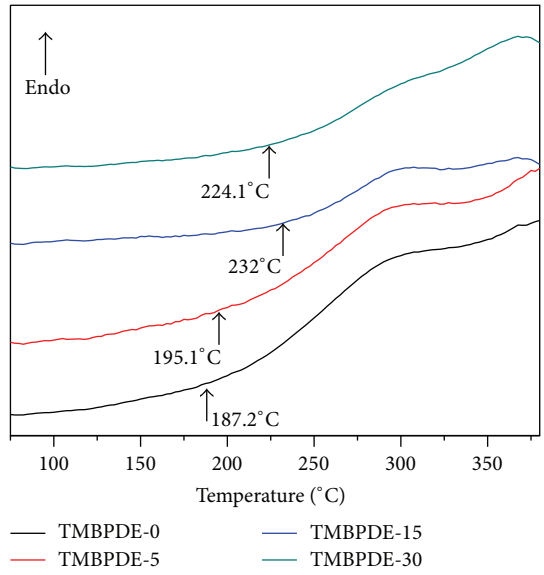

Figure 7: The glass transition temperatures of UFUR/TMBPDE composite resins with different TMBPDE contents.

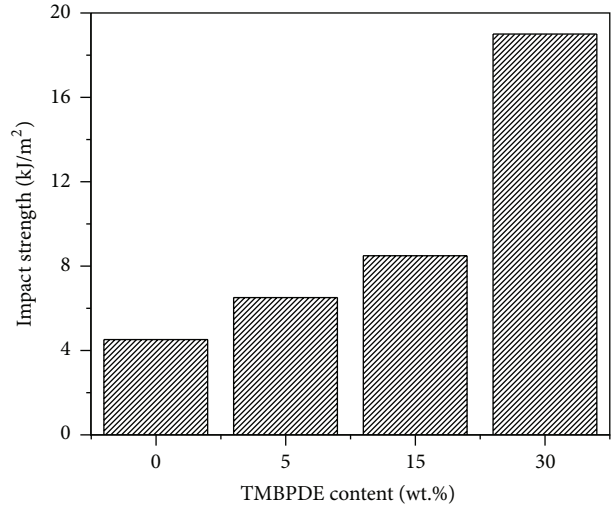

Figure 9: Impact strength of UFUR/TMBPDE composite resins with different TMBPDE contents.

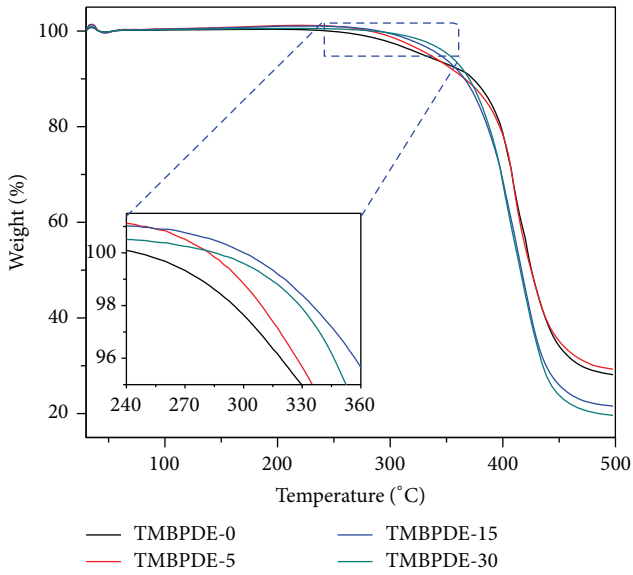

Figure 8: Thermogravimetric analysis of UFUR/TMBPDE composite resins with different TMBPDE contents.

resulting in improvement of the toughness. Therefore, the fracture surface exhibited ductile fracture with a river pattern where the multiple lines begin as a single line at the initiation point. For the composite resin with 30% TMBPDE, the furrow pattern at the starter crack region is found to be much bigger and coarser than that with 15% TMBPDE. Therefore, the toughness of TMBPDE-30 was higher than TMBPDE-15 by SEM.

The LC possesses a unique hierarchical microstructure in which, in the absence of external fields, they tend to form a macroscopically disordered polydomain, where each LC domain is defined as a region of uniform orientation [24]. For the LC thermoset, it exhibits exceptionally high fracture toughness. At low stress, crazes first take place within the isotropic amorphous domains and grow along the stress direction. Finally the crazes are hampered by the LC domains, which improved the impact strength of the LC thermoset [25]. For the UFUR/TMBPDE composite resin in our study, during curing, the LC phase of TMBPDE was "frozen" into the network, forming anisotropic LC domains surrounded by a macroscopically disordered polydomain. Therefore, the microdeformation and fracture mechanism of the LC thermoset could be extended to the case of the UFUR/TMBPDE networks and explain the reason for the impact strength improvement of the composite resin.

4. Conclusions

TMBPDE was utilized to modify the urushiol derivative, UFUR. The results showed that the T_g significantly increased after the addition of TMBPDE. The UFUR/TMBPDE composite resin with 15% TMBPDE had a higher T_g by 45°C compared with the pure UFUR. TGA analysis showed that the cured UFUR/TMBPDE composite resin exhibited increasing thermodecomposition temperature as the TMBPDE concentration increased, indicating its great potential for high temperature applications. Moreover, the presence of TMBPDE enhanced the toughness of UFUR as observed by impact test and reflected in the morphologies observed from SEM images of fracture surfaces. In conclusion, TMBPDE significantly enhanced the toughness of UFUR without sacrificing high T_g and thermodecomposition temperature. It is supposed that the improvements of the properties are the effects of the mesogenic domains distributed in the network. These results also suggest that it would be a novel and effective way to modify other urushiol derivatives by a LC polymer.

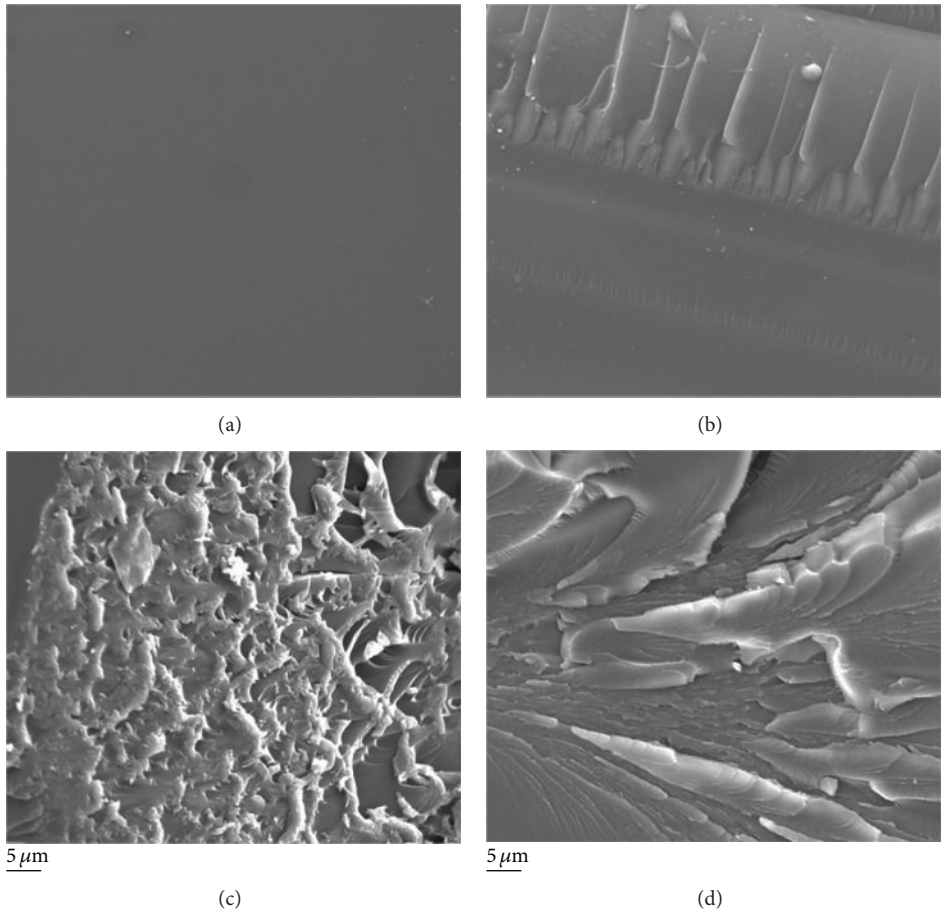

Figure 10: Impact surfaces of UFUR/TMBPDE composite resins ((a) TMBPDE-0; (b) TMBPDE-5; (c) TMBPDE-15; (d) TMBPDE-30).

Conflict of Interests

The authors declare that there is no conflict of interests regarding the publication of this paper.

Acknowledgments

This work was supported by Natural Science and Technology Ministry of China (ID: 2011BAD33B03) and the Key Technologies R&D Program of Tianjin, China (ID: 14ZXCXGX00680).

References

[1] X. L. Sun, G. M. Wu, and Z. W. Kong, "Research progress of modification and application of raw lacquer," *Biomass Chemical Engineering*, vol. 48, no. 2, pp. 41–46, 2014.

[2] F. L. Zhang, "Origin of lacquer civilization in China," *Journal of Chinese Lacquer*, vol. 29, no. 2, pp. 16–25, 2010.

[3] D. X. Li and F. L. Zhang, "Extraction of active constituents and progress in the studies on Lacquer tree," *Journal of Chinese Lacquer*, vol. 33, no. 1, pp. 27–32, 2014.

[4] F. L. Zhang and H. Zhang, "Lacquer tapping and refined processing technology in ancient China," *Journal of Chinese Lacquer*, vol. 30, no. 2, pp. 22–27, 2011.

[5] R. Lu, N. Ebata, F.-L. Zhang, and T. Miyakoshi, "Development of a new type lacquer based on *Rhus vernicifera* sap with chitosan," *Progress in Organic Coatings*, vol. 77, no. 2, pp. 439–443, 2014.

[6] J. Kumanotani, "Urushi (oriental lacquer)-a natural aesthetic durable and future-promising coating," *Progress in Organic Coatings*, vol. 26, no. 2–4, pp. 163–195, 1995.

[7] F. L. Zhang, "Molecular mechanism of lacquer film formation," *Journal of Chinese Lacquer*, vol. 31, no. 1, pp. 13–20, 2012.

[8] T. Ishimura, R. Lu, K. Yamasaki, and T. Miyakoshi, "Effects of hybridization of lacquer sap with organic silane on drying properties," *Progress in Organic Coatings*, vol. 62, no. 2, pp. 193–198, 2008.

[9] Q. Wang, Y. Shi, and F. L. Zhang, "Development progress on the modification of natural raw lacquer," *Shanghai Coatings*, vol. 48, no. 2, pp. 30–33, 2010.

[10] I. Takahisa, L. Rong, and M. Tetsuo, "Studies on the reaction mechanism between urushiol and organic silane," *Progress in Organic Coatings*, vol. 55, no. 1, pp. 66–69, 2006.

[11] S. Kanehashi, H. Oyagi, R. Lu, and T. Miyakoshi, "Development of bio-based hybrid resin, from natural lacquer," *Progress in Organic Coatings*, vol. 77, no. 1, pp. 24–29, 2014.

[12] B. Hu, J. Lin, and Y. Xu, "The improvement of raw lacquer and the study on urushiol-metal polymer," *Journal of Chinese Lacquer*, vol. 19, no. 3, pp. 1–7, 2000.

[13] F. L. Zhang and N. He, "Synthesis and characterization of urushiol organic boron resin," *Shanghai Coatings*, vol. 31, no. 2, pp. 3–5, 2012.

[14] Y. Liu, "Epoxy modified urushiol-furfural resin," *Paint & Coatings Industry*, vol. 3, pp. 1–4, 1995.

[15] Y. Li, P. Badrinarayanan, and M. R. Kessler, "Liquid crystalline epoxy resin based on biphenyl mesogen: thermal characterization," *Polymer*, vol. 54, no. 12, pp. 3017–3025, 2013.

[16] C. Carfagna, E. Amendola, and M. Giamberini, "Liquid crystalline epoxy based thermosetting polymers," *Progress in Polymer Science*, vol. 22, no. 8, pp. 1607–1647, 1997.

[17] M. Harada, N. Okamoto, and M. Ochi, "Fracture toughness and fracture mechanism of liquid-crystalline epoxy resins with different polydomain structures," *Journal of Polymer Science, Part B: Polymer Physics*, vol. 48, no. 22, pp. 2337–2345, 2010.

[18] P. Punchaipetch, V. Ambrogi, M. Giamberini, W. Brostow, C. Carfagna, and N. A. D'Souza, "Epoxy + liquid crystalline epoxy coreacted networks: I. Synthesis and curing kinetics," *Polymer*, vol. 42, no. 5, pp. 2067–2075, 2001.

[19] P. Punchaipetch, V. Ambrogi, M. Giamberini, W. Brostow, C. Carfagna, and N. A. D'Souza, "Epoxy+liquid crystalline epoxy coreacted networks: II. Mechanical properties," *Polymer*, vol. 43, no. 3, pp. 839–848, 2002.

[20] H. J. Sue, J. D. Earls, and R. E. Hefner Jr., "Fracture behaviour of liquid crystal epoxy resin systems based on the diglycidyl ether of 4,4′-dihydroxy-α-methylstilbene and sulphanilamide: part I Effects of curing variations," *Journal of Materials Science*, vol. 32, no. 15, pp. 4031–4037, 1997.

[21] P. Chang, R. Zuo, R. Wang, and L. Chen, "Toughening of epoxy resins with a liquid-crystalline epoxy resin," *Acta Polymerica Sinica*, no. 5, pp. 682–684, 2002.

[22] Y.-L. Liu, Z.-Q. Cai, X. Wen et al., "Thermal properties and cure kinetics of a liquid crystalline epoxy resin with biphenyl-aromatic ester mesogen," *Thermochimica Acta*, vol. 513, no. 1-2, pp. 88–93, 2011.

[23] Z. F. Huang, S. T. Tan, and X. Y. Wang, "Modification of an o-cresol formaldehyde epoxy resin by the thermotropic liquid crystalline polymer," *Journal of Applied Polymer Science*, vol. 97, no. 4, pp. 1626–1631, 2005.

[24] C. Ortiz, R. Kim, E. Rodighiero, C. K. Ober, and E. J. Kramer, "Deformation of a polydomain, liquid crystalline epoxy-based thermoset," *Macromolecules*, vol. 31, no. 13, pp. 4074–4088, 1998.

[25] C. Ortiz, L. Belenky, C. K. Ober, and E. J. Kramer, "Microdeformation of a polydomain, smectic liquid crystalline thermoset," *Journal of Materials Science*, vol. 35, no. 8, pp. 2079–2086, 2000.

Hindawi Publishing Corporation
International Journal of Polymer Science
Volume 2015, Article ID 547907, 9 pages
http://dx.doi.org/10.1155/2015/547907

Research Article

Enzymatic Digestion and Mass Spectroscopies of N-Linked Glycans in Lacquer Stellacyanin from *Rhus vernicifera*

Oyunjargal Tumurbaatar[1] and Takashi Yoshida[1,2]

[1] *Department of Biological and Environmental Chemistry, Kitami Institute of Technology, 165 Koen-cho, Kitami, Hokkaido 090-8507, Japan*
[2] *Research Center for Environmentally Friendly Materials Engineering, Muroran Institute of Technology, 27-1 Mizumoto-cho, Muroran, Hokkaido 050-8585, Japan*

Correspondence should be addressed to Takashi Yoshida; yoshida@chem.kitami-it.ac.jp

Received 5 January 2015; Accepted 15 February 2015

Academic Editor: Yulin Deng

Lacquer stellacyanin was isolated and purified from lacquer acetone powder by continuous Sephadex column chromatographies using Sephadex C-50, DEAE A-50, and C-50 gels. The purified lacquer stellacyanin had a blue color with one major and three minor bands around 26 k Dain SDS PAGE. Trypsin- and chymotrypsin-treated lacquer stellacyanins were examined by LC/MS/MS to determine three N-glycosylation sites (N28, N60, and N102) and were further analyzed by MALDI TOF MS, indicating that the N-linked glycans were attached to the three asparagine (Asn) sites, respectively. In addition, after trypsin digestion and PNGase A and PNGase F treatments to cleave N-linked glycans from the Asn sites, it was found that lacquer stellacyanin had a xylose containing a biantennary N-linked glycan with core fucosylation consisting of 13 sugar residues (a complex type N-linked glycan) by MALDI TOF MS analysis. This is the first report on the structure of an N-linked glycan in lacquer stellacyanin.

1. Introduction

Lacquer sap is a naturally occurring paint that is polymerized by laccase, an oxidoreductive enzyme of catechols, to give a durable film with a glorious surface. Lacquer sap is a water-in-oil emulsion composed mainly of urushiols, polysaccharides, glycoproteins, laccase, and stellacyanin [1]. Among them, stellacyanin, like laccase, is a copper-containing glycoprotein; it was first characterized as a blue glycoprotein by Keilin and Mann in 1940 [2]. Lacquer stellacyanin is a low molecular weight (approximately 20 kDa) protein with a single polypeptide chain of 107 amino acid residues and a Cu atom. Since the glycoprotein was identified as stellacyanin [3], proteins similar to lacquer stellacyanin have been isolated from cucumber [4], zucchini peel [5], spinach leaf [6], and horseradish root [7]. These glycoproteins are plant specific glycoproteins belonging to the phytocyanin subclass of the cupredoxins. Stellacyanin is an electron transfer protein [8] and is involved in a redox process during primary defence, lignin formation, and cell-to-cell signalling transmission; however, the exact physiological function is still unclear [9–11]. In addition, N-linked glycans in plant glycoproteins have been shown to affect catalytic activity, thermostability, lignin formation, folding or subcellular localization, and secretion [12, 13]. Recently, it was found that N-linked glycans may play a role in plant pathogen integration and functional pattern recognition receptors [14]. Removal of complex type N-glycans from plant glycoproteins by mutational modification of N-linked glycans in several plants, *Arabidopsis* and tobacco, has demonstrated no or little effect on plant growth [15]. For the structural analysis of the carbohydrate composition of lacquer stellacyanin, no results have been published except a paper on chromatographic separation of monosaccharides of stellacyanin hydrolysate by Peisach et al. in 1967 [16].

We have investigated the structure and specific biological activities of lacquer polysaccharides in Japanese and Chinese

lacquer saps. The lacquer polysaccharides with the number-average molecular weight of $\overline{M}_n = 10 \times 10^3 - 30 \times 10^3$ were analysed by high resolution NMR measurement, revealing that the lacquer polysaccharides were acidic polysaccharides and had a $(1 \rightarrow 3)$-β-D-galactopyranan main chain with complex branches consisting of glucuronic acid in the terminal [17]. The lacquer polysaccharides were found to reduce the growth of sarcoma 180 tumour in mice and had blood coagulation-promoting activity compared to that of control [18]. After sulfation, lacquer polysaccharides showed potent anti-HIV and low blood anticoagulant activities. These specific biological activities should originate from the acidic branched structure [18]. In addition, treatment with diluted alkaline aqueous solution revealed that lacquer polysaccharides were constructed of association of low molecular weight polysaccharides [19].

Glycosylation is one of the most common and important modifications of peptides that changes the functions of proteins. In general, N-linked glycans are located at an asparagine (Asn) residue of the tripeptide sequence, Asn-X-Ser or Thr, where X is any amino acid except proline [20]. There are three possible N-glycosylation sites (Asn-X-Seror Thr) in the amino acid sequence of stellacyanin (N28, N60, and N102) [21]. Mass spectrometry (MS) is valuable and rapid analytical techniques to analyse structures of glycans in proteomics and proteins by a combination with enzymatic treatments [22]. In this study, we report for the first time the structural analysis of N-linked glycans present in lacquer stellacyanin by both matrix assisted laser desorption/ionization time of flight mass spectrometry (MALDI TOF MS) and liquid chromatography mass spectrometry coupled with electrospray ionisation tandem mass spectrometry (LC/MS/MS) after enzymatic digestion for the elucidation of stellacyanin functionality in lacquer sap.

2. Materials and Methods

2.1. Materials. Lacquer acetone powder was prepared by addition of acetone to lacquer sap according to the method reported by Reinhammar [23]. CM-Sephadex C-50 and DEAE-Sephadex A-50 were purchased from Healthcare Bio-Sciences AB, Sweden. Trypsin from porcine pancreas (≥10,000 units/mg), α-chymotrypsin from bovine pancreas (61.75 units/mg), dithiothreitol (DTT), iodoacetamide (IAA), and trifluoroacetic acid (TFA) were obtained from Sigma Aldrich, Japan. Peptide-N-Glycosidase A (PNGase A) from almond and Peptide-N-Glycosidase F (PNGase F) were purchased from Roche. Other reagents, *Arthrobacter ureafaciens* sialidase from Nakalai, a BlotGlyco glycan purification and labeling kit (BS-45603) from Sumitomo Bakelite Co., Ltd., 2,5-dihydroxybenzoic acid (DHB) as a matrix for MALDI-TOF/MS from Bruker Daltonics GmbH, 10–20% gradient gels (E-T1020L), EZ marker standards (AE-1440), and Coomassie blue for SDS-PAGE analysis from ATTO Corporation, Japan, were used.

2.2. Isolation and Purification of Lacquer Stellacyanin from Acetone Powder. Lacquer acetone powder (20 g), which was prepared by the method of Reinhammar [23], was dissolved in 200 mL of 0.01 M potassium phosphate buffer solution (pH 6.0) and then stirred overnight at 4°C. The mixture was centrifuged and then filtered to remove any insoluble materials. The filtrate was chromatographed on a CM-Sephadex C-50 column (250 mm × 40 mm) to collect lacquer laccase and stellacyanin as blue colorbands eluted with 0.1 M and 0.2 M phosphate buffer solution (pH 6.0), respectively. Lacquer stellacyanin was further purified by DEAE-Sephadex A-50 column chromatography (500 mm × 20 mm) and subsequent CM-Sephadex C-50 column chromatography (500 mm × 20 mm) gradually eluted with 0.005 M, 0.025 M, 0.05 M, and 0.1 M phosphate buffer solutions. The eluent with a blue colour was finally desalted by dialysis with deionized water overnight and then freeze-dried to give 0.233 g (1.17%) and 0.083 g (0.42%) of pure lacquer laccase and stellacyanin, respectively.

2.3. Preparation of Copper-Free Stellacyanin. Blue stellacyanin (56 mg) was dissolved in 20% aqueous trichloroacetic acid solution (10 mL), and the mixture was stirred until the blue color disappeared. After dialysis against deionized water overnight, it was then freeze-dried to give colorless stellacyanin without copper. The purity and molecular weights of the purified stellacyanin were measured by SDS-PAGE and MALDI TOF MS, respectively.

2.4. Enzymatic Digestion and N-Glycan Labeling. Lacquer stellacyanin (1 mg) was suspended in 0.1 M NH_4HCO_3 solution, DTT (5 μL, 120 mM) was added, and then the mixture was incubated for 30 min at 60°C. To the mixture was added 10 μL of IAA (123 mM) and it was incubated in the dark for 1 h at room temperature to give carboxamide-methylated stellacyanin, which was used without purification for the next enzymatic digestion. Trypsin (1 mg) or chymotrypsin (1 mg) solution in 1 mL of 0.1 M NH_4HCO_3 (10 μL) was added to the above carboxamide-methylated stellacyanin solution and incubated overnight at 37°C and 25°C, respectively, to digest stellacyanin, and then the mixture was heated to 95°C to denature trypsin or chymotrypsin.

The trypsin-digested stellacyanin was deglycosylated by adding 0.25 U PNGase A at pH 5.0 (adjusted by 0.1%HCOOH) and 5 U PNGase F at pH 8.5, respectively, overnight at 37°C. The digested N-glycans were labeled with N^{α}-((aminooxy)acetyl)tryptophanylarginine methyl ester (aoWR) by using a BlotGlyco glycan purification and labeling kit according to the manufacturer's protocol and then the aoWR-labelled glycans were purified by a clean-up column according to the manufacturer's protocol [24]. The chymotrypsin-digested stellacyanin was also treated with 0.25 U PNGase A and 5 U PNGase F, respectively, by the same procedure as above to give aoWR-labelled glycans.

2.5. Sialidase Treatment. Lacquer stellacyanin (0.5 mg) was treated with *Arthrobacter ureafaciens* sialidase (1.0 U in 50 mM Tris/HCI buffer) overnight at pH 5.6 and 37°C to confirm the presence or absence of sialic acid in the glycans.

2.6. MALDI TOF MS. The MALDI TOF MS spectrum was recorded on an Ultraflex II instrument (Bruker Daltonics) in reflection mode with an acceleration voltage of 25 kV in

the positive ion mode (positive voltage polarity). The MS spectrum was automatically provided by using FlexControl software 3.0 version. External calibration was carried out with singly charged monoisotopic peaks of peptide standards (1046.5 Da angiotensin II, 1296.6 Da angiotensin I, 1347.7 Da substance P, 1619.8 Da bombesin, and 2093.0, 3474.5 ACTH CLIP peptides). DHB matrix in acetonitrile/water (3 : 7, v/v) was used for the MALDI TOF MS measurements of the aoWR-labelled N-glycans, trypsin-digested peptide, and glycopeptide mixture. The aoWR-labelled N-glycans were mainly detected as protonated molecular ions $[M+H]^+$. Sialic acid residues in glycan were esterified by a methyl group (-COOH→-$COOCH_3$; mass signal increases +14.02), and the exact masses of glycans were calculated as glycan exact mass [M] = [observed m/z] − 447.21 + 18.01 − (14.02 ×n) − 1.00, where 447.21 is the mass of the aoWR labelling reagent and n is the number of sialic acids.

2.7. LC/MS/MS. LC/MS/MS was performed using a liquid chromatography (Shimadzu LC system) tandem mass spectrometry (AB SCIEX API 4000 Q TRAP) system with Turbo spray source and electrospray ionization (ESI). An ODS column (TSK-Gel ODS-80Ts (5 μm) with ID 2.5 mm × 15 cm and a TSK guard cartridge (5 μm) with ID 3.2 mm × 1.5 cm) was used at 30°C. The eluents used were (A) 0.1% TFA in 90% acetonitrile and (B) 0.1% TFA in 10% acetonitrile with a flow rate of 0.2 mL/min in a gradient program for 120 min. And MS/MS spectra were acquired in the positive ionization mode with an acquisition time of 0.63 spectra per second.

Also, the following MS data were acquired by enhanced MS (EMS), in which the scan rate was 4000 Da/s, scan range was 100–2800 Da, fixed linear ion trap (LIT) full time was 10 ms, and Q0 was off check. The enhanced resolution MS (ER), in which scan rate was 250 Da/s, fixed LIT full time was 10 ms, and Q0 was on, and information dependent acquisition (IDA) criteria were inserted to select the 1–3 most intense peaks; ions greater than 400 (m/z) and smaller than 1500 (m/z) and peak intensity which exceeds 50000 cps were chosen. Finally, two enhanced product ion (EPI) experiments were performed, in which scan rate was 4000 Da/s, scan range was 100–2500, fixed LIT full time was 50 ms, and Q0 was trapping on.

MS data were processed with DataAnalyst 4.0 by using a default setting for glycopeptide analysis. Peptide sequences in glycopeptides obtained by proteases were annotated by BioAnalyst (peptide sequence), and MS/MS analyses of attached glycans were interpreted manually. Protein information is available in UniProt with ID number P00302 and entry name STEL_TOXVR (http://www.uniprot.org/uniprot/P00302).

3. Results and Discussion

3.1. Purification and Molecular Weight of Lacquer Stellacyanin. Scheme 1 shows the analytical scheme of the lacquer stellacyanin by enzymatic hydrolysis. The lacquer stellacyanin was isolated and purified from lacquer acetone powder, which was obtained by addition of acetone to lacquer sap, by continuous column chromatographies of Sephadex C50 and DEAE A50 gels. Figure 1 shows the (a) SDS-PAGE profile, (b) MALDI TOF MS profile, and (c) amino acid sequence of lacquer stellacyanin. The purified lacquer stellacyanin was confirmed by SDS-PAGE, which revealed that the lacquer stellacyanin had one major and three minor bands around 26 kDa. The bands were very close to each other as shown in Figure 1(a). We used this lacquer stellacyanin without further purification. Figure 1(b) shows the MALDI TOF MS spectrum of the lacquer stellacyanin using DHB as the matrix, in which several signals, at least four peaks, appeared around 17000–19000 Da with one strong and three weak signals. The strongest signal appeared around 18700 Da. These results suggested that the lacquer stellacyanin is not a single protein but consists of isoenzymes of the same protein. The molecular weights by the SDS-PAGE electrophoresis were larger than those of MALDI TOF MS, probably due to the linear structure by SDS. Figure 1(c) exhibits the amino acid sequence of the lacquer stellacyanin according to the literature [21]. The lacquer stellacyanin had 107 amino acid residues and the molecular weight of the amino acid residues was 12296 Da. Therefore, the molecular weight of the carbohydrate portions of the lacquer stellacyanin is around 7000 Da.

3.2. LC/MS/MS Analysis of Glycopeptides. For identification of the N-glycosylation sites in the lacquer stellacyanin, trypsin-digested peptides and glycopeptides were directly analysed by LC/MS/MS without any separation and purification because LC/MS/MS is a high resolution tool for analysis of mixed samples with the liquid chromatography (LC) system. We used two different proteases, trypsin and chymotrypsin, to obtain three possible N-glycosylation sites that contain Asn with an N-linked glycan from the amino acid sequence of stellacyanin. For identification of glycopeptides, the mixture of the trypsin-digested peptides and glycopeptides was selectively detected by extracted ion chromatography (XIC) to reveal that it contains a glycan marker ion of m/z 204.1 due to glucosamine, $GlcNAc^+$. The marker ion was extracted by total ion chromatography (TIC) in the LC/MS profile, and then it appears in several separated areas in the XIC. We identified the three glycopeptides with an N-linked glycan at Asn28, Asn60, and Asn102, based on the peptides' theoretical masses; these were $WASN_{28}K$ (m/z = 605.2), $NYQSCN_{60}DTTPIASYNTGBBR$ (m/z = 2291.9), and $VHIN_{102}VTVR$ (m/z = 937.5) as shown in Table 1. The MS/MS spectrum of the glycopeptides was analysed, and then the signals at m/z = 204.1 ($GlcNAc_1$), m/z = 366.1 (Gal+GlcNAc), and m/z = 512.1 (Fuc+Gal+GlcNAc) due to fragment ions of N-linked glycans as well as the b and y type fragment ions of oligopeptides cleaved at the glycosidic bond were very frequently observed. After confirmation of the N-glycopeptides derived by trypsin in the MS/MS, the characterization of the attached N-linked glycans was based on their product ion spectra.

The LC/MS/MS spectra of trypsin-digested lacquer stellacyanin are shown in Figure 2. The TIC and XIC containing the m/z = 204.1 ion signal due to GlcNAc are presented in Figures 2(a) and 2(b). A glycopeptide $WASN_{28}K$ with Asn at Asn28 was observed around 13–15 min in the TIC, and the most intense ion signal at m/z = 605.2 corresponded to the molecular weight of the oligopeptide part.

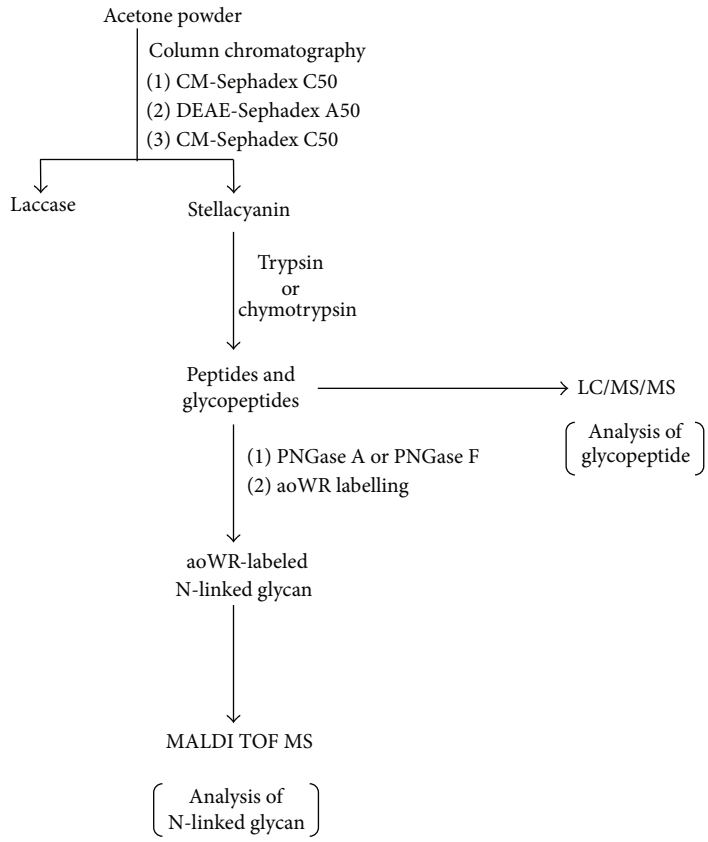

Scheme 1: Isolation and purification of glycoproteins and N-linked glycan from lacquer stellacyanin.

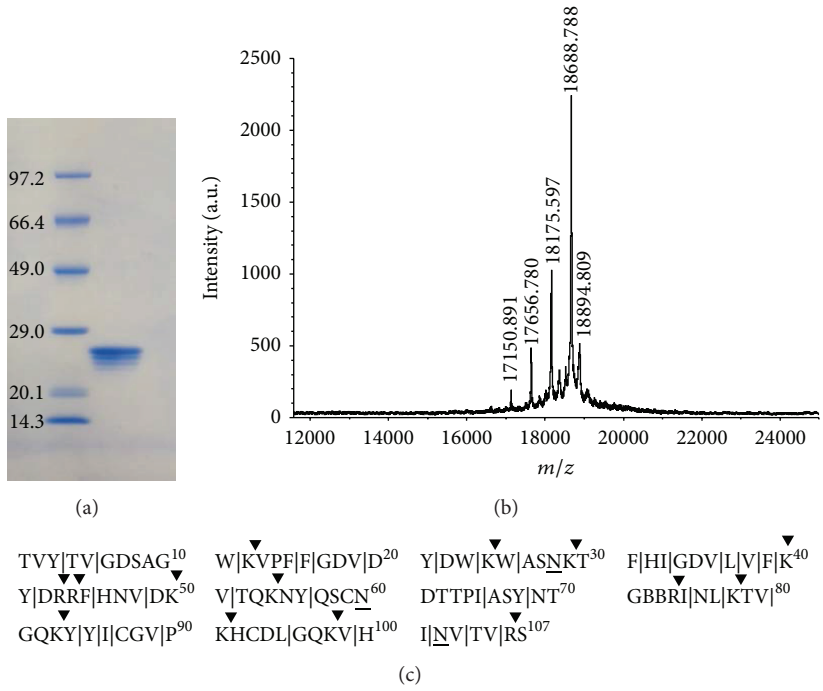

Figure 1: Stellacyanin isolated from lacquer sap: (a) SDS-PAGE profile, (b) MALDI TOF MS profile, and (c) amino acid sequence of lacquer stellacyanin. N-glycosylation sites at Asn28, Asn60, and Asn102 are underlined. ▼ and |: trypsin and chymotrypsin cleavage sites, respectively, and B: unidentified amino acid residue, N (asparagine) or D (aspartic acid).

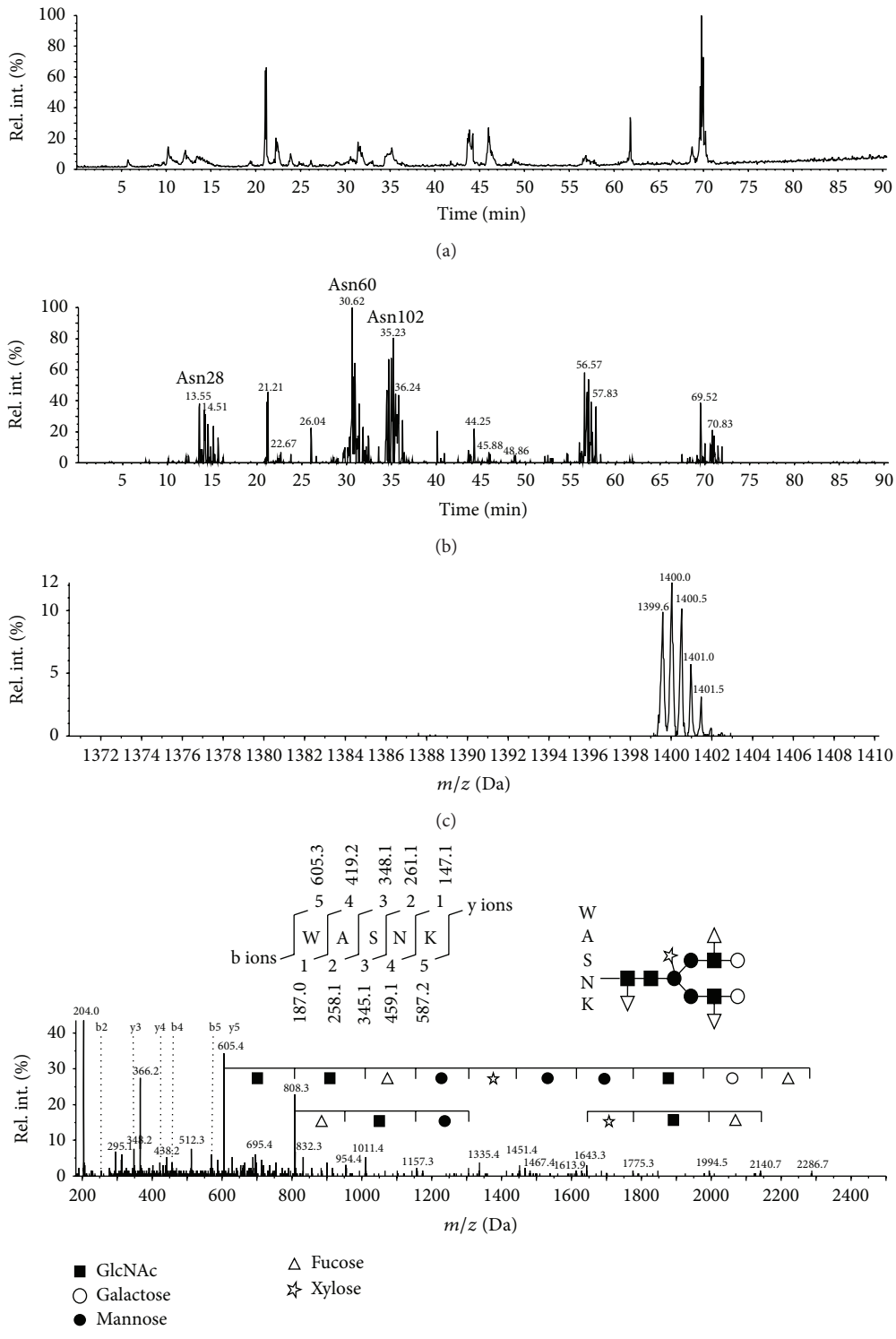

Figure 2: LC/MS/MS analysis of trypsin-derived N-glycopeptide WASNK (Asn28) of lacquer stellacyanin. (a) Total ion chromatography, (b) extracted ion chromatography, (c) enhanced mass spectrum of m/z 1399.6 (2+) acquired at 13.53 min, and (d) MS/MS spectrum of 1399.6 (2+) as a precursor.

Table 1: Observed N-glycopeptides derived enzymatic digestion of lacquer stellacyanin.

Glycosylation Site	Trypsin-derived glycopeptides		Chymotrypsin-derived glycopeptides		N-glycan	
	Peptide (mass)	Obs. m/z	Peptide (mass)	Obs. m/z	Mass	Composition[a]
Asn 28	WASNK (604.29)	888.12/2	ASNKTF (666.34)	919.19/2	1188.42	GlcNAc2 Hex3 Fuc1 Xyl1
		1070.85/2		1101.88/2	1553.56	GlcNAc3 Hex4 Fuc1 Xyl1
		1144.03/2		1175.03/2	1699.61	GlcNAc3 Hex4 Fuc2 Xyl1
		1326.56/2		1357.50/2	2064.75	GlcNAc4 Hex5 Fuc2 Xyl1
		1399.88/2		1430.63/2	2210.80	GlcNAc4 Hex5 Fuc3 Xyl1
Asn 60	NYQSCNDTTPIASYNGTBBR (2290.93)	1154.68/3	QSCNDTTPIASY (1356.57)	1264.51/2	1188.42	GlcNAc2 Hex3 Fuc1 Xyl1
		1276.85/3		nd[b]	1553.56	GlcNAc3 Hex4 Fuc1 Xyl1
		1324.24/3		1014.33/2	1699.61	GlcNAc3 Hex4 Fuc2 Xyl1
		1496.33/3		1184.74/3	2210.80	GlcNAc4 Hex5 Fuc3 Xyl1
Asn 102	VHINVTVR (936.55)	981.40/2	HINVTV (681.38)	nd	1042.37	GlcNAc2 Hex3 Xyl1
		703.41/3		926.74/2	1188.42	GlcNAc2 Hex3 Fuc1 Xyl1
		776.31/3		nd	1407.50	GlcNAc3 Hex4 Xyl1
		825.35/3		nd	1553.56	GlcNAc3 Hex4 Fuc1 Xyl1
		1237.38/2			1553.56	GlcNAc3 Hex4 Fuc1 Xyl1
		873.47/3		1182.87/2	1699.61	GlcNAc3 Hex4 Fuc2 Xyl1
		1310.40/2			1699.61	GlcNAc3 Hex4 Fuc2 Xyl1
		1044.45/3		1438.56/2	2210.80	GlcNAc4 Hex5 Fuc3 Xyl1

[a]Monosaccharides represented as GlcNAc, N-acetylglucosamine; Hex, mannose or galactose; Fuc, fucose; Xyl, xylose.
[b]nd: not detected.

Table 2: MALDI TOF MS assignment of the N-linked glycans from lacquer stellacyanin.

Peak number	Observed m/z[a]		Theoretical m/z[b]		N-linked glycan[c]
	PNGase A	PNGase F	N-glycan	aoWR-glycan	
1	2642.08	2641.60	2192.27	2640.48	(HexNAc)4 (Hex)5 (Fuc)3 Xyl
2	2495.98	2495.83	2046.74	2494.95	(HexNAc)4 (Hex)5 (Fuc)2 Xyl
3	—	2349.64	1900.50	2347.71	(HexNAc)4 (Hex)5 (Fuc) Xyl
4	2130.84	2130.08	1681.60	2129.81	(HexNAc)3 (Hex)4 (Fuc)2 Xyl
5	1984.78	1984.60	1535.55	1983.76	(HexNAc)2 (Hex)4 (Fuc) Xyl
6	1838.68	1838.63	1389.49	1837.70	(HexNAc)3 (Hex)4 Xyl
7	1619.5	—	1170.41	1618.62	(HexNAc)2 (Hex)3 (Fuc) Xyl

[a]MALDI TOF MS signal digested with PNGase A and PNGase F.
[b]Theoretical molecular weight of N-linked glycan.
[c]HexNAc: N-acetylglucosamine, Hex: mannose or glucose, Fuc: fucose, and Xyl: xylose.

From the observed molecular weight in Figure 2(c) and the MS/MS profile of the glycopeptides between 605.4 and 2286.7 [8], the N-linked glycan at Asn28 was characterized as (HexNAc)4(Hex)5(Fuc)3Xyl, a complex type glycan obtained from the product ion spectrum with doubly charged m/z = 1399.87. Other forms of the complex type glycans were observed in Asn28, as shown in Table 2.

The trypsin-derived N-glycopeptide NYQSCNDTTPI-ASYNTGBBR (m/z = 2291.7) bearing Asn60 was observed as a long peptide with only one GlcNAc residue attached to the peptide in the MS/MS spectrum as presented in Figure 3(a). However, when we used chymotrypsin for the digestion of lacquer stellacyanin, an N-linked glycan was obtained in an oligopeptide, QSCNDTTPIASY (m/z = 1356.5) by LC/MS/MS analysis as shown in Figure 3. As a result, the same N-linked glycan structure of $HexNAc_4Hex_5Fuc_3Xyl_1$ was also identified at Asn60. We also found that the same complex type glycan was connected at Asn102 by both trypsin and chymotrypsin digestions and subsequent LC/MS/MS analyses. These results are summarized in Table 1.

Trypsin-digested oligopeptides and oligoglycosyl peptides were also applied to MALDI TOF MS without any further purification. Signals between m/z = 700 and 4500 were observed from both trypsin-digested oligopeptides and oligoglycosyl peptides (data are shown in supporting information). The strongest signal appeared at m/z = 4487.4 due to the glycopeptides at Asn60 bearing a complex type N-linked glycan with the molecular weight of 2192. From the MALDI

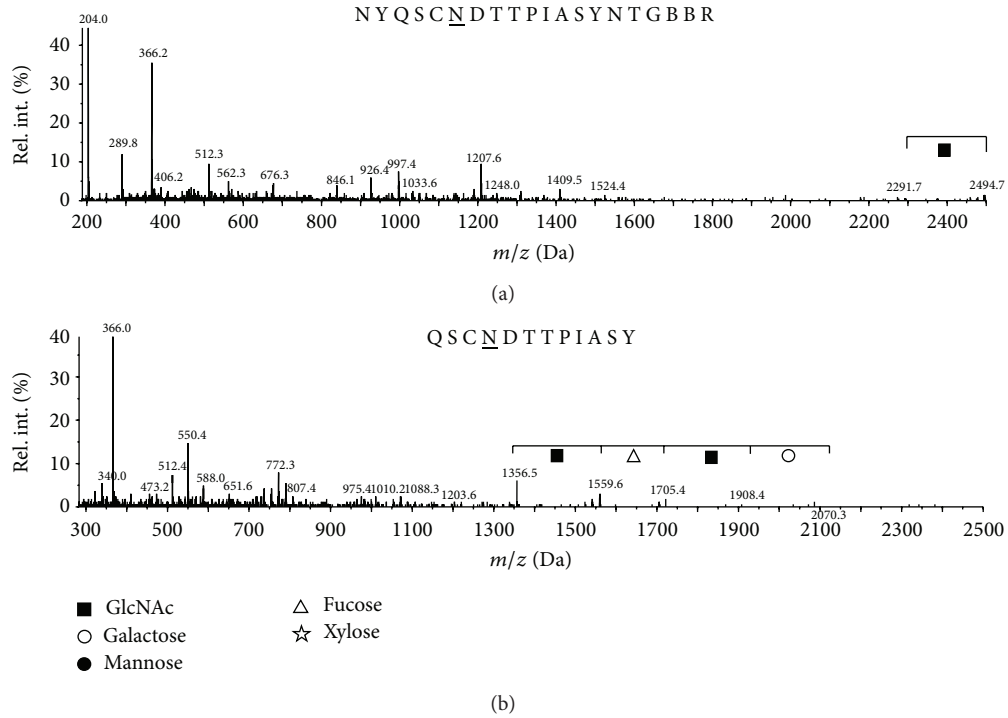

Figure 3: LC/MS/MS spectra of (a) trypsin- and (b) chymotrypsin-derived N-glycopeptide from lacquer stellacyanin. Observed mass numbers at m/z = 2291.7 (a) and m/z = 1356.5 (b) were due to oligopeptides, NYQSCNDTTPIASYNTGBBR and QSCNDTTPIASY at Asn60 site, respectively.

TOF MS analysis, the fucose and xylose-containing complex type biantennary glycan was linked at the three Asn sites in lacquer stellacyanin. Fucose and xylose should be attached to the GlcNAc next to Asn and at the central mannose residues, respectively.

3.3. MALDI TOF MS Analysis of N-Linked Glycans in Lacquer Stellacyanin. After isolation and purification of the lacquer stellacyanin, trypsin and chymotrypsin digestions were carried out, respectively, to give digested peptides and glycopeptides. Each product was further treated with PNGase A and PNGase F, respectively, to cleave N-linked glycans from Asn to afford N-linked glycans, which were labelled by using the BlotGlyco glycan purification and labeling kit to give the aoWR-labelled N-linked glycans. The aoWR-labelled N-linked glycans were mixed with the matrix (DHB) and then subjected to MALDI TOF MS to provide initial information on the relative quantities of N-linked glycans presented in lacquer stellacyanin. Figure 4 shows the MALDI TOF MS spectra of the aoWR-labelled N-linked glycans after (a) PNGase A and (b) PNGase F digestion of the lacquer stellacyanin. The observed mass numbers increased 447.21 due to the aoWR labelling reagent compared to the underived N-linked glycans. Although the signals appeared at the same m/z positions in Figures 4(a) and 4(b), the intensity was slightly different. These results suggest that the N-linked glycan in the lacquer stellacyanin has fucose at the glucosamine next to Asn because PNGase A releases N-linked glycans with and without α-1,3-fucosylated GlcNAc next to Asn and PNGase F cleaves N-linked glycans with α-1,6-fucosylated GlcNAc. Table 2 shows the structure of N-linked glycans based on the m/z in MALDI TOF MS spectra in Figure 4. The most intense peak (number 1) at the m/z of 2642 was assigned to a complex type N-linked glycan consisting of four glucosamines (HexNAc), five hexoses (Hex), three fucoses (Fuc), and one xylose (Xyl), that is, (HexNAc)4(Hex)5(Fuc)3Xyl (those that follow have the same description) [2], suggesting that the major oligosaccharide in lacquer stellacyanin was the complex type N-linked glycan. This type of N-linked glycan is the most common structure in plants, which has an α-1,3 linked fucosylated GlcNAc next to Asn, and a β-1,2 linked xylose should be attached to the central mannose residue [20]. Other signal peaks, numbers 2–7 in Figure 4, decreased the mass numbers from the m/z of 2642, indicating that one or more sugar residues were cleaved from the N-linked glycan (HexNAc)4(Hex)5(Fuc)3Xyl as illustrated in Figure 4. These results suggest that lacquer stellacyanin has the same complex type N-linked glycan in the three Asn sites.

In the MALDI TOF MS spectra of the lacquer stellacyanin treated and untreated with sialidase, the two spectra were identical. In addition, the signals at m/z = 292.1 due to NeuAc, m/z = 274 due to NeuAc-H_2O, and m/z = 657.1 due to Hex+HexNAc+NeuAc are diagnostic or marker ions originating from sialylated glycopeptides. However, none of these signals appeared in the LC/MS/MS spectra. These results suggest that the N-linked glycan in lacquer stellacyanin had no sialic acids.

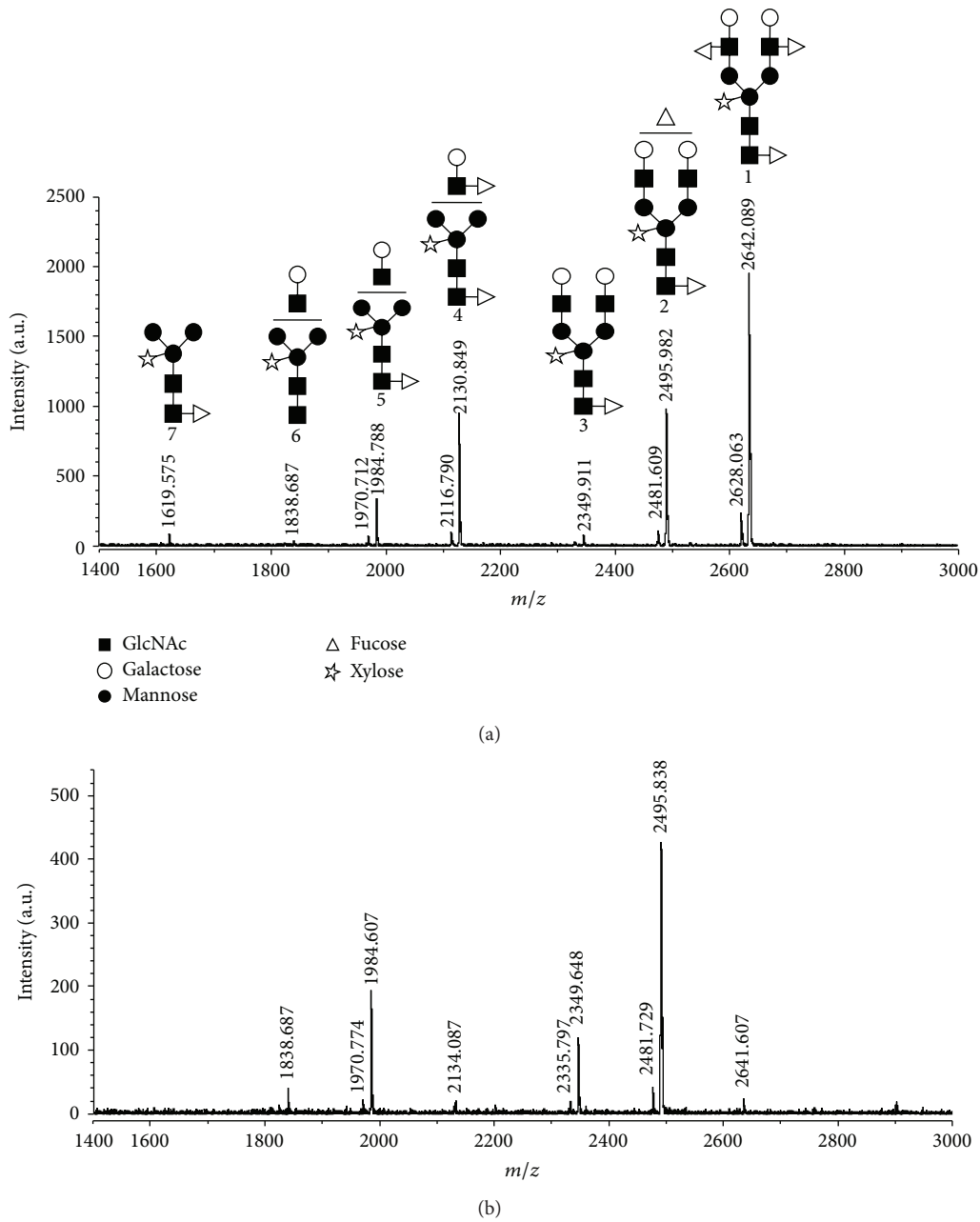

Figure 4: MALDI TOF MS profiles of aoWR-labelled N-linked glycans after (a) PNGase A and (b) PNGase F treatment of lacquer stellacyanin. N-glycan mass = [observed mass − 447.21 + 17].

4. Conclusion

By enzymatic digestions and a combination of MALDI TOF MS and LC/MS/MS analyses, we revealed the structures of the N-linked glycan and oligoglycopeptides at the three Asn residues (Asn28, Asn60, and Asn102) in lacquer stellacyanin, indicating that the N-linked glycan had the same structure at the three Asn sites and was a biantennary complex type N-linked glycan containing fucose at GlcNAc next to Asn and xylose at the central mannose residues. The complex type N-linked glycan confirmed in lacquer stellacyanin is the most common N-linked glycan in plants. No sialic acids were identified in the lacquer stellacyanin. This is the first report on the structural characterization of N-linked glycans in lacquer stellacyanin from *Rhus vernicifera*, a phytocyanin family of plant glycoproteins. Characterization of N-linked glycans in lacquer laccase is also under investigation.

Conflict of Interests

The authors declare that there is no conflict of interests regarding to the publication of this paper.

Acknowledgment

This research was partly supported by a Grant-in-Aid for Scientific Research from Japan Society for the Promotion of Science 2012–2014 (no. 24550129).

References

[1] J. Kumanotani, "Urushi (oriental lacquer)—a natural aesthetic durable and future-promising coating," *Progress in Organic Coatings*, vol. 26, no. 2–4, pp. 163–195, 1995.

[2] D. Keilin and T. Mann, "Carbonic anhydrase. Purification and nature of the enzyme," *Biochemistry*, vol. 34, pp. 1163–1176, 1940.

[3] T. Omura, "Studies on laccases of lacquer trees: IV purification and properties of a blue protein obtained from latex of *Rhus vernicifera*," *The Journal of Biochemistry*, vol. 50, no. 4, pp. 394–399, 1961.

[4] V. T. Aikazyan and R. M. Nalbandyan, "Copper-containing proteins from *Cucumis Sativus*," *FEBS Letters*, vol. 104, no. 1, pp. 127–130, 1979.

[5] A. Marchesini, M. Minelli, H. Merkle, and P. M. Kroneck, "Mavicyanin, a blue copper protein from *Cucurbita pepo medullosa*. Purification and characterization," *European Journal of Biochemistry*, vol. 101, no. 1, pp. 77–84, 1979.

[6] L. K. Sarkissian and R. M. Nalbandyan, "A novel copper-containing protein from spinach: a blue oxidase with unique properties," *Bioscience Reports*, vol. 3, no. 10, pp. 915–920, 1983.

[7] K.-G. Paul and T. Stigbrand, "Umecyanin, a novel intensely blue copper protein from horseradish root," *Biochimica et Biophysica Acta—Protein Structure*, vol. 221, no. 2, pp. 255–263, 1970.

[8] O. Ikeda and T. Sakurai, "Electron transfer reaction of stellacyanin at a bare glassy carbon electrode," *European Journal of Biochemistry*, vol. 219, no. 3, pp. 813–819, 1994.

[9] A. Ranieri, G. Battistuzzi, M. Borsari, C. A. Bortolotti, G. D. Rocco, and M. Sola, "PH and solvent H/D isotope effects on the thermodynamics and kinetics of electron transfer for electrode-immobilized native and urea-unfolded stellacyanin," *Langmuir*, vol. 28, no. 42, pp. 15087–15094, 2012.

[10] A. M. Nersissian, P. J. Hart, and J. S. Valentine, "Stellacyanin, a member of the phytocyaninfamily of plant proteins," *Encylopedia of Inorganic and Bioinorganic Chemistry*, pp. 1–17, 2011.

[11] G. H. H. Borner, K. S. Lilley, T. J. Stevens, and P. Dupree, "Identification of glycosylphosphatidylinositol-anchored proteins in Arabidopsis. A proteomic and genomic analysis," *Plant Physiology*, vol. 132, no. 2, pp. 568–577, 2003.

[12] W. Song, M. G. L. Henquet, R. A. Mentink et al., "*N*-glycoproteomics in plants: perspectives and challenges," *Journal of Proteomics*, vol. 74, no. 8, pp. 1463–1474, 2011.

[13] A. Ceriotti, M. Duranti, and R. Bollini, "Effects of N-glycosylation on the folding and structure of plant proteins," *Journal of Experimental Botany*, vol. 49, no. 324, pp. 1091–1103, 1998.

[14] H. Häweker, S. Rips, H. Koiwa et al., "Pattern recognition receptors require *N*-glycosylation to mediate plant immunity," *The Journal of Biological Chemistry*, vol. 285, no. 7, pp. 4629–4636, 2010.

[15] R. Strasser, "Biological significance of complex *N*-glycans in plants and their impact on plant physiology," *Frontiers in Plant Science*, vol. 5, article 363, 6 pages, 2014.

[16] J. Peisach, G. L. Walter, and W. E. Blumberg, "Structural properties of stellacyanin, a coppermucoprotein from *Rhus vernicifera*, the Japanese lac tree," *The Journal of Biological Chemistry*, vol. 242, no. 12, pp. 2847–2858, 1967.

[17] R. Lu and T. Yoshida, "Structure and molecular weight of Asian lacquer polysaccharides," *Carbohydrate Polymers*, vol. 54, no. 4, pp. 419–424, 2003.

[18] R. Lu, T. Yoshida, H. Nakashima et al., "Specific biological activities of Chinese lacquer polysaccharides," *Carbohydrate Polymers*, vol. 43, no. 1, pp. 47–54, 2000.

[19] Y. Bai and T. Yoshida, "Separation of lacquer polysaccharides and interaction with poly-l-lysine," *Carbohydrate Polymers*, vol. 98, no. 1, pp. 270–275, 2013.

[20] C. Rayon, P. Lerouge, and L. Faye, "The protein *N*-glycosylation in plants," *Journal of Experimental Botany*, vol. 49, no. 326, pp. 1463–1472, 1998.

[21] C. Bergman, E. K. Gandvik, P. O. Nyman, and L. Strid, "The amino acid sequence of stellacyanin from the lacquer tree," *Biochemical and Biophysical Research Communications*, vol. 77, no. 3, pp. 1052–1059, 1977.

[22] H. Geyer and R. Geyer, "Strategies for analysis of glycoprotein glycosylation," *Biochimica et Biophysica Acta—Proteins and Proteomics*, vol. 1764, no. 12, pp. 1853–1869, 2006.

[23] B. Reinhammar, "Purification and properties of laccase and stellacyanin from *Rhus vernicifera*," *Biochimica et Biophysica Acta*, vol. 205, no. 1, pp. 35–47, 1970.

[24] BlotGlycoR Glycan Purification and Labeling Kit BS-45603Z, Operation protocol, Sumitomo Bakelite Co Ltd.

Hindawi Publishing Corporation
International Journal of Polymer Science
Volume 2015, Article ID 843290, 6 pages
http://dx.doi.org/10.1155/2015/843290

Research Article

Preparation and Characterization of Urushiol Methylene Acetal Derivatives with Various Degrees of Unsaturation in Alkyl Side Chain

Chengzhang Wang,[1,2,3] Yuanfeng He,[1] Hao Zhou,[1,2,3] Ran Tao,[1,2] Hongxia Chen,[1,2,3] Jianzhong Ye,[1] and Yusi Zhang[1]

[1] *Institute of Chemical Industry of Forest Products, CAF, Nanjing 210042, China*
[2] *Key Lab of Biomass Energy and Material, Nanjing Jiangsu 210042, China*
[3] *Institute of New Technology of Forestry, CAF, Beijing 100091, China*

Correspondence should be addressed to Chengzhang Wang; wangczlhs@sina.com

Received 15 February 2015; Revised 16 April 2015; Accepted 16 April 2015

Academic Editor: Rong Lu

Preparation of urushiol derivatives was carried out in response to the drug industry's increasing demand for new synthetic anticancer agents. Urushiol methylene acetal derivatives were synthesized in high yields by reaction of urushiol with methylene chloride under the catalytic action of NaOH. Four kinds of urushiol methylene acetal monomers were separated by silica-gel column and preparative HPLC, and their structures were elucidated by extensive spectroscopic methods, including 1D-NMR and 2D-NMR (^{1}H, ^{13}C-NMR, ^{1}H-^{1}HCOSY, HSQC, and HMBC) as well as TOF-MS. They were identified as 3-[pentadecyl] benzene methylene ether (compound 1), 3-[8′-pentadecatrienyl] benzene methylene ether (compound 2), 3-[8′,11′-pentadecatrienyl] benzene methylene ether (compound 3), and 3-[8′,11′,14′-pentadecatrienyl] benzene methylene ether (compound 4). This research provides a theoretical reference for exploration of these interesting and potentially bioactive compounds.

1. Introduction

Urushiols are major components of the sap of the lacquer tree (*Rhus verniciflua* Stokes, Anacardiaceae) that is widely cultivated in northeastern Asian countries including China, Korea, and Japan [1]. Urushiol is a typical phenolic compound which consists of o-dihydroxybenzene (catechol) coupled with a saturated or unsaturated alkyl side chain of 15 or 17 carbons and is an amphipathic compound [2]. Urushiol has been used as a traditional folk medicine in China and has antioxidant, antimicrobial, and anticancer activities [3]. However, urushiol can cause hypersensitive reaction, and it is sensitive to oxidation and polymerization, which reduce its activities [4]. As a result, the usefulness of urushiol as a potential therapeutic agent has been limited. Therefore, nonallergenic urushiol derivatives may be useful as bioactive compounds in the human body. It is thought that the phenolic hydroxyl group of urushiol is the main cause of allergic reaction and polymerization [5]. Synthesis of the urushiol ester and silyl derivatives has been reported and their anticancer activities have been demonstrated [6, 7]. Recently, studies showed that acetal derivatives of phenolic compounds also have prominent antioxidant, antimicrobial, and anticancer activities, and the acetal-type groups have the advantages of including simultaneous protection of two hydroxyls and easy removal of a partial deprotection [8, 9], but, till now, there has been no report about the preparation of acetal derivatives of urushiol and its monomers.

In view of the research status of urushiol and the great potential of urushiol as a potent material in new drug research and development, our study was aimed at synthesizing urushiol methylene acetal derivatives, separating urushiol methylene acetal monomers of various unsaturated degrees, and characterizing their structures. The urushiol methylene acetal derivatives were obtained by linking methylene acetal chains to the two adjacent hydroxide groups of urushiol,

and urushiol methylene acetal monomers of 0–3 degrees of unsaturation were separated by silica-gel column and preparative high performance liquid chromatography. The structures of the urushiol methylene acetal monomers with 0–3 degrees of unsaturation were elucidated by extensive spectroscopic methods, including 1D-NMR and 2D-NMR (^{1}H, ^{13}C-NMR, ^{1}H-^{1}HCOSY, HSQC, and HMBC) as well as TOF-MS and chemical analysis. Our studies provide potentially important information for further development of new urushiol derivatives and provide new leading compounds for the research on clinical drugs.

2. Experiments

2.1. General Experimental Procedures. IR spectra were measured on a Horiba FT-710 spectrophotometer. NMR spectra were recorded at 303 K on a Bruker AV-500 NMR (^{1}H NMR, 500 MHz; ^{13}C NMR, 125 MHz) instrument with TMS in $CDCl_3$ as the internal standard. The 2D-NMR, HSQC, HMBC, and ^{1}H-^{1}H COSY experiments were performed using standard Bruker pulse sequences. The TOF-MS experiment was performed on an Agilent orthogonal TOF-MS system equipped with an ESI source. The GC-MS system consisted of an Agilent 6890 N gas chromatograph and an Agilent 5973 N mass spectrometer. Column chromatography was performed on silica gel (100–200 μm, Qingdao Marine Chemical Co., Ltd., China). Preparative HPLC was performed using a Shimadzu LC-20A instrument. Thin-layer chromatography (TLC) was performed on precoated silica gel GF254 plates (Qingdao Marine Chemical Co.).

2.2. Materials. Urushiol was obtained by extraction of the sap of a Chinese lacquer tree with acetone and removal of the solvent with vacuum concentration. All solvents and reagents were purchased from Nanjing Jitian Chemical Reagents Company (Nanjing, China) and were of analytical grade.

2.3. Synthesis of Urushiol Methylene Acetal Derivatives. This compound was prepared by a modified procedure based on the method of Werschkun and Thiem [10]. A 2 L, 4-neck round bottom flask (equipped with an N_2 inlet, overhead magnetic stir drive, addition funnel, thermocoupler, and condenser) was filled with 100 mL CH_2Cl_2 and 300 mL DMSO, heated to 110°C, and refluxed for 0.5 h; then, 100 g urushiol in 500 mL DMSO via one addition funnel and NaOH (40 g) in 100 mL water via another addition funnel were simultaneously added to the flask over 1 hour. The temperature was kept at 110°C for 3 h; after completion of the reaction, the mixture was diluted with water and stirred for 30 min at room temperature. It was then extracted with petroleum ether (3 × 1 L), and the combined petroleum ether layer was washed with water (3 × 500 mL), dried with anhydrous Na_2SO_4, and concentrated in a rotary evaporator to give the crude urushiol methylene acetal derivatives.

2.4. Separation of Urushiol Methylene Acetal Monomers. Crude urushiol methylene acetal derivatives (60 g) were subjected to silica gel column chromatography (diameter 60 mm × length 800 mm) and eluted with a stepwise gradient mixture of EtOAc-Pet. ether (1 : 99; 2 : 98; 3 : 97; 5 : 95; 6 : 94; 8 : 92; 10 : 90). Fractions of 100 mL each were collected and controlled by TLC examination, and fractions with similar R_f values were combined, yielding three major fractions (A–C). Fraction A (15 g) was subjected to preparative HPLC (Hypersil ODS-2, 250 × 10 mm i.d., CH_3CN–H_2O (95 : 5, v/v), 4 mL/min) to afford compounds 1, 2, 3, and 4.

Table 1: ^{13}C NMR spectral data of compounds 1, 2, 3, and 4 in pyridine-d_5 (δ ppm).

Carbon	1	2	3	4
1	146.5	146.9	146.8	146.9
2	145.3	145.4	145.5	145.4
3	124.4	129.5	129.4	129.4
4	122.5	124.4	124.5	124.5
5	121.2	122.2	122.5	122.2
6	116.2	116.5	116.2	116.5
1′	29.7	29.8	29.7	29.8
2′	29.6	29.7	29.6	29.7
3′	29.6	29.6	29.6	29.6
4′	29.6	29.5	29.6	29.6
5′	29.5	29.5	29.5	29.5
6′	29.4	29.4	29.4	29.4
7′	29.3	27.4	27.3	27.3
8′	29.3	130.2	130.4	130.5
9′	29.3	130.4	128.6	127.7
10′	29.4	27.6	26.4	25.8
11′	29.3	29.3	128.5	127.5
12′	29.5	29.5	130.6	129.8
13′	31.9	31.9	27.9	26.7
14′	22.6	22.6	22.6	114.8
15′	14.1	14.1	13.9	136.9
-O-CH_2-O-	76.5	77.0	77.2	77.4

2.5. Compound 1 (3-[Pentadecyl] Benzene Methylene Ether). Compound 1 is a colorless oil: IR (KBr) γmax (cm^{-1}): 1640, 1052; ^{1}H (500 MHz, DMSO-d6) and ^{13}C NMR (125 MHz, DMSO-d6) (see Tables 1 and 2); TOF-MS (*m/z*): 331 [M–H]$^-$, 135[M–$C_{14}H_{29}$], 105[M–$C_{15}H_{31}$–CH_2–2H], and 77[M–$C_{15}H_{31}$–CH_2O_2 + 2H] (calculated for $C_{22}H_{36}O_2$, 332).

2.6. Compound 2 (3-[8′-Pentadecatrienyl] Benzene Methylene Ether). Compound 2 is a colorless oil: IR (KBr) γmax (cm^{-1}): 1640, 1598, and 1052; ^{1}H (500 MHz, DMSO-d6) and ^{13}C NMR (125 MHz, DMSO-d6) (see Tables 1 and 2); TOF-MS (*m/z*): 329 [M–H]$^-$, 148[M–H–$C_{13}H_{25}$], 135[M–$C_{14}H_{27}$], 105[M–$C_{15}H_{29}$–CH_2–2H], 91[M–$C_{15}H_{29}$–CH_2–O], and 77[M–$C_{15}H_{29}$–CH_2O_2 + 2H] (calculated for $C_{22}H_{34}O_2$, 330).

2.7. Compound 3 (3-[8′,11′-Pentadecatrienyl] Benzene Methylene Ether). Compound 3 is a colorless oil: IR (KBr) γmax (cm^{-1}): 1630, 1598, and 1052; ^{1}H (500 MHz, DMSO-d6) and

Table 2: ^{1}H NMR spectral data of compounds 1, 2, 3, and 4 in pyridine-d5 (δ in ppm, J in H_Z).

Carbon	1	2	3	4
1				
2				
3				
4	6.72(m)	6.77(m)	6.79(m)	6.79(m)
5	6.68(m)	6.69(m)	6.70(m)	6.71(m)
6	7.25(s)	7.27(s)	7.28(s)	7.27(s)
1′	2.56(t, J = 7.50)	2.61(t, J = 7.50)	2.59(t, J = 7.50)	2.61(t, J = 7.50)
2′	1.60(m)	2.61(m)	1.63(m)	1.77(m)
3′	1.58(m)	2.58(m)	1.60(m)	1.74(m)
4′	1.58(m)	2.58(m)	1.53(m)	1.33(m)
5′	1.58(m)	2.55(m)	1.48(m)	1.60(m)
6′	1.58(m)	2.55(m)	1.46(m)	1.65(m)
7′	1.30(m)	2.55(m)	2.56(m)	2.09(m)
8′	1.30(m)	5.38(t, J = 3.5)	5.44(t, J = 4.5)	5.68(t, J = 4.0)
9′	1.25(m)	5.35(t, J = 4.0)	5.39(t, J = 4.0)	5.65(t, J = 4.0)
10′	1.25(m)	2.04(m)	2.81(m)	2.89(m)
11′	1.25(m)	1.65(m)	5.37(t, J = 5.0)	5.48(t, J = 3.5)
12′	1.25(m)	1.63(m)	5.34(t, J = 4.5)	5.46(t, J = 4.0)
13′	1.25(m)	1.33(m)	2.06(m)	2.84(m)
14′	1.25(m)	1.31(m)	1.41(m)	5.42(m)
15′	0.87(t, J = 6.3)	0.92(t, J = 6.3)	0.95(t, J = 6.3)	5.39(d, J = 5.0)
-O-CH_2-O-	5.92(s)	5.94(s)	5.94(s)	5.99(s)

^{13}C NMR (125 MHz, DMSO-d6) (see Tables 1 and 2); TOF-MS (m/z): 327 $[M–H]^-$, 175$[M–C_{11}H_{19}–2H]$, 161$[M–C_{12}H_{21}–2H]$, 148$[M–H–C_{13}H_{23}]$, 135$[M–C_{14}H_{25}]$, 91$[M–C_{15}H_{27}–CH_2–O]$, and 77$[M–C_{15}H_{27}–CH_2O_2 + 2H]$ (calculated for $C_{22}H_{32}O_2$, 328).

2.8. Compound 4 (3-[8′,11′,14′-Pentadecatrienyl] Benzene Methylene Ether). Compound 4 is a colorless oil: IR (KBr) γmax (cm^{-1}): 1630, 1598, and 1052; ^{1}H (500 MHz, DMSO-d6) and ^{13}C NMR (125 MHz, DMSO-d6) (see Tables 1 and 2); TOF-MS (m/z): 325 $[M–H]^-$, 135$[M–C_{14}H_{23}]$, 105$[M–C_{15}H_{25}–O]$, 91$[M–C_{15}H_{25}–CH_2–O]$, and 79$[M–C_{15}H_{25}–CH_2O_2 + 4H]$ (calculated for $C_{22}H_{30}O_2$, 326).

3. Result and Discussion

3.1. Synthesis of Urushiol Methylene Acetal Derivatives. Catechol methylene acetal is an important pharmaceutical intermediate that is vital for the synthesis of quinolones; it is traditionally synthesized through a nucleophilic substitution reaction of catechol with methylene chloride under the catalytic action of NaOH [11]. Urushiol is a typical phenolic compound possessing a catechol structure and an alkyl side chain of 15 or 17 carbons [12]; it has two adjacent phenolic hydroxyl groups on the benzene ring, so a practical method for preparation of catechol methylene acetal is desirable for natural product synthesis and process chemistry of urushiol. It is well known that the phenolic hydroxyl groups of urushiol can cause skin problems and is easy to oxidate [13], so it is necessary to modify and protect the phenolic hydroxyl groups of urushiol. Because acetal-type protecting groups possess significant advantages, such as simultaneous protection of two hydroxyls, easy removal, and the possibility of a partial deprotection [14], the preparation of urushiol methylene acetal can not only increase the stability but also preserve the original biological activity of urushiol.

Conversion of urushiol to the urushiol methylene acetal consists of three steps, and the reaction mechanism is shown in Figure 1. First, the two adjacent phenolic hydroxyl groups of urushiol lose two hydrogen ions in the presence of NaOH, resulting in formation of catechol anions; secondly, catechol anions react with methylene chloride by bimolecular nucleophilic substitution with NaOH being the base to give the intermediate product of catechol methyl chloromethyl ether anions; finally, the intramolecular substitution reaction of the intermediate product gives the final product of urushiol methylene acetal.

To obtain the best yields of urushiol methylene acetal, the reaction conditions including reaction time and reaction temperature were optimized; the results showed that the best reaction time is 2-3 h, the best reaction temperature is 105–115°C, and the yield of urushiol methylene acetal can reach over 80%. In addition, during the reaction process, some urushiols may oxidize and polymerize, leading to the destruction of the catechol structure, thus the reaction of polymerized urushiols will not give the product of urushiol methylene acetal, but produce by-products possessing an alcohol structure. It was reported that the yields of by-products could be reduced by preventing increases in the concentration of catechol anions by adding NaOH gradually

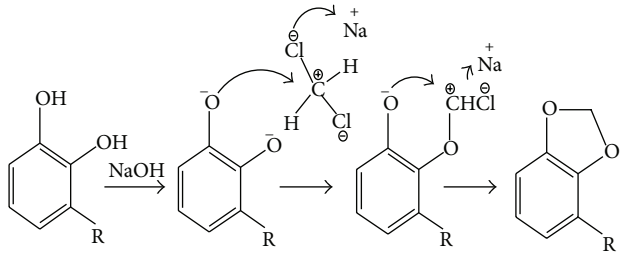

Figure 1: Aldolization mechanism of synthesis of urushiol methylene acetal.

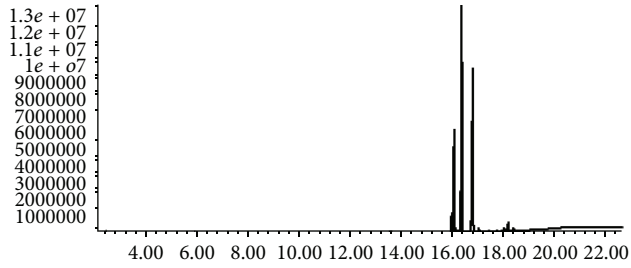

Figure 2: Total ion chromatography of urushiol methylene acetal by GC-MS.

and using enough DMSO solvent [15]. Furthermore, because the reaction products are composed of a water phase (NaOH solution) and an organic phase (DMSO, methylene chloride, urushiol methylene acetal, and by-products), in view of the low polarity of urushiol methylene acetal, petroleum ether was selected to extract urushiol methylene acetal from the reaction products.

After the reaction and extraction of petroleum ether, the chemical structures and yield of crude urushiol methylene acetal were determined from the IR spectrum and HPLC. The IR spectrum showed the characteristic peak of ether bonding groups at 1100 cm^{-1}, and the hydroxyl groups of urushiol at 3431 cm^{-1} disappeared, which indicates that the hydroxyl groups were all converted to ether-bonding groups by the reaction. The results of HPLC analysis indicate that the yield of urushiol methylene acetal was 83.5%.

3.2. Separation of Urushiol Methylene Acetal Monomers. The crude urushiol methylene acetal obtained was further purified by silica gel column chromatography and preparative HPLC to obtain urushiol methylene acetal monomers. First, crude urushiol methylene acetal was subjected to silica gel column chromatography and eluted by a gradient of EtOAc and Pet. Ether, yielding three major fractions (A–C) according to the TLC examination. The results of TLC analysis showed that the R_f value of fraction A is 0.5, which is similar to that of urushiol, and the R_f values of fractions B and C were 0.8–0.95, which indicated that fractions B and C had greater polarity than fraction A. It was judged that fractions B and C consisted of by-products of the reaction and polymers of urushiol. When fraction A was analyzed by GC-MS (Figure 2), the GC-MS chromatogram revealed four major peaks, whose *m/z* were 332, 330, 328, and 326, respectively.

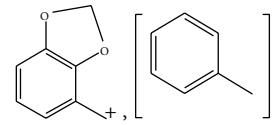

Figure 3: Fragment of urushiol methylene acetal under EI.

Meanwhile, the mother nucleus fragment at 135 *m/z* was found in all four major peaks through analysis of fragment ions from samples. It was deduced that the mother nucleus fragment of 135 *m/z* was produced by splitting of urushiol methylene acetal, and its structure is shown in Figure 3. Based on the GC-MS analysis, fraction A was demonstrated to be purified total urushiol methylene acetal. Finally, fraction A was separated by preparative HPLC affording four kinds of urushiol methylene acetal monomers: compound 1 (0.86 g), compound 2 (1.03 g), compound 3 (1.17 g), and compound 4 (0.92 g).

3.3. Characterization of Urushiol Methylene Acetal Monomers. The compounds' structures were elucidated mainly by 500-MHz NMR analysis, including 1D-NMR and 2D-NMR (^{1}H, ^{13}C-NMR, ^{1}H-^{1}HCOSY, HSQC, HMBC, and ROESY), and TOF-MS, and by comparison with literature data [16, 17].

Compound 1 was assigned a molecular formula of $C_{22}H_{36}O_2$, as deduced from the $[M–H]^-$ ion at *m/z* 331 in negative ion mode TOF-MS. Its IR spectrum exhibited strong absorption bands at 1640 and 1052 cm^{-1} due to a benzene ring and ether functional groups. The ^{1}H NMR spectrum of compound 1 showed signals indicative of three protons on a benzene ring at δH 6.72, 6.68, and 7.25 (H-4, H-5, and H-6) and an alkyl group at δH 0.87–1.60 (H-1′–15′). These signals are characteristic of 1,2-dihydroxy-3-alkyl-benzene, strongly suggesting that compound 1 is an urushiol-type compound. The characteristic NMR signals for a methylene acetal group were observed in the ^{1}H NMR spectrum of 1, with a singlet of two methylene protons at δ_H 5.92. The existence of the HMBC correlation between H-1′ (δ_H 2.56), C-2 (δC 145.3), and C-4 (δC 122.5) confirmed that C-1′ of the alkyl group bonded at C-3 of a benzene ring. The molecular formula and ^{1}H and ^{13}C NMR spectra indicated that the alkyl group contained 15 carbons. Based on the above-discussed results and comparison of spectral data with the literature, the structure of compound 1 was identified as 3-[pentadecyl] benzene methyl.

Compound 2 was assigned a molecular formula of $C_{22}H_{34}O_2$, as deduced from the $[M–H]^-$ ion at *m/z* 329 in negative ion mode TOF-MS. Its IR spectrum exhibited strong absorption bands at 1640, 1598, and 1052 cm^{-1} due to a benzene ring, olefinic, and ether functional groups. The ^{1}H and ^{13}C NMR spectra of compound 2 were similar to those of 1 (Table 1), indicating that compound 2 was also an urushiol-type compound. The IR, molecular formula, and ^{1}H and ^{13}C NMR spectra indicated that the alkyl group of compound 2 had one double bond. The position of the double bond in the alkyl group was determined by the H–H COSY, HSQC, and HMBC spectra. In the HSQC spectrum,

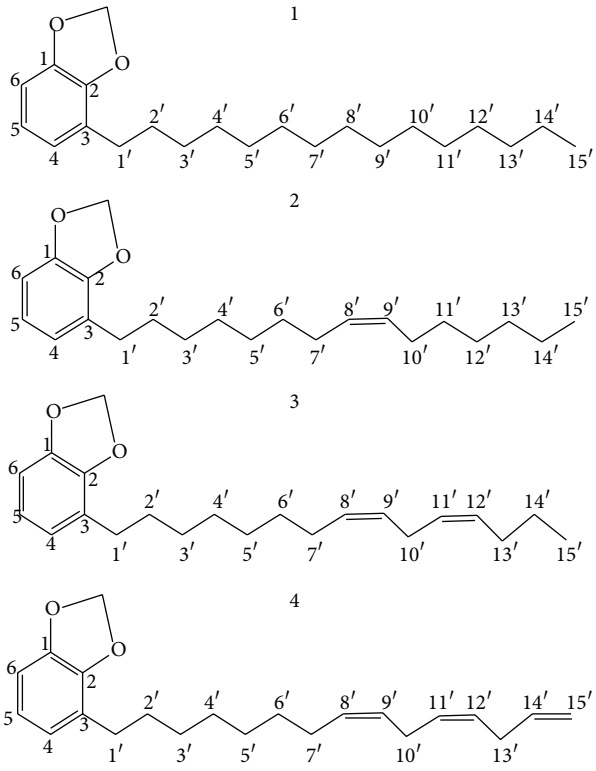

Figure 4: Structures of urushiol methylene acetal monomers (compounds 1, 2, 3, and 4).

the methyl proton (H-15′) signal of a triplet at δ_H 0.92 correlated with the ^{13}C signal at δ_C 14.1, showing that the ^{13}C signal was assigned to C-15′. The cross-peak between C-15′ signal at δ_C 14.1 and proton signal at δ_H 1.33 observed in the HMBC spectrum assigned the proton signal to H-13′. The H-13′ signal at δ_H 1.33 had a cross-peak with the ^{13}C signal at δ_C 29.3, indicating that the ^{13}C signal was C-11′. The H-11′ signal at δ_H 1.65 which correlated with the ^{13}C signal at δ_C 29.3 from the HSQC spectrum showed a cross-peak with the ^{13}C signal δ_C 130.4, in the HMBC spectrum, so the ^{13}C signal was assigned to C-9′, indicating that the double bond was located at C-9′–C-8′. In the HMBC spectrum, C-9′ showed a cross-peak with the proton signal at δ_H 2.55 assignable to H-7′ adjacent to a double bond at C-8′, and C-8′ showed a cross-peak with the proton signal at δ_H 2.04 assignable to H-10′ adjacent to a double bond at C-9′.

Based on the above-discussed results, the structure of compound 2 was identified to be 3-[8′-pentadecatrienyl] benzene methylene ether (see Figure 4).

Compound 3 was assigned the molecular formula of $C_{22}H_{32}O_2$, as deduced from the [M–H]- ion at *m/z* 327 in negative ion mode TOF-MS. Its IR spectrum exhibited strong absorption bands at 1630, 1598, and 1052 cm^{-1} due to benzene ring, olefinic, and ether functional groups. The ^{1}H and ^{13}C NMR spectra of compound 3 were similar to those of 1 (Table 1), indicating that compound 3 was also an urushiol-type compound. The IR, molecular formula, and ^{1}H and ^{13}C NMR spectra indicated that the alkyl group of compound 3 had two double bonds. The position of the double bond in the alkyl group was determined by the H–H COSY, HSQC, and HMBC spectra. In the HSQC spectrum, the methyl proton (H-15′) signal of a triplet at δ_H 0.95 correlated with the ^{13}C signal at δ_C 13.9, showing that the ^{13}C signal was assignable to C-15′. The H-15′ signal at δ_H 0.95 was coupled with the proton signal at δ_H 1.41 in the H–H COSY spectrum assignable to H-14′; furthermore, the H-14′ signal at δ_H 1.41 coupled with the proton signal at δ_H 2.06 was assignable to protons adjacent to a double bond, and these signal relationships indicated that a double bond was located at C-12′–C-11′. The H-13′ signal at δ_H 2.06 had a cross peak with the ^{13}C signal at δ_C 128.5, indicating that the ^{13}C signal was C-11′. The H-11′ signal at δ_H 5.37 which correlated with the ^{13}C signal at δ_C 128.5 from the HSQC spectrum showed a cross-peak with the ^{13}C signal δ_C 128.6 in the HMBC spectrum, so the ^{13}C signal was assigned to C-9′; this indicated that the second double bond was located at C-9′–C-8′. In the HMBC spectrum, C-9′ showed a cross-peak with the proton signal at δ_H 2.56 assignable to H-7′ adjacent to a double bond at C-8′, and C-8′ showed a cross-peak with the proton signal at δ_H 2.81 assignable to H-10′ adjacent to a double bond at C-9′. Based on the above-discussed results, the structure of compound 3 was identified to be 3-[8′,11′-pentadecatrienyl] benzene methylene ether (see Figure 4).

Compound 4 was assigned a molecular formula of $C_{22}H_{30}O_2$, as deduced from the [M–H]- ion at *m/z* 325 in negative ion mode TOF-MS. Its IR spectrum exhibited strong absorption bands at 1630, 1598, and 1052 cm^{-1} due to benzene ring, olefinic, and ether functional groups. The ^{1}H and ^{13}C NMR spectra of compound 4 were similar to those of 1 (Table 1) indicating that compound 4 was also an urushiol-type compound. The IR, molecular formula, and ^{1}H and ^{13}C NMR spectra indicated that the alkyl group of compound 4 had three double bonds. The position of the double bonds in the alkyl group was determined by the H–H COSY, HSQC, and HMBC spectra. The proton signal of a doublet at δ_H 5.39 which correlated with the ^{13}C signal at δ_C 136.9 from the HSQC spectrum showed a cross-peak with the proton signal at δ_H 5.42 in the H–H COSY spectrum, which indicated that one double bond was located at C-15′–C-14′. In the HMBC spectrum, C-15′ also showed a cross-peak with the proton signal at δ_H 2.84 assignable to H-13′ adjacent to a double bond at C-14′. The H-14′ signal at δ_H 5.42 which correlated with the ^{13}C signal at δ_C 114.8 from the HSQC spectrum had a cross-peak with the ^{13}C signal at δ_C 129.8, indicating that the ^{13}C signal was C-12′ and that the second double bond was located at C-12′–C-11′. In the HMBC spectrum, C-12′ also showed a cross-peak with the proton signal at δ_H 2.89 assignable to H-10′ adjacent to a double bond at C-11′. The cross-peak between proton signal at δ_H 5.46 assigned to H-12′ from the HSQC spectrum and proton signal at δ_H 5.48 observed in the H–H COSY spectrum assigned the proton signal to H-11′. The H-11′ signal at δ_H 5.48 showed a cross-peak with the ^{13}C signal δ_C 127.7, in the HMBC spectrum, so the ^{13}C signal was assigned to C-9′. This indicated that the third double bond was located at C-9′–C-8′. In the HMBC spectrum, C-9′

also showed a cross-peak with the proton signal at δ_H 2.09 assignable to H-7′ adjacent to a double bond at C-8′. Based on the above-discussed results, the structure of compound 4 was identified to be 3-[8′,11′,14′-pentadecatrienyl] benzene methylene ether (see Figure 4).

4. Conclusions

We synthesized novel urushiol methylene acetal derivatives and separated four kinds of urushiol methylene acetal monomers which possess 0, 1, 2, and 3 double bonds in the alkyl side chain. This study produced valuable leading compounds to help further the design and development of more potent anticancer agents. In addition, further studies on the structure-anticancer activity relationship of urushiol methylene acetal derivatives will be carried out.

Conflict of Interests

The authors declare that there is no conflict of interests regarding the publication of this paper.

Acknowledgment

This project was supported by the National Special Project of International Technology Cooperation (no. 2014DFR31300).

References

[1] K. T. Suk, S. K. Baik, H. S. Kim et al., "Antibacterial effects of the urushiol component in the sap of the lacquer tree (*Rhus verniciflua* stokes) on *Helicobacter pylori*," *Helicobacter*, vol. 16, no. 6, pp. 434–443, 2011.

[2] V. S. Byers, N. Castagnoli Jr., and W. L. Epstein, "In vitro studies of poison oak immunity. II. Effect of urushiol analogues on the human in vitro response," *Journal of Clinical Investigation*, vol. 64, no. 5, pp. 1449–1456, 1979.

[3] J.-Y. Choi, C.-S. Park, J. Choi, H. Rhim, and H. J. Chun, "Cytotoxic effect of urushiol on human ovarian cancer cells," *Journal of Microbiology and Biotechnology*, vol. 11, no. 3, pp. 399–405, 2001.

[4] X.-M. Ma, R. Lu, and T. Miyakoshi, "Recent advances in research on lacquer allergy," *Allergology International*, vol. 61, no. 1, pp. 45–50, 2012.

[5] Z. Xia, T. Miyakoshi, and T. Yoshida, "Lipoxygenase-catalyzed polymerization of phenolic lipids suggests a new mechanism for allergic contact dermatitis induced by urushiol and its analogs," *Biochemical and Biophysical Research Communications*, vol. 315, no. 3, pp. 704–709, 2004.

[6] J. C. Murphy, E. S. Watson, and E. C. Harland, "Toxicology evaluation of poison oak urushiol and its esterified derivative," *Toxicology*, vol. 26, no. 2, pp. 135–142, 1983.

[7] P. D. Adawadkar and M. A. ElSohly, "An urushiol derivative from poison sumac," *Phytochemistry*, vol. 22, no. 5, pp. 1280–1281, 1983.

[8] Z. Jakab, A. Mándi, A. Borbás et al., "Synthesis, regioselective hydrogenolysis, partial hydrogenation, and conformational study of dioxane and dioxolane-type (9′-anthracenyl)methylene acetals of sugars," *Carbohydrate Research*, vol. 344, no. 18, pp. 2444–2453, 2009.

[9] F. C. Bove and V. B. Haarstad, "Pharmacological activities of acetal derivatives of hemicholinium No. 3," *European Journal of Pharmacology*, vol. 57, no. 2-3, pp. 149–163, 1979.

[10] B. Werschkun and J. Thiem, "Synthesis of novel types of divalent saccharide structures by a ketene acetal Claisen rearrangement," *Tetrahedron Asymmetry*, vol. 16, no. 2, pp. 569–576, 2005.

[11] K. Takai, Y. Nawate, T. Okabayashi, H. Nakatsuji, A. Iida, and Y. Tanabe, "Practical and robust method for stereoselective preparations of ketene silyl (thio)acetal derivatives and NaOH-catalyzed crossed-Claisen condensation between ketene silyl acetals and methyl esters," *Tetrahedron*, vol. 65, no. 28, pp. 5596–5607, 2009.

[12] D. Kim, S. L. Jeon, and J. Seo, "The preparation and characterization of urushiol powders (YPUOH) based on urushiol," *Progress in Organic Coatings*, vol. 76, no. 10, pp. 1465–1470, 2013.

[13] J. Y. Kim, J.-Y. Cho, Y. K. Ma, Y. G. Lee, and J.-H. Moon, "Nonallergenic urushiol derivatives inhibit the oxidation of unilamellar vesicles and of rat plasma induced by various radical generators," *Free Radical Biology and Medicine*, vol. 71, pp. 379–389, 2014.

[14] U. Ellervik, "9-Anthraldehyde acetals as protecting groups," *Tetrahedron Letters*, vol. 44, no. 11, pp. 2279–2281, 2003.

[15] P. J. L. M. Quaedflieg, C. M. Timmers, V. E. Kal, G. A. van der Marel, E. Kuyl-Yeheskiely, and J. H. van Boom, "An alternative approach towards the synthesis of (3′→5′) methylene acetal linked dinucleosides," *Tetrahedron Letters*, vol. 33, no. 21, pp. 3081–3084, 1992.

[16] M. A. ElSohly, P. D. Adawadkar, C.-Y. Ma, and C. E. Turner, "Separation and characterization of poison ivy and poison oak urushiol components," *Journal of Natural Products*, vol. 45, no. 5, pp. 532–538, 1982.

[17] K. Kadokura, K. Suruga, T. Tomita et al., "Novel urushiols with human immunodeficiency virus type 1 reverse transcriptase inhibitory activity from the leaves of *Rhus verniciflua*," *Journal of Natural Medicines*, vol. 69, no. 1, pp. 148–153, 2015.

Hindawi Publishing Corporation
International Journal of Polymer Science
Volume 2015, Article ID 725467, 11 pages
http://dx.doi.org/10.1155/2015/725467

Research Article

Simultaneous Organic and Inorganic Analysis of Colored Oriental Lacquerware by Pyrolysis-Gas Chromatography/Mass Spectrometry

Yoshimi Kamiya,[1] Takayuki Honda,[2] Atsushi Ohbuchi,[3] and Tetsuo Miyakoshi[2]

[1] *Tokyo Metropolitan Industrial Technology Research Institute, Tama Techno Plaza, Textile and Chemical Technology Group, Department of Materials Chemistry Application, 3-6-1 Azuma-cho, Akishima-shi, Tokyo 196-0033, Japan*
[2] *Department of Applied Chemistry, Meiji University, 1-1-1 Higashi-Mita, Tama-ku, Kawasaki-shi, Kanagawa 214-8571, Japan*
[3] *Rigaku Corporation, X-Ray Research Laboratory, Application Laboratories, XRD Analysis Group, 3-9-12 Matsubara-cho, Akishima-shi, Tokyo 196-8666, Japan*

Correspondence should be addressed to Yoshimi Kamiya; kamiya.yoshimi@iri-tokyo.jp

Received 10 February 2015; Accepted 7 May 2015

Academic Editor: Michael Schilling

Organic analysis and inorganic analysis are generally based on different physical principles, and for this reason it is difficult to analyze resins and pigments simultaneously. For these reasons, we have performed Py-GC/MS measurements of red-, yellow-, and green-colored lacquer films applied to lacquerware items to assess the feasibility of simultaneously detecting resin ingredients together with certain pigments. We have also compared our findings to the results of SEM-EDS, X-ray fluorescence spectrometry (XRF), and X-ray diffractometry (XRD) measurements. XRD analysis yielded molecular-level information (information on binding states) regarding mercury (Hg) and iron (Fe); however, the information obtained for arsenic (As) and sulfur (S) was insufficient. In contrast, Py-GC/MS analyses simultaneously yielded molecular-level information on arsenic (As) and sulfur (S) together with detection of the primary ingredients of the lacquer. For this reason, it shows that several pieces of information is provided easily and quickly when the colored lacquer cultural heritage is measured using the Py-GC/MS method.

1. Introduction

Studies of valuable cultural heritage generally call for nondestructive methods of analysis. However, lacquered cultural heritage items are compound objects that generally incorporate a variety of distinct materials, including lacquers, wood, paper, cloth, soil, minerals, and metals. Such studies necessarily involve a combination of multiple analytical methods: observations using various microscopy techniques to assess an artifact's state of deterioration and reveal its internal structure; analysis of organic substances to assess whether or not a given object contains lacquers, oils, or similar ingredients; and elemental analysis to identify species of inorganic substances such as pigments or metals used for decoration. Most of these analytical methods involve destructive analyses, and the precious nature of cultural heritage makes it essential to restrict the quantity of measurement samples subject to destructive analyses to the absolute minimum required. This poses a challenge for methods of destructive analysis, to extract the greatest possible amount of information from the smallest possible volume and quantity of measurement samples.

The lacquer used in lacquerware is an organic substance and a resin. A general-purpose tool that has long been used to analyze organic substances of this type is *Fourier-transform infrared spectroscopy* (FR-IR). However, when the measurement sample is a mixture, or otherwise exhibits a complicated composition, FT-IR methods not only may fail to identify certain components but may also pose the risk of erroneous analysis. For this reason, the *pyrolysis-gas chromatography-mass spectrometry* (Py-GC/MS) method is increasingly being used to analyze organic substances. The use of Py-GC/MS to analyze lacquer films allows the identification of chemical species in lacquer resins that cannot be identified in analyses

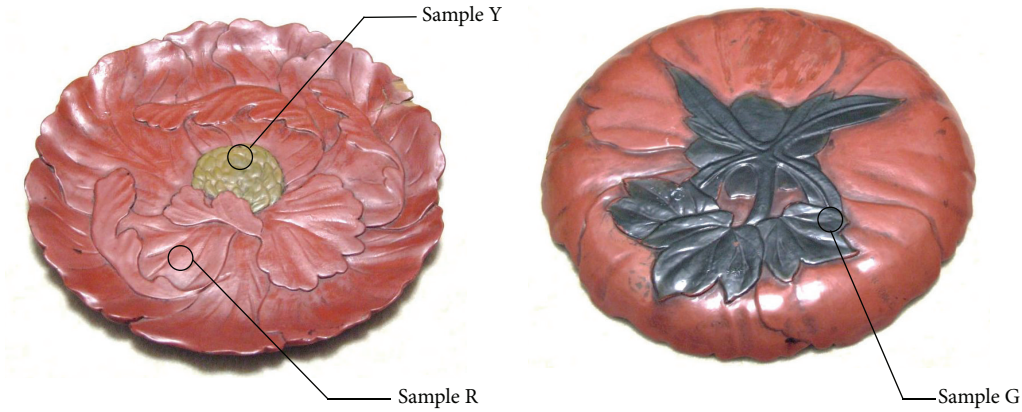

(a) Top (b) Underside

Figure 1: Photographs of a *Kamakura-bori* tray decorated with a peony design (diameter: 31 cm); (a) top, (b) underside. Locations of collected samples (○) are indicated.

using IR spectra [1]. For inorganic analysis of ingredients, such as inorganic pigments blended into paint layers or metallic powders and foils used to decorate lacquerware, many X-ray-based elemental analyses have been performed. However, the analyses of samples with multilayered structures that have been reported to date suffer from one or more of the following drawbacks. A first problem is the depth to which nondestructive X-ray analysis can probe beneath the surface layers. To remedy these difficulties, an analytical method based on *scanning electron microscopy augmented by energy dispersive X-ray spectrometry* (SEM-EDS) was proposed. This analytical method allows measurements that are pinpointed within individual layers. However, SEM-EDS requires the measurement sample to be rigidly fixed in place, and the carbon tape or other materials used to achieve this purpose may interfere with other analyses. This is the second of the problems mentioned above.

Understanding the material composition of lacquered artifacts of this sort requires the use of multiple analytical methods to gather data; full analyses can require large amounts of time and may be highly inefficient. For this reason, analytical methods that yield multiple types of information easily and rapidly from precisely targeted specific measurement sites are highly desirable. However, organic analysis and inorganic analysis are generally based on different physical principles, and for this reason it is difficult to analyze resins and pigments simultaneously. For these reasons, we have focused on analyses using Py-GC/MS, which allows analysis of tiny samples and offers outstanding ability to separate and identify sample constituents. A team of Italian researchers recently reported that Py-GC/MS could be used to detect the presence of mercury [2] and arsenic sulfide from analysis of analytical reagents [3]. According to their results, Py-GC/MS analysis can offer molecular information (information on binding states) on arsenic (As) and sulfur (S). However, although the use of Py-GC/MS to detect mercury in lacquerware has been reported [2], no report has offered evidence to support the use of Py-GC/MS to detect arsenic in lacquerware [4, 5]. Arsenic sulfide has been used since antiquity as a yellow coloring agent, and it has a history of use in painting and craftwork. In the 1970s, arsenic sulfide was determined to be poisonous for nonpharmaceutical uses; its production as a pigment for lacquerware was terminated in Japan, and arsenic-containing yellow pigments for lacquerware were destroyed. As a result, notwithstanding the use since antiquity of arsenic sulfide as a lacquerware pigment, the detailed composition of yellow pigments containing arsenic sulfide remains unclear. We have obtained yellow lacquerware pigments used in ancient times by craftsmen in the Japanese city of Wajima; after analyzing 7 varieties of these pigments, we concluded that all were sulfur compounds containing no arsenic. Among these was the yellow pigment clearly identified as orpiment, but this was not arsenic sulfide. This demonstrates that information on arsenic sulfide used as a lacquerware pigment was mixed in those days. The continuing ambiguity surrounding the characteristics of the yellow pigments used in the lacquerware production of the past is problematic from the standpoint of the preservation of lacquerware cultural heritage.

For these reasons, we have performed Py-GC/MS measurements of red, yellow, and green-colored lacquer films applied to lacquerware items to assess the feasibility of simultaneously detecting resin ingredients together with certain pigments. We have also compared our findings to the results of SEM-EDS, X-ray fluorescence spectrometry (XRF), and X-ray diffractometry (XRD) measurements. The results we report demonstrate that a single measurement of a small-volume sample extracted from a pinpointed region of an artifact can simultaneously yield information on organic components and some inorganic components.

2. Materials and Methods

2.1. Samples. The test item was a tray in the *Kamakura-bori* style decorated with a peony pattern colored with red, yellow, and green pigments, and samples were taken of each of the colors. Figure 1 shows the front and back surfaces of the full artifact, as well as the sampling points. The samples

taken from the yellow, green, and red regions of the craft work for analysis are hereafter referred to as Samples Y, G, and R, respectively. *Kamakura-bori* is a style of Japanese craftsmanship in which lacquer coatings were painted in layers onto a design carved from wood; in this lacquerware tradition, ingredients such as *makomo* (wild rice) were used to accentuate the shading due to surface roughness in carved wood. This craft work uses both the top and the underside surfaces to express a carved image of a peony flower. The pistil at the center of the flower is colored yellow, while the leaves and other regions are colored green. Careful inspection of the leaf regions of the underside surface reveals a deep green color used to indicate the base of each leaf, which evolves gradually into a green color strongly inflected with yellow coloring as one proceeds out to the tip of the leaf; this lends the impression of a three-dimensional depiction of a leaf.

2.2. Analysis Methods

2.2.1. Surface and Cross-Section Observations. Surface observation was conducted using a digital camera attached to an optical microscope (BX51 TRF-6 [D] and DP73-CU [D], resp., Olympus Co. Ltd.). Cross-section observations were conducted using a digital camera attached to an optical microscope (KH-770 and MX (G)-10C: OL-140II, HIROX Co. Ltd.). The relevant polished cross-sections were characterized by optical microscopy in order to examine all layers comprising the tray. Each sample was embedded in epoxy resin. After the epoxy resin had completely hardened, the surfaces of the embedded samples were ground flat and polished with wet sandpaper.

2.2.2. XRF. X-ray fluorescence spectrometry (XRF) was performed using a NEX CG (polarized optics energy dispersive XRF, Rigaku Ltd.); Pd radiation was used for the X-ray tube. Secondary targets of two types were used, RX9 for sulfur (S) and molybdenum (Mo) for iron (Fe), arsenic (As), and mercury (Hg). The SDD detector was used.

2.2.3. SEM-EDS. The inorganic materials in cross-sectional samples of the three colored areas were characterized by SEM-EDS. The SEM-EDS analysis was performed using a SEM (JSM-6610LV, JEOL Ltd.) coupled with an energy dispersive spectrometer (NSS 312E, Thermo Fisher Scientific K.K.). The accelerating voltage was set at 15 kV and the working distance at 10 mm. The range of qualitative analyses included elements in the periodic table ranging from boron to uranium. Analyses of two types of small-volume samples were conducted to ensure a cross-check on the results: (1) the outermost surface and (2) cross-sectional samples for each layer. In both cases, conducting carbon tape was used to fix the sample to the sample stage and analyses were conducted without evaporative coating.

2.2.4. XRD. XRD was performed using a diffractometer (UltimaIV, Rigaku Ltd.) equipped with a sample vertical goniometer (radius of 285 mm) and Cu Kα radiation with a Ni filter operated at 40 kV and 50 mA. Conventional Bragg-Brentano focusing geometry was used in combination with a 1/3° divergence slit, an 8 mm scattering slit, and a 13 mm receiving slit. A one-dimensional silicon strip detector (D/teX Ultra, Rigaku Ltd.) was used.

2.2.5. Py-GC/MS. Very small samples were taken from each of the color regions of the craft work and analyzed by Py-GC/MS. Py-GC/MS measurements were carried out using a vertical microfurnace-type pyrolyzer (PY-2020iD, Frontier Lab. Co. Ltd.) with a 6890N/5975 GC/MS system (Agilent Technologies, Ltd.). A stainless steel capillary column (30 m, 0.25 mm I.D.) coated with 0.25 μm Ultra Alloy PY-1(MS/HT) (100% methyl silicone) was used for the separation. The sample (0.5 mg) was placed in a stainless steel sample cup (Eco-cup, Frontier Lab. Co. Ltd.). The cup was placed on top of the pyrolyzer at near ambient temperature. The sample cup was introduced into the furnace when the furnace at 500°C and the temperature of the pyrolyzer interface and injector were set at 280°C, and then the temperature program of the gas chromatograph oven was started. The gas chromatograph oven was set at 40°C and held for 2 min, then programmed to provide a constant temperature increase at 12°C/min from 40°C to 320°C, and held for 10 min at 320°C. The flow rate of the helium gas was 1 mL/min. All pyrolysis products were identified by mass spectrometry. The mass spectrometry ionization energy was 70 eV (EI-mode), the cycle time was 1.94 scans per second, and the mass range was 29–800 m/z. Collected data were processed and analyzed by MSD ChemStation Software (Agilent Technologies, Ltd.).

3. Results and Discussion

3.1. Surface Analysis

3.1.1. Observing the State of the Outermost Surface. Figure 2 shows magnified microscope images depicting the state of the outermost surface of each of the three color regions. Samples Y and R exhibited more surface roughness than Sample G, indicating that painted surfaces were in a slightly roughened state. We attribute this to the fact that, in ordinary use, the front surface of a tray receives more light illumination than the back surface. Indeed, lacquer films have the disadvantage of being vulnerable to infrared light, and lacquer films tend to decompose due to the influence of ultraviolet radiation.

3.1.2. XRF. Table 1 summarizes the results of XRF measurements. While sulfur (S), iron (Fe), and arsenic (As) were detected in Sample Y, sulfur (S), iron (Fe), arsenic (As), and mercury (Hg) were detected in Samples G and R. From these

Table 1: Results of surface analysis by XRF.

Sample	Color	Elements
Y	Yellow	S, Fe, As
G	Green	S, Fe, As, Hg
R	Red	S, Fe, As, Hg

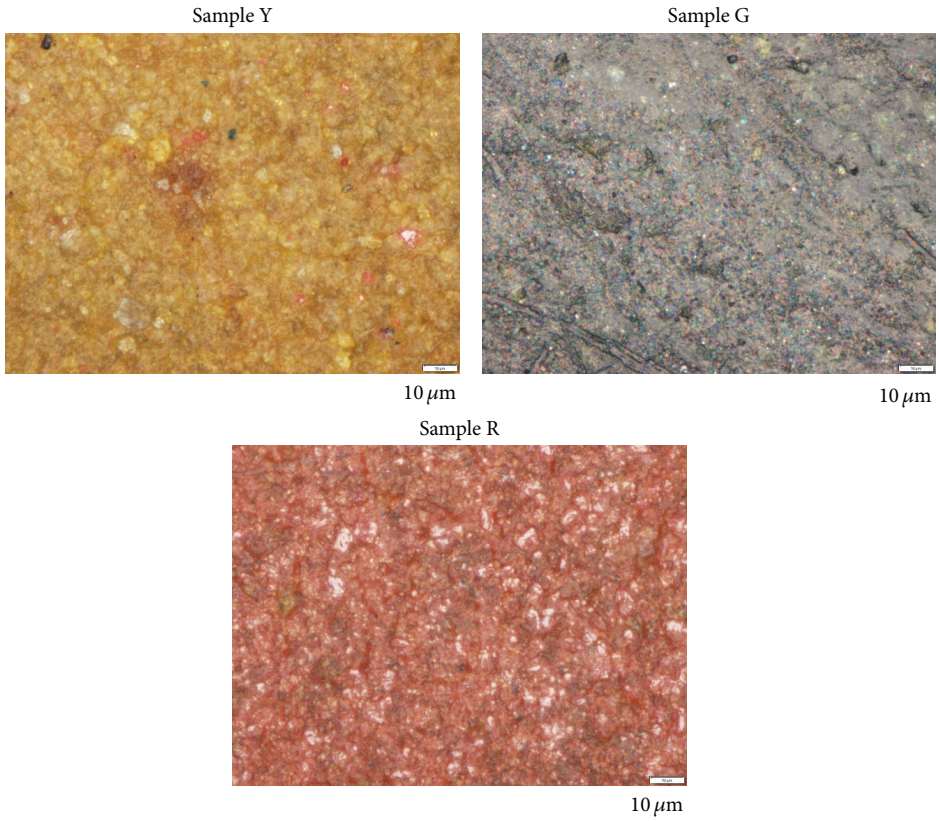

Figure 2: Microphotographs showing surface conditions of Samples Y, G, and R.

Table 2: Results of surface analysis by SEM-EDS.

Sample	Color	Elements
Y	Yellow	C, O, Al, Si, S, Ca, K, Fe, As
G	Green	C, O, Si, S, Cl, K, Ca, Fe, As, Hg
R	Red	C, O, Al, S, Fe, Cu, As, Hg

findings, we surmise that arsenic sulfide was used as a yellow pigment, while cinnabar (mercury sulfide, HgS) was used as a red pigment. However, binding information could not be obtained in cases where sulfur (S) and arsenic (As) formed compounds; thus we are unable to state definitively that the compound was orpiment (As_2S_3).

3.1.3. SEM-EDS. Table 2 lists the elements detected by SEM-EDS. It was determined with high certainty that Sample Y contained sulfur (S), iron (Fe), and arsenic (As); Sample Y was also believed to contain trace amounts of aluminum (Al), silica (Si), potassium (K), and calcium (Ca). It was determined with high certainty that Sample G contained sulfur (S), iron (Fe), arsenic (As), and silica (Si); Sample G was also believed to contain trace amounts of chlorine (Cl), potassium (K), calcium (Ca), and mercury (Hg). Sample R showed strong spectra of sulfur (S), arsenic (As), and mercury (Hg); also detected in trace amounts in Sample R were aluminum (Al), iron (Fe), and copper (Cu).

3.1.4. XRD. Qualitative analysis for elements and crystalline phases of all samples are shown in Table 3. In Sample Y, sulfur (S), iron (Fe), and arsenic (As) were detected, and realgar (As_4S_4), arsenolite (As_2O_3), and magnetite (Fe_3O_4) were identified. In Sample G, S, Fe, As, and Hg were detected, and arsenic (As), realgar (As_4S_4), arsenolite (As_2O_3), hematite (Fe_2O_3), magnetite (Fe_3O_4), and cinnabar (HgS) were identified. In Sample R, S, Fe, As, and Hg were detected; arsenic (As) and cinnabar (HgS) were identified. In Sample Y, cinnabar (HgS) occurred mainly in crystalline form/in the crystalline phase.

Figure 3 shows the results of crystal analyses of Samples Y, G, and R. The analysis of Sample R was straightforward, but the analyses of Samples Y and G were considerably more complicated. Indeed, in the crystal analysis of Samples Y and G, it was necessary to inspect the spectra with proper consideration of the possibility of ingredients that might have been used as mineral pigments in the lacquerware tradition; this makes the analysis more difficult. Kitano performed XRD analyses of arsenic sulfide contained in unearthed lacquerware items and showed that the detection rate for arsenic sulfide was lower for green lacquer than for yellow lacquer [6]. In the present case, assessing the realgar (As_4S_4) thought to be contained in Samples Y and G amounts to the question of whether or not the sample contains a very small quantity of the substance; we were unable to compare the quantities present in the two samples. A comparison with the results of Kitano's measurements is difficult because

Table 3: Results of surface analysis by XRD.

Sample	Color	Crystalline phases
Y	Yellow	Arsenic (As), realgar (As_4S_4), magnetite (Fe_3O_4)
G	Green	Arsenic (As), realgar (As_4S_4), hematite (Fe_2O_3), magnetite (Fe_3O_4), cinnabar (HgS)
R	Red	Arsenic (As), cinnabar (HgS)

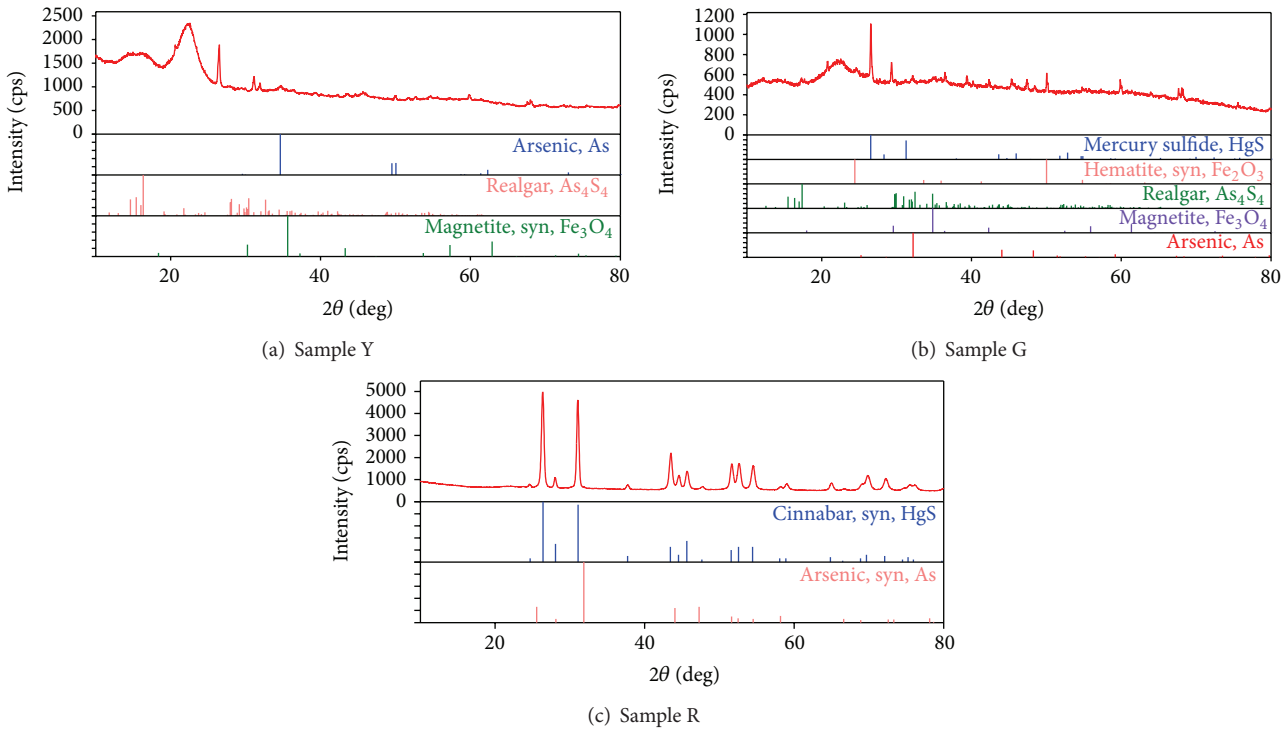

(a) Sample Y

(b) Sample G

(c) Sample R

Figure 3: XRD crystal diffraction experiments.

the detailed methods of those measurements are unclear; it is possible that the measurement sample was ground into a powder to enable the measurements. The present study is concerned with nondestructive measurements, and hence we do not grind measurement samples into powders; still, our finding that XRD spectra are more complicated when the lacquer sample contains arsenic sulfide is in good agreement with the findings reported by Kitano. In XRD measurements, determining the presence of arsenic sulfide is more difficult for samples of lacquer mixtures than for individual samples of arsenic sulfide (single-body mineral samples). Thus, although the question is somewhat dependent on the quantity of arsenic sulfide contained in the sample, in general it is best to avoid reliance on XRD measurements alone when determining whether or not oriental lacquer films contain arsenic sulfide.

3.2. Cross-Sectional Analysis

3.2.1. Cross-Sectional Observations. Figure 4 shows microscope images of cross-sectional samples from the various color regions. Images (a) and (b) are both of cross-sectional samples taken from Sample Y, while images (c) and (d) are cross-sectional samples of Samples G and R, respectively. All of these samples included an underlayer of black paint.

Comparing the two images of cross-sectional samples taken from Sample Y (Figures 4(a) and 4(b)), we see that although the uppermost painted layer in the Sample Y region is yellow in color, some samples taken from this region—depending on the site from which the sample was collected—contain red paint films as well. No red paint film lying beneath the yellow paint film was observed for the sample collected from the point closer to the center. We conclude that samples exhibiting red paint films were those taken from regions corresponding to petals of the peony; these regions surround the central region of the flower, which is covered in yellow paint. Presumably the artist was not excessively meticulous when painting the artifact, resulting in a coating of yellow paint. Inspection of the image of Sample G in Figure 4(c) reveals a yellow-painted region lying above a black paint film and marbled with regions of strong green and dark green coloration. This indicates that two shades of green paint were blended on the artifact before the wet paint solidified to form paint films. As seen in Figure 1, the dark green color present at the petiole of the leaves turns gradually into a green color with a strong yellow tint as one traces the leaf to its tip, conveying

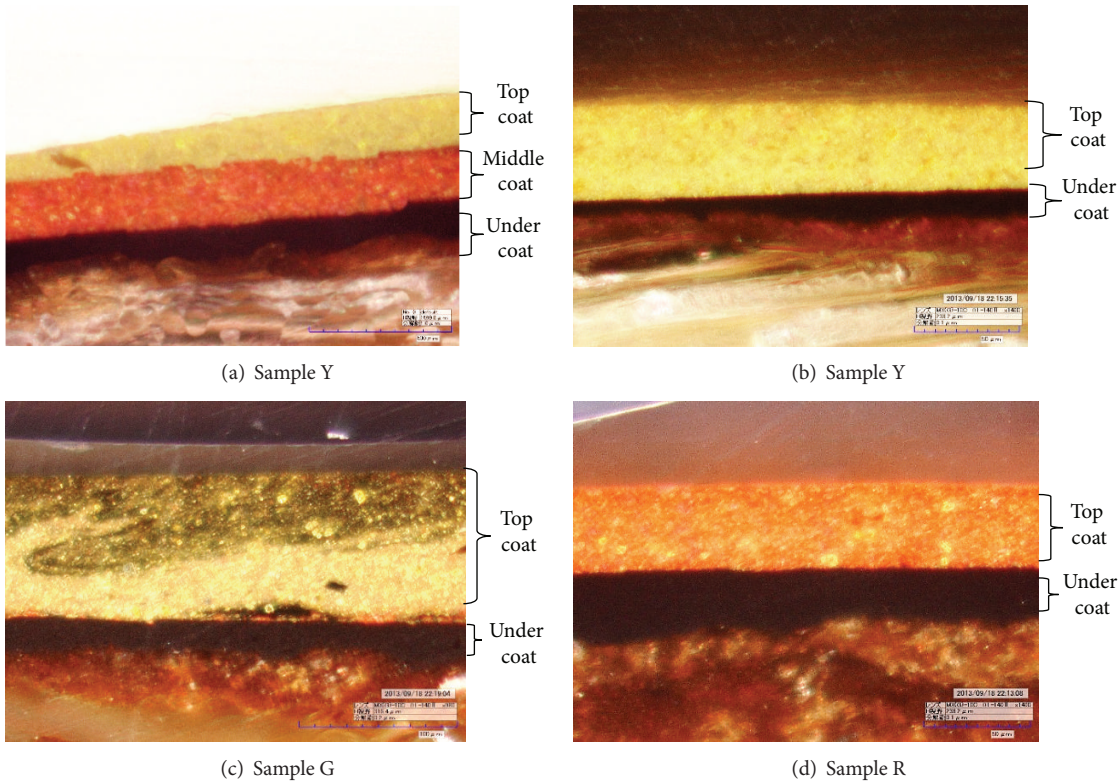

(a) Sample Y (b) Sample Y

(c) Sample G (d) Sample R

Figure 4: Cross-sectional photos of Sample Y (a) and (b), Sample G (c), and Sample R (d).

a sense of the three-dimensional nature of the leaf; we believe that this explains the cross-sectional structure observed in Figure 4(c). The image of Sample R in Figure 4(d) shows a red paint film lying atop a black paint film. The upper paint layer (the red layer) is dotted with yellow particles large in size compared to the red particles, suggesting the possibility that red and yellow pigments were blended. This was most likely done to yield a bright orange color for the petals of the peony that this tray seeks to depict.

3.2.2. SEM-EDS. Figure 5 shows the results of elemental mappings conducted via SEM-EDS on the cross-sectional samples. Analysis of the red-colored layers observed in Figures 4(a) and 4(d) revealed that the same elements were detected in these two samples. For this reason, Figure 5(a) shows the results of analysis of the cross-sectional sample of Figure 4(a). Figure 5(b) shows the results of analysis of the cross-sectional sample of Figure 4(c). No elements originating from pigments were detected in the black-painted underlayers. The yellow-, green-, and red-painted layers observed in Figure 4 were all observed to contain elements believed to originate from pigments.

Inspecting the element mapping of the Y layer in Figure 5(a), we see that the points at which arsenic (As) is present roughly coincide with the points at which sulfur (S) is present, strongly suggesting the presence of arsenic sulfide. In contrast, in the R layer of Figure 5(a), the points at which arsenic (As) and sulfur (S) are present do not agree to the same extent; on the other hand, the points at which mercury (Hg) and sulfur (S) are present agree quite well. We thus conclude that the R layer of Figure 5(a) contains only small quantities of arsenic sulfide; instead, mercury sulfide constitutes the majority of the pigment in this region. Looking at the element mapping of the G layer in Figure 5(b), we see a lesser presence of arsenic sulfide than in the Y layer of Figure 5(a). Mercury (Hg) is also scattered throughout this region.

3.3. Chemical Analysis

3.3.1. Analysis of Resins via Py-GC/MS. To identify the resins used as paints, we performed Py-GC/MS data analysis. Figure 6 shows an ion chromatogram (m/z 108)—extracted from the *total ion chromatogram* (TIC)—that originates from alkylphenol and is used in the principle component analysis of oriental lacquer. Essentially identical pyrolysis products were observed from all samples (Samples Y, G, and R). Our identification of these pyrolysis products allows us to determine [7, 8] the substance in question as *Toxicodendron vernicifluum* (the academic name for a tree) for which urushiol is a primary component. *T. vernicifluum* is an oriental lacquer tree cultivated in Japan, China, and Korea. It shows that the paint applied to all colored regions of the *Kamakura-bori* tray used sap tapped from *T. vernicifluum*. The substance detected with the greatest intensity camphor may be used as a diluting agent when applying coats of oriental lacquer. Because the wood carving of our sample exhibits surface roughness, the application of only an impasto coat of oriental lacquer would create a high risk of paint defects. We surmise

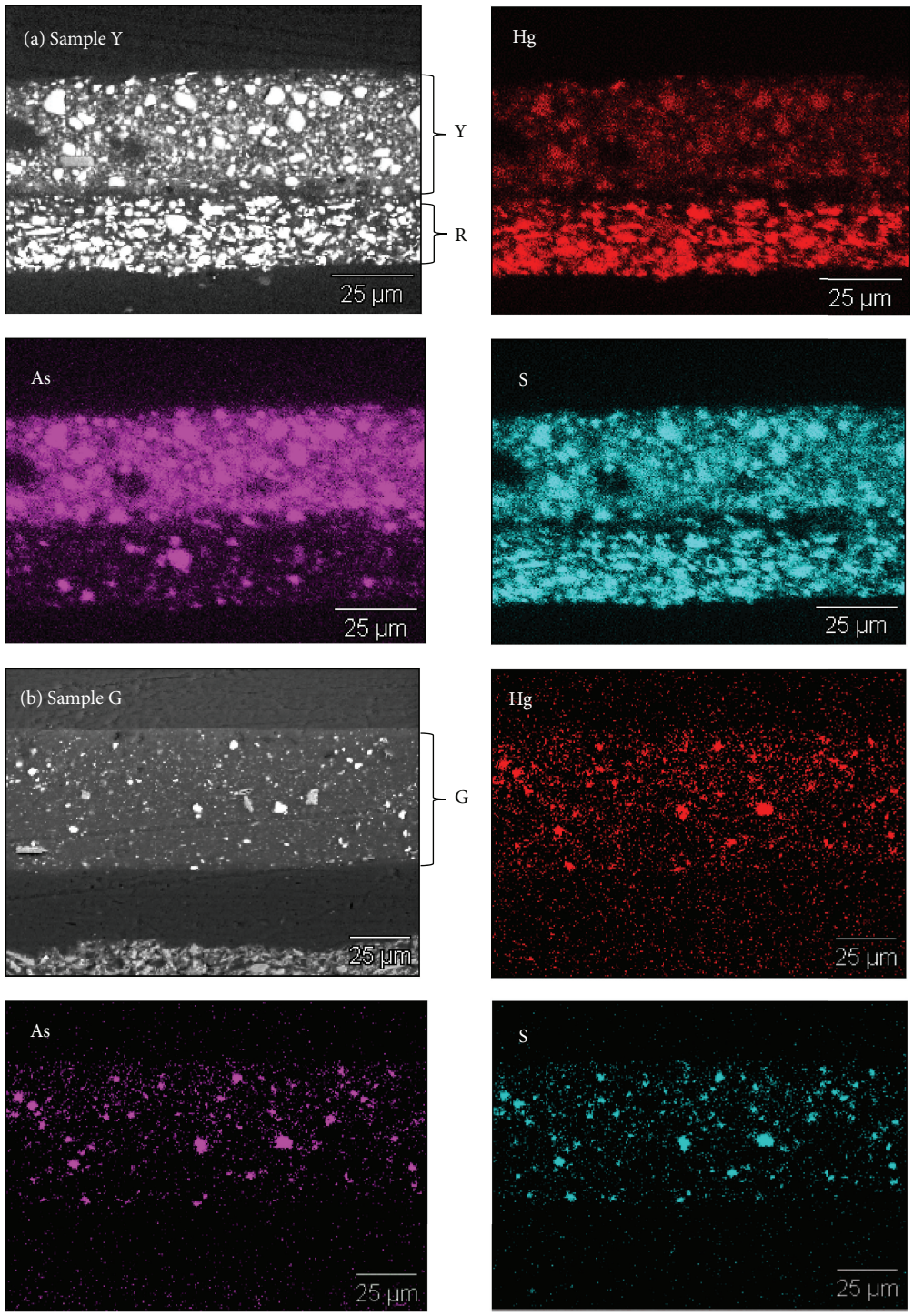

Figure 5: Cross-sectional element mapping experiments. (a) Sample Y, (b) Sample G.

that camphor was used to dilute the oriental lacquer applied to the item to mitigate this risk.

3.3.2. Py-GC/MS Analysis of Pigments. To investigate the ways in which S, As, and Hg—which may have been used as pigments—were present in our samples, we analyzed the results of Py-GC/MS analyses.

(1) Investigation of Sulfur (S) and Arsenic (As). Samples Y and G gave nearly identical results by Py-GC/MS analysis; the results of Sample R were also similar but of weaker intensity. Figure 7 collects the results for Sample Y. Figure 7(a) shows the TIC, while Figures 7(b), 7(c), and 7(d) show the mass spectra near the high-intensity Peaks B, C, and D labeled in Figure 7(a). The mass spectrum of Peak B is consistent with

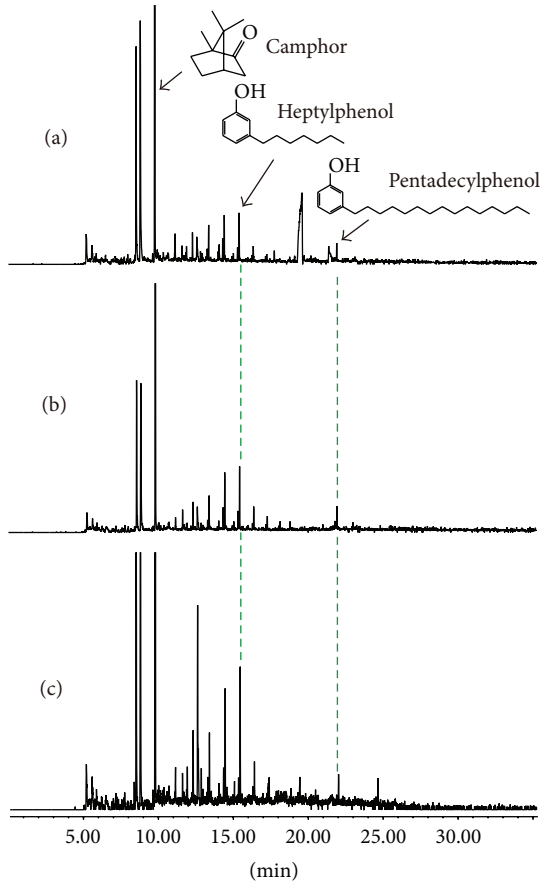

Figure 6: Ion chromatograms of the m/z 108 fragment ion of the alkylphenol of Sample Y (a), Sample G (b), and Sample R (c).

As_4 (MW 300) and shows a typical fragmentation by sequential loss of As atoms (Figure 7(b)). This agrees with the results reported by Chiavari et al. [3, 9]. In the mass spectrometry analysis of Sample Y, elemental As was detected at m/z 74.9 for 1x As, m/z 149.8 for 2x As, m/z 224.7 for 3x As, and m/z 299.6 for 4x As. Chiavari et al. reported that the presence of As_4 indicates the use of orpiment (As_2S_3) as a yellow pigment [3]. We performed Py-GC/MS measurements of orpiment (As_2S_3) and realgar (As_4S_4) from commercial suppliers. Measured results for the mineral samples of orpiment reveal mass spectra identical to those observed near Peaks B and C (Figures 7(b) and 7(c)). However, the As_3S_3 and As_4S_4 features observed near Peak D (Figure 7(b)) were not seen for the orpiment mineral sample. In contrast, the mass spectra detected for the mineral sample of realgar contained the As_3S_3 and As_4S_4 features seen near Peak D (Figure 7(b)). On the other hand, none of the samples we measured indicated As_2S_3 (MW 246) in their mass spectra. Chiavari et al. did not perform measurements with As_2S_3 as a standard reagent [3], while the mass spectra reported by Ma et al. [4] were not able to confirm a mass spectrum of As_2S_3 but nonetheless identified the substance as orpiment (As_2S_3). In the future, further analyses focusing on the binding states of arsenic (As) and sulfur (S) are necessary to investigate the detailed composition of yellow pigments containing arsenic sulfide.

Figure 8 shows ion chromatograms with m/z 300 (solid curves) and m/z 427.6 (dashed curves). Results for Sample Y are shown in Figures 8(a) and 8(b), and results for Sample G are shown in Figures 8(c) and 8(d). Samples Y and G both contained As_4, corroborating the results obtained by both XRD analysis and SEM-EDS mapping analyses, which suggested the presence of isolated arsenic (As). As_4 was also strongly detected in Sample R. While As_4S_4 was strongly detected in Sample Y, irrespective of the position on the artifact from which the sample was collected for analysis, the intensity of the As_4S_4 that was detected was variable in Sample G. The reason for this disparity may be due to the varying amounts of differently colored lacquer that were blended together when the artifact was made; for example, in order to elicit stronger coloration in the green-colored region of Sample G, yellow-green lacquer containing a strong yellow tint was blended with a deep green lacquer containing a weak black-inflected yellow tint to produce the two distinct lacquer layers that are visible in the cross-section shown in Figure 4(c). Consequently, the intensity with which As_4S_4 was detected varied depending on the precise location from which the material was collected for Py-GC/MS analysis.

Most reports of scientific investigations involve the use of X-ray techniques to confirm the presence of the elements arsenic and sulfur—findings which are habitually attributed to As_2S_3 (orpiment) despite the absence of molecular-level information. Many studies in the field of cultural artifact research have used methods of Raman spectroscopy to identify molecular-level signatures of arsenic sulfide [10]. However, in the case of lacquerware artifacts, the existence of light emission from lacquer-coating layers prevents the collection of analyzable spectra, and thus Raman spectroscopy cannot be used for such objects. On the other hand, these findings showed that information on binding states, which is difficult to infer based on XRD analysis, can easily and rapidly be obtained from Py-GC/MS analysis. Indeed, depending on the analytical methods employed, a single measurement can yield a variety of information regarding the use of pigments.

(2) Investigation of Mercury. Many naturally occurring elements are composed of multiple stable isotopes of different mass numbers [11]. For mercury, there are 7 stable isotopes, and the use of Py-GC/MS allows the stable isotopes of mercury to be detected with ease [2]. The total ion chromatography (TIC) and the m/z 202 ion chromatograms of standard HgS powder are shown in Figure 9 together with mass spectra and isotope ratios inset. The values listed in the table of isotope ratios were derived as follows. Following the literature by taking the ^{198}Hg isotope to be 100, the isotope ratios of ^{196}Hg, ^{198}Hg, ^{199}Hg, ^{200}Hg, ^{201}Hg, and ^{204}Hg were each computed from the mass spectra, and the measured values were compared to values available in the literature. From the TIC peak in Figure 9, a total of 6 isotope peaks were detected, with m/z 202 being the primary peak (Figure 9 inset). The isotope ratios are close to those reported in the literature, whereupon we conclude that these mass spectra originate from mercury [12].

The TIC and the m/z 202 ion chromatograms of Sample R are shown in Figure 10. Because the mercury isotope peaks

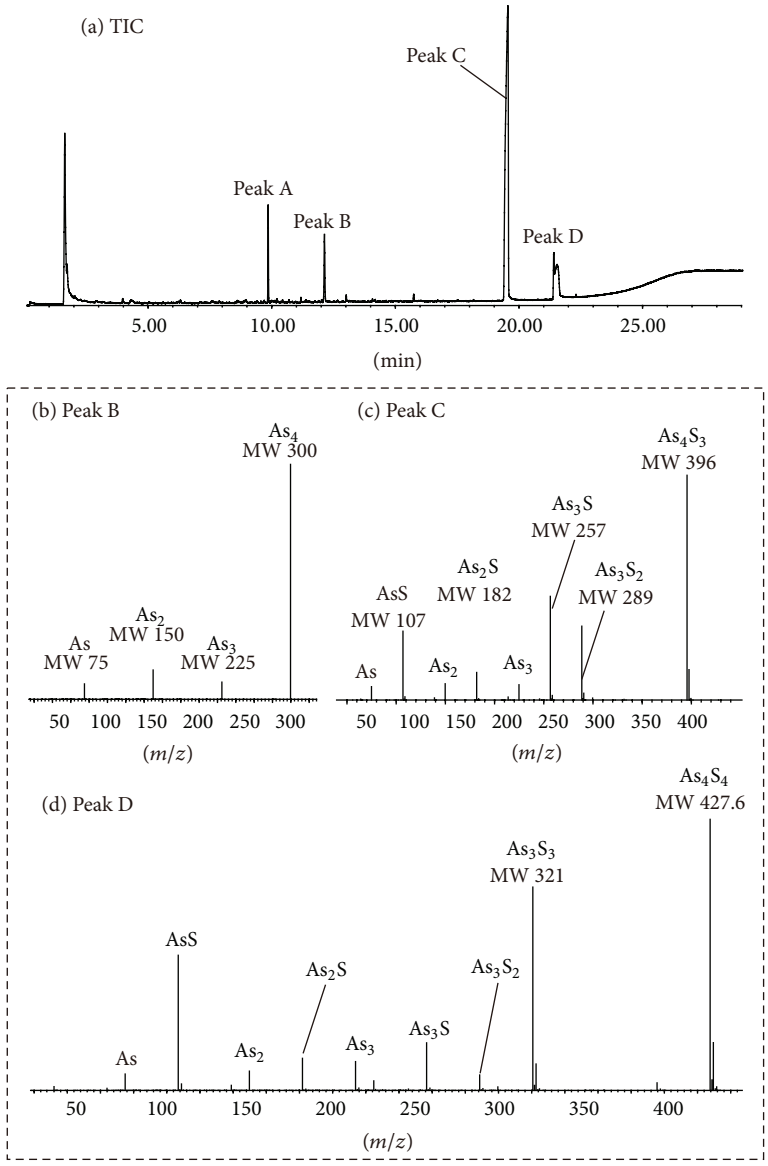

Figure 7: Py-GC/MS analyses of Sample Y. (a) TIC, (b) ion chromatograms of Peak B, (c) ion chromatograms of Peak C, and (d) ion chromatograms of Peak D.

were detected with greatest intensity in Sample R, Figure 10 shows results of measurements on Sample R. Isotope peaks were not detected for Sample Y. On the other hand, for Sample G, isotope peaks similar to those of Sample R but of weaker intensity were detected. The results of these measurements agree well with the results of XRF, SEM-EDS, and XRD analyses. Inspecting the table of isotope ratios in the inset of Figure 10, we see results that lie closer to literature values than the measured values in the inset of Figure 9. However, in Figure 9, which measured powders of a mercury sulfide (HgS) reagent, a strong spectrum was observed at 7 minutes and 30 seconds; in contrast, for Sample R, a strong spectrum was observed at 11 minutes and 30 seconds. Because we did not make any significant modifications to the state of the measurement apparatus, the origin of this discrepancy in the retention time is unclear and remains a question for future work.

4. Conclusions

Upon comparing the results of the XRF and XRD analyses, SEM-EDS measurements of the outermost layers and the cross-sectional layers, and Py-GC/MS measurements, we arrive at the following conclusions.

(1) Observations regarding Arsenic Sulfide. The results of elemental analyses conducted via XRF and SEM-EDS afford knowledge of the presence of As and S. By further combining the SEM-EDS-based elemental mapping analyses for As and S, we may determine whether or not the sites at which these

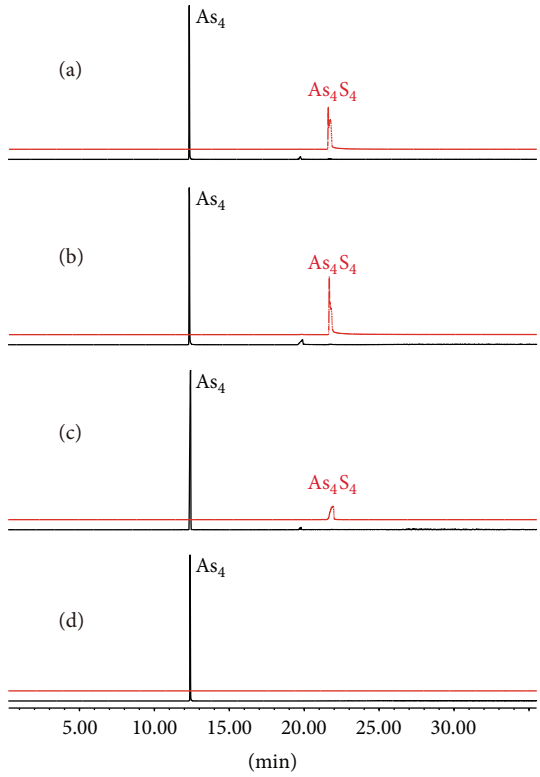

Figure 8: Ion chromatograms of the m/z 300 and m/z 427.6 fragment ions of Sample Y (a) and (b), Sample G (c) and (d).

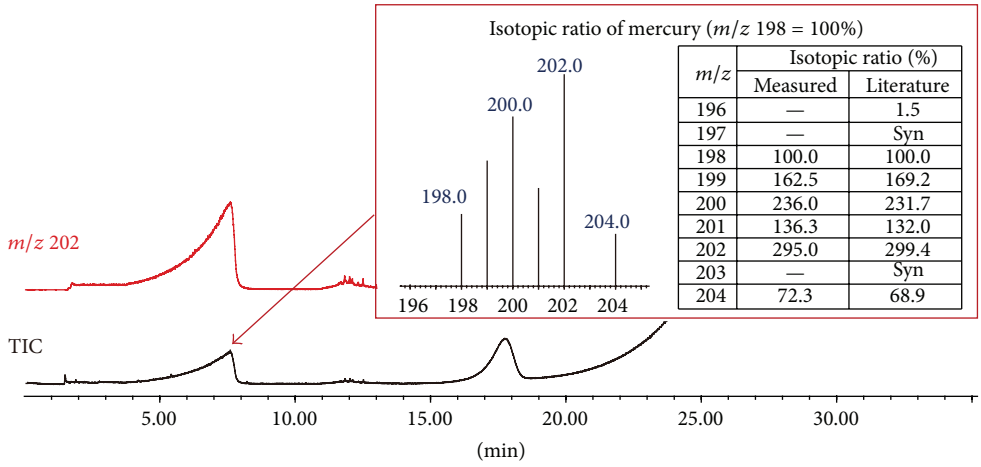

m/z	Isotopic ratio (%)	
	Measured	Literature
196	—	1.5
197	—	Syn
198	100.0	100.0
199	162.5	169.2
200	236.0	231.7
201	136.3	132.0
202	295.0	299.4
203	—	Syn
204	72.3	68.9

Figure 9: TIC and ion chromatograms of the m/z 202 fragment ion of standard HgS powder.

two elements are present coincide. However, it is difficult to pinpoint the binding configuration of the As and S atoms. The use of XRD measurements allows determination of the binding states of As and S; however, in cases involving mixtures with lacquer, the peaks that allow detailed analysis are difficult to observe, and it is challenging to confirm the presence of substances. In contrast, the use of Py-GC/MS readily allows determination of specific binding states of As and S—such as As_4S_4—whereupon the presence of such substances may be rapidly discovered.

(2) Observations regarding Substances Other Than Arsenic Sulfide. We were able to verify the presence of mercury via elemental analyses using XRF, SEM-EDS, and XRD, while Py-GC/MS identified mercury by detecting the mass spectra of its isotopes. We were able to verify the fact that mercury was present in the form of cinnabar (mercury sulfide) from the results of XRD analyses. The presence of iron was confirmed by XRF, SEM-EDS, and XRD. The results of XRD analyses indicated the possibility that iron was present in the form of hematite (Fe_2O_3) or magnetite (Fe_3O_4).

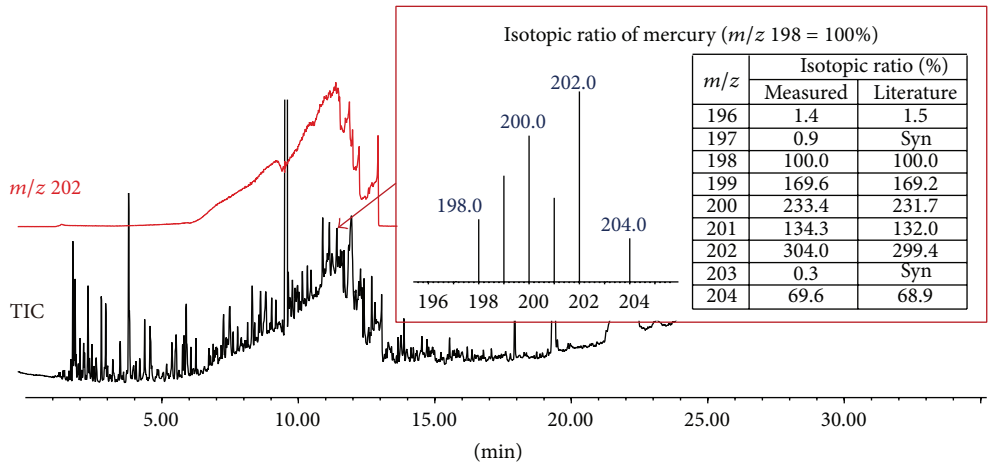

m/z	Isotopic ratio (%)	
	Measured	Literature
196	1.4	1.5
197	0.9	Syn
198	100.0	100.0
199	169.6	169.2
200	233.4	231.7
201	134.3	132.0
202	304.0	299.4
203	0.3	Syn
204	69.6	68.9

Figure 10: TIC and ion chromatograms of the m/z 202 fragment ion of Sample R.

Therefore, Py-GC/MS analyses simultaneously yielded molecular-level information on arsenic (As) and sulfur (S) together with detection of the primary ingredients of the lacquer. We were also able to confirm the presence of mercury (Hg), in agreement with the results of previous work [2]. These findings demonstrate that Py-GC/MS is capable of identifying the presence of arsenic (As), sulfur (S), and mercury (Hg), even when mixed together in a lacquer film; thus Py-GC/MS may be used for simultaneous analysis of organic and inorganic substances.

Conflict of Interests

The authors declare that there is no conflict of interests regarding the publication of this paper.

Acknowledgment

This work was supported by a Grant-in-Aid for Scientific Research (B), Grant number 25282076.

References

[1] R. Lu, Y. Kamiya, and T. Miyakoshi, "Applied analysis of lacquer films based on pyrolysis-gas chromatography/mass spectrometry," *Talanta*, vol. 70, no. 2, pp. 370–376, 2006.

[2] G. Chiavari and R. Mazzeo, "Characterisation of paint layers in Chinese archaelogical relics by pyrolysis-GC-MS," *Chromatographia*, vol. 49, no. 5-6, pp. 268–272, 1999.

[3] G. Chiavari, D. Fabbri, and G. C. Galletti, "Pyrolysis/gas chromatography/mass spectrometry of arsenic inorganic compounds," *Rapid Communications in Mass Spectrometry*, vol. 9, no. 7, pp. 559–562, 1995.

[4] X. M. Ma, R. Lu, and T. Miyakoshi, "Application of pyrolysis gas chromatography/mass spectrometry in lacquer research: a review," *Polymers*, vol. 6, no. 1, pp. 132–144, 2014.

[5] T. Honda, R. Lu, M. Yamabuki et al., "Investigation of Ryukyu lacquerwares by pyrolysis-gas chromatography/mass spectrometry," *Journal of Analytical and Applied Pyrolysis*, 2014.

[6] N. Kitano, *The Industrial Technique and the Organization of Modern Lacquer Ware*, Yuzankaku, 2005, (Japanese).

[7] N. Niimura and T. Miyakoshi, "Characterization of natural resin films and identification of ancient coating," *Journal of the Mass Spectrometry Society of Japan*, vol. 51, no. 4, pp. 439–457, 2003.

[8] R. Lu, Y. Kamiya, and T. Miyakoshi, "Preparation and characterization of *Melanorrhoea usitata* lacquer film based on pyrolysis-gas chromatography/mass spectrometry," *Journal of Analytical and Applied Pyrolysis*, vol. 78, no. 1, pp. 172–179, 2007.

[9] G. Chiavari, D. Fabbri, G. C. Galletti, and R. Mazzeo, "Use of analytical pyrolysis to characterize Egyptian painting layers," *Chromatographia*, vol. 40, no. 9-10, pp. 594–600, 1995.

[10] I. M. Bell, R. J. H. Clark, and P. J. Gibbs, "Raman spectroscopic library of natural and synthetic pigments (pre-~1850 AD)," *Spectrochimica Acta Part A: Molecular and Biomolecular Spectroscopy*, vol. 53, no. 12, pp. 2159–2179, 1997.

[11] J. D. Blum and B. A. Bergquist, "Reporting of variations in the natural isotopic composition of mercury," *Analytical and Bioanalytical Chemistry*, vol. 388, no. 2, pp. 353–359, 2007.

[12] A. Takeuchi, Y. Shibata, and A. Tanaka, "Mercury (Hg) isotope biogeochemistry," *Journal of Environmental Chemistry*, vol. 19, no. 1, pp. 1–11, 2009 (Japanese).

Hindawi Publishing Corporation
International Journal of Polymer Science
Volume 2015, Article ID 729132, 8 pages
http://dx.doi.org/10.1155/2015/729132

Research Article

Properties of Polymer-Composite Used as Fills of Asian Lacquerware: Issues on Restoration Processes of Lacquered Objects from Cultural Heritage

Anne-Solenn Le Hô,[1] Isabelle Fabre-Francke,[2] and Caroline Thiphavong[3]

[1]*Centre de Recherche et de Restauration des Musées de France (C2RMF), Ministère de la Culture et de la Communication, Palais du Louvre-Porte des Lions, 14 quai François Mitterrand, 75001 Paris, France*
[2]*Laboratoire de Physicochimie des Polymères et des Interfaces (LPPI), Institut des Matériaux, Université de Cergy-Pontoise, 5 mail Gay-Lussac, Neuville-sur-Oise, 95031 Cergy-Pontoise Cedex, France*
[3]*Institut National du patrimoine (INp), Département des Restaurateurs, 150 avenue du Président Wilson, 93210 Saint Denis La Plaine, France*

Correspondence should be addressed to Anne-Solenn Le Hô; anne-solenn.leho@culture.gouv.fr

Received 29 January 2015; Revised 16 June 2015; Accepted 25 June 2015

Academic Editor: Michael Schilling

One of the common problems encountered in lacquerware issued from cultural heritage is the appearance of lifting areas and some losses of material. Composite systems made of commercial polymer and different fills were tested as filling agents for the cracking, splitting, and losses compensation of Asian lacquer. For that purpose, the stability of traditional and modern commercially available materials usually used in the restoration practice of historical lacquerware was assessed. Their thermomechanical and chemical properties and surface state were evaluated by a set of techniques (TGA, DMA, mechanical test, contact angle value, and microtopography). There is a drastic change of the behavior of the interface between fill and Asian lacquer, dependent on the nature of the composite fillers. So the evaluation of materials and processes for the restoration of Asian lacquer were emphasized. The commercial Paraloid B72 used with glass microspheres as additives appeared to be the most stable of all of the investigated fillers.

1. Introduction

Asian lacquer is one of the most important materials and practices in the history and culture of oriental civilization from the Neolithic to nowadays. Concurrently lacquerware is one of the leading contributors of Far East in the cultural heritage, especially decorative arts, in the Europe. The objects constitutive of Asian lacquer were largely imported from East Asia to Europe from the sixteenth century by maritime routes as luxury and exotic products. So they are now largely widespread in Occidental museum collections. Even though it is considered as an ideal natural, durable, and plastic coating, lacquer can suffer from substantial damage, mainly caused by improper reparation, its poor UV stability, and its brittleness under dry conditions. The poor UV stability and the brittleness of lacquer cause permanent mechanical damage such as cracking, lifting, and losses of material within substrate or lacquer layers. Once cracks have been formed, they evolve from the lacquer surface to the ground preparation and finally to the substrate. The lacquer splits away from the substrate. These common problems are commonly encountered in the Occident where the climate is often dryer than in Asia [1–4].

In the last past decades, different treatments were experimented in the Occident to fill exfoliation and losses of lacquer. To repair these structural deteriorations, fills are applied to lacquer in order to penetrate into losses of lacquer and complete voids. Nevertheless, lacquer can be a difficult material to work for Western conservators because the lacquer technology poorly migrated from Asia to West. Furthermore,

lacquer is not a reversible material. In the Western museum conservation-restoration principle, repairs appear acceptable if they are compatible with the original ones and can be removed easily without causing damage. So the Asian traditional practice with the use of materials based on lacquer, as *kokuso*—a mixture of lacquer, cotton or hemp fibers, and wood powder—to fill holes, gaps, and cracks is almost not considered in Western museums. This concept of reversibility of conservation treatments is a central motivation in the Occident [5]. For that reason, Western conservators have adopted the use of synthetic or even other natural fillers instead of the traditional Asian lacquer fillers. In the last 20 years, a lot of fill materials were experimented based on waxes (beeswax, microcrystalline, paraffin, and carnauba), dammar terpenic resin, or modern synthetic compounds such as polyester resin, polyvinyl alcohol, and epoxy resin [6]. Nevertheless various problems can be encountered as thermochromatic changes, brittleness of the filler, or a lack of reversibility.

This paper deals with fills for cracks and losses, even the deeper and largest ones occurring from the surface to the substrate. These ones are the most problematic to repair. The goal of this work was not to prescribe a fill recipe or application method but rather to provide useful comparative data to aid in choosing different fillers and lacquer loss compensation treatments. With greater knowledge of the properties of filler compounds, it may be possible to better control the filler. So the significant factor guiding this research was detailed; then the properties of materials commonly used by conservators for restoration of lacquer were studied. Our strategy was to measure and compare performances and characteristics of restoration material by a set of thermophysical and chemical techniques to have a better assessment. With this in mind, extensive testing of different fills was chosen to go beyond aesthetic observations and visual considerations.

An appropriate fill has to balance characteristics to attain the best combination of strength, adhesive compatibility, nominal shrinkage, retreatability, stability, and aesthetic compensation [6–8].

Thus the thermomechanical, chemical, and optical properties of a set of synthetic and natural fills were characterized with the purpose of evaluating the fillers used in the restoration of lacquerware. Fillers made of copolymer of acrylate and methacrylate, polyvinyl alcohol, hydroxypropyl cellulose, or vegetal, mineral waxes, and terpenic resin were tested.

The behavior of the tested filler mixture was compared with the original material to fill in (lacquer or ground layer) by an analytical methodology: thermal analyses by TGA and DMA to test the stability of fills, mechanical tests to investigate their strength properties, contact angle values to characterize their hydrophobic or hydrophilic properties and solubility measurements.

The roughness is a key optical parameter on appearance phenomena. The more the fill is rough, the more matt, scarred, and imperfect the treated surface will appear. This will lead to changes in gloss and color saturation in the surface finishes (final surface of the fill and top coat). Furthermore, adhesion is dependent on chemistry and also roughness of the surfaces to be adhered.

So the overall appearance of the treated surface was also investigated by microtopography to measure the roughness of the fills.

2. Experimental

2.1. Sample Preparation. The selection of these filler materials was based on products and recipes usually described in the literature and used in the lacquer restoration practice in the Occident [6, 9, 10]. A preliminary survey has been made addressed to Western lacquer conservators to take an inventory of filler materials and processes that are in common used to compensate for losses on lacquer.

Five polymer-composite fills were chosen from among those typically used in art restoration of lacquer. The composition of the different filler materials is given in Table 1. Paraloid B72 (ethyl methacrylate and methyl acrylate copolymer) (Rhom and Haas), Gelvatol (polyvinyl alcohol) (CTS), Klucel G/$CaCO_3$ (hydroxypropyl cellulose) (Stouls), ethanol (VWR, GPR Rectapur 95–97%), acetone (VWR, technical), phenolic micro balls (20–90 μm in size, CTS), micro glass beads Scotchlite K-15 (size between 30 and 80 μm, 3 M), carnauba wax (La Cérésine), $CaCO_3$ (Sennelier). Dammar resin, ozokerite, and talcum were taken from the laboratory of the restoration department at the Institut National du patrimoine (Saint-Denis).

The fills were prepared similarly to common restoration practices and using similar conditions. Most of the composite fills were obtained by stirring each of the compounds at room temperature. The carnauba wax/dammar resin filling was the only one to be prepared at 90°C. The obtained mixtures were then poured into a silicone mould, measuring 2 cm × 3 cm × 0.5 cm. For DMA, films of fills were prepared in moulds of smaller size. Typical dimensions of the DMA samples were 6 mm × 20 mm × 1 mm (Figure 1). Then they were dried at laboratory temperature and 40–50% RH under free air for 12 hours, except for the mixture wax/resin which was dried for few minutes.

For microtopography, fills were successively polished with 240, 600, 800, 1600, and 3600 grade Micro-Mesh© abrasive cloth [11]. Then the surface roughness was measured on polished fills.

Furthermore one Asian traditional material was also tested as reference of original compound encountered in lacquerwares. This reference was prepared using a real Asian processing method. A kuro-nakanuri lacquer, originated from China and processed in Japan, was selected (Watanabe Syoten, Tokyo, Japan). The kuro-nakanuri is usually used for intermediate layers of lacquer and made by the adding of black pigments to lacquer. A reference of kuro-nakanuri lacquer was prepared by the restorer. Five layers of kuro-nakanuri were successively applied with a paintbrush onto a silicone plate.

The Paraloid PB72 is used as an extremely stable and non-yellowing polymer on internal exposure in a gallery [12, 13]. PVA/$CaCO_3$ can be applied easily, dries quickly, and can also be burnished to a very smooth finish [6]. It is stable under light, and its yellowing occurs beyond 80°C. Klucel G/$CaCO_3$ seems a good candidate for its strong adhesive properties. It

Table 1: Composition of fills.

Fills	Percentage of each compound (% in weight)			
PB72/μphenolic balls	75% of PB72 in 25% of ethanol/ acetone (1/1) solution	25% of phenolic micro balls		
PB72/μglass beads	90% of PB72 in 25% of ethanol/ acetone (1/1) solution	10% of glass bubbles Scotchlite		
PVA/$CaCO_3$	25% of Gelvatol in 8% of H_2O	75% of $CaCO_3$		
Klucel G/$CaCO_3$	40% of Klucel G/$CaCO_3$ in 6% of ethanol	60% of $CaCO_3$		
Wax/resin	23% of carnauba wax	30% of dammar resin	23% of ozokerite	23% of talcum

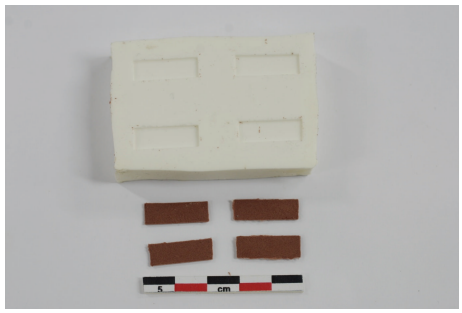

Figure 1: Fills after preparation in moulds.

is used for leather and pigment consolidation [14, 15]. The wax/resin is commonly used because it is easy to spread.

2.2. Accelerated Ageing. Samples of fillers were submitted to accelerate thermal ageing to evaluate their stability. The samples were submitted to 60°C for 113 hours at 85% relative humidity and 10°C for 168 hours and 20% relative humidity, in an APT Line KBF WTB Binder climatic chamber. Samples were removed after the ageing to perform their physicochemical measurements.

2.3. Physicochemical Measurements. The thermal techniques used for the evaluation of fills were thermogravimetric analysis (TGA) and dynamic mechanical thermal analysis (DMTA) because these techniques are sensitive to changes in ageing of materials. The selected ranging temperature (room temperature to 250°C) gives accurate indication of the inherent mechanical and chemical properties of the fills (softness, stiffness, molecular nature, movements of structure, etc.). The ability of the polymer chains to move past one another and adjust to a changed situation (mobility of chains, movements of molecular structure) may be also tested. The ranging temperature is an ideal way to test material and polymer for conservation purposes. It allows an evaluation of their properties.

Thermogravimetric analysis (TGA) was performed on a TGA Q50 model (TA Instruments) under synthetic air (60 mL·min^{-1}) from room temperature to 250°C, at 5°C·min^{-1} heating rate.

DMA measurements were carried out on sample films with a Q800 apparatus (TA Instruments) operating in tension mode. Experiments were performed at a frequency of 1 Hz and heating rate of 5°C·min^{-1} from 35 to 250°C. Typical dimensions of the samples were 6 mm × 20 mm × 1 mm. The setup provides the storage and loss modulus (E' and E'') and the damping parameter or loss factor is defined as $\tan\delta = E''/E'$. In fact the loss factor $\tan\delta$ is the ratio of loss modulus to storage modulus. It is a measure of the energy loss, expressed in terms of the recoverable energy, and represents mechanical damping or internal friction in a viscoelastic system. The loss factor $\tan\delta$ is expressed as a dimensionless number. A high $\tan\delta$ value is indicative of a material that has a high, nonelastic strain component, while a low value indicates a more elastic material. The storage data was normalized at 1000 MPa at 35°C.

Shearing tests were performed on Instron 1122 with applied force to 5 KN at room temperature with a rate of deformation of 0.5 mm·m^{-1}. These tests lead to study the adhesion and the resistance to failure of different composite fills. The shear was applied to the fill in the plane of the bond line. Typical dimensions of the samples were 20 mm × 10 mm. Sandwich specimens made for the tests constituted of two plates of beech between which was disposed filling material of 0.5 mm thickness. These specimens modeled infilling of extensive and large losses that penetrate deep into the object, that is, from the lacquer surface to wooden substrate of lacquerware. They modeled wooden substrate with losses of lacquer where a fill is required to bulk out large voids and fill losses in the surface and deeper areas. It means the fills but also the surrounding wood and their compatibilities were tested. The influence of the fill on the response of wooden substrate was also appreciated.

Contact angle measurements were performed using a DSA-P instrument (Kruss, Germany) and water. It is of prime importance to perform contact angle measurements with water. A main factor in the deterioration of Asian lacquer is its sensitivity to water. The surface of damaged lacquer may be soluble. Aqueous substances also cause discoloration. Lacquer should be exposed to water if preliminary tests have been carried out. Asian lacquer is often coated onto a number of layers (substrate, ground, and finishing layers). In many cases, many of these layers are water-soluble. The sensitive nature of lacquer to water must be taken into account during filling losses. Additionally, hygroscopic fillers may allow the fill to contract or expand with varying relative humidity.

One drop of water (25 μL, Millipore Ultrapure) was deposited on each polymer-composite sample. The static contact angle was measured by means of a Young-Laplace drop

profile fitting. The reported values correspond to the average of three measurements with an error bar corresponding to the standard deviation.

Microtopography was carried out on a station of STIL micromeasurements (model Micromesure) equipped with a CHR 150-N high resolution optical sensor. This non-destructive technique allows, starting from measurements of altitude variations, the calculation of the roughness of a surface at the microscale [4]. It is one of the very few non-contact techniques for 3D metrology recommended by the ISO 25178 international standard.

The selected parameters were as follows: optical pen 3000 μm, frequency of 300 Hz, scanned surface over a distance of 2.5 mm (x-axis) × 2.5 mm (y-axis), rate of 1000 μm·s^{-1}, and step size of 10 μm on x- and y-axis. The two-dimensional root-mean-square deviation of the profile, R_q, which demonstrates the root-mean-square value of the profile deviation compared to the line of reference of least squares, is expressed as:

$$R_q = \text{RMS} = \sqrt{\frac{1}{N}\sum_{i=1}^{N} y_i^2}, \quad (1)$$

where N represents the number of deviations taken into account.

3. Results and Discussion

3.1. Thermogravimetric Analysis. Thermogravimetric study of unaged fills was done. In order to study their thermal stability, the measurements were performed up to 250°C. As shown in Figure 2, all materials are stable up to 100°C and no weight loss is observed. A significant weight loss of 15% can be observed starting from 100°C for PVA/$CaCO_3$. This mass loss, which is water loss, is most likely due to the presence of water during the material preparation and can be observed up to 100°C. Furthermore a continuous weight loss is observed for the PB72/μphenolic ball fill probably due to the presence of solvent or monomer. Other materials are relatively stable up to 250°C.

In addition, a reference material was also analyzed under the same conditions, that is, a reference to the corresponding kuro-nakanuri lacquer. A mass loss of less than 5% was observed up to 250°C corresponding to the water used during the preparation of the sample. All of these materials are therefore stable in the 25 to 250°C temperature range.

Then, aged fills were also studied (Figure 3). In general, the aged materials have the same behavior as the unaged ones except PVA/$CaCO_3$. Indeed, no mass loss was observed in aged material. For PVA/$CaCO_3$, thermal ageing causes the elimination of volatile species, along with the removal of the preparation residual water.

All of these measurements show that polymer-composite fills and lacquer reference are relatively stable for use and storage between ambient temperature and 250°C. Moreover the accelerated ageing of these materials has no noticeable effect on their thermal stability. In conclusion, at this point of the study, it is difficult to promote a filler system compared to another.

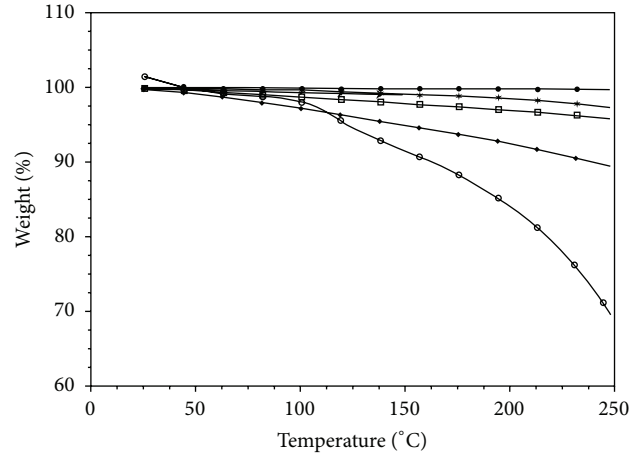

Figure 2: Behavior of weight loss for different unaged fills and reference: (●) Klucel G/$CaCO_3$, (◆) PB72/μphenolic balls, (∗) PB72/μglass beads, (o) PVA/$CaCO_3$, (➢) wax/resin, and (□) kuro-nakanuri lacquer.

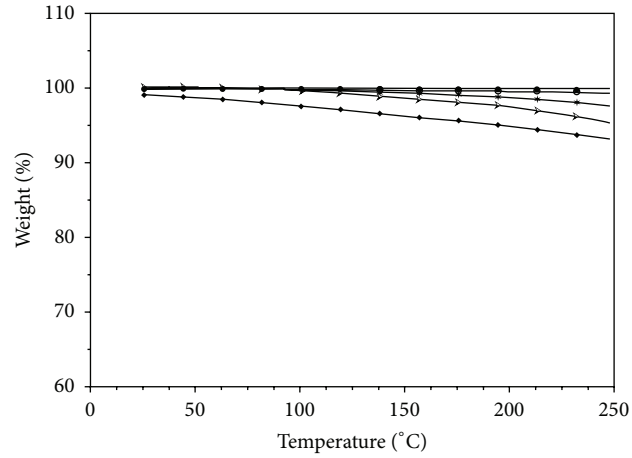

Figure 3: Weight loss of aged fills: (●) Klucel G/$CaCO_3$, (◆) PB72/μphenolic balls, (∗) PB72/μglass beads, (o) PVA/$CaCO_3$, (➢) wax/resin, and (□) kuro-nakanuri lacquer.

3.2. Dynamic Mechanical Analysis (DMA). DMA measurements were performed on unaged materials. Loss factor ($\tan\delta$) and storage moduli (E') are represented between ambient and about 250°C temperature in Figures 4 and 5. The maximum of loss factor corresponds to the α mechanical relaxation. The storage modulus E' is characteristic of the rigidity of the material, and this study used to compare the strength of the various fills.

Depending on the composition of the materials, some samples were not analyzed by this technique because of their fragility and brittleness: wax/resin which was very breakable, PVA/$CaCO_3$ with a high percentage of charges (75% of $CaCO_3$) influencing the mechanical properties of the filler compound and making it brittle.

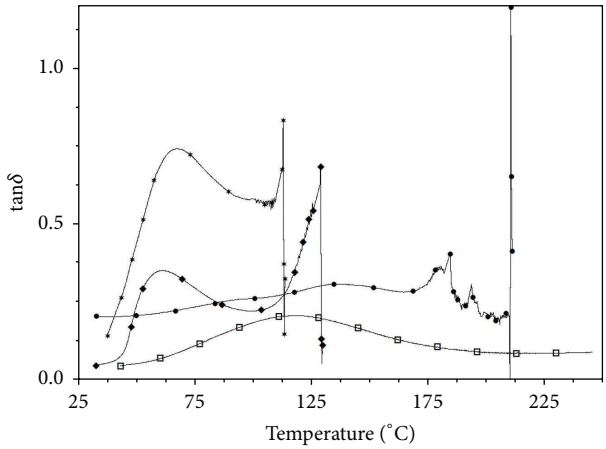

FIGURE 4: Mechanical relaxation temperature and loss factor of unaged fills: (●) Klucel G/$CaCO_3$, (◆) PB72/μphenolic balls, (∗) PB72/μglass beads, and (□) kuro-nakanuri lacquer.

The reference kuro-nakanuri lacquer shows a α mechanical relaxation temperature ($T\alpha$) of 119°C in Figure 4. Both of mixtures polyacrylates PB72/μphenolic balls and PB72/μglass beads have $T\alpha$ of 56°C and 66°C, respectively. These mechanical relaxation temperatures are in the range of values usually measured for non-cross-linked acrylate polymers [16]. Finally, the Klucel G/$CaCO_3$, a cellulose derivative, was described as having complicated thermomechanical spectra and damping at room temperature was distinctly higher than that of the other polymers [17]. The Klucel G/$CaCO_3$ fill does not exhibit a very marked mechanical relaxation. Only a small relaxation was detected at about 136°C with the presence of a shoulder at 100°C. This material is very rigid in a broad temperature range.

Figure 3 also presents maximal values of $\tan\delta$ at 0.21, 0.31, 0.36, and 0.74, respectively, for kuro-nakanuri lacquer reference, Klucel G/$CaCO_3$, PB72/μglass beads, and PB72/μphenolic balls. PB72/μphenolic balls have a high, nonelastic strain component contrary to the other fills and lacquer.

The values of storage moduli at 35°C are, respectively, 231, 393, 648, and 1034 MPa for PB72/μglass beads, PB72/μphenolic balls, Klucel G/$CaCO_3$, and kuro-nakanuri lacquer reference. This result confirms that the Klucel G/$CaCO_3$ is the most rigid material after the lacquer.

Secondly, all moduli were normalized to 1000 MPa at 35°C in order to be compared (Figure 5). Some materials have poor mechanical properties due to creep. The latter corresponds to the sliding of the polymer chains with respect to each other to break the material. This break is reflected by a significant drop in the storage modulus. At the same time, it is translated by the increase of $\tan\delta$ (Figure 4). Indeed the value of $\tan\delta$ varies from 0.31–0.36 to 1 for the Klucel G/$CaCO_3$ and PB72/μglass and from 0.74 to 1.5 for PB72/μphenolic balls. This is not observed for lacquer. The kuro-nakanuri lacquer does not creep unlike PB72/μphenolic balls, PB72/μglass beads, and Klucel G/$CaCO_3$. Thus the highly cross-linked lacquer will become more malleable from $T\alpha$ = 119°C but not even flow if the temperature reaches 250°C. Polyacrylate materials, respectively, flow to about 116°C for the PB72/μphenolic balls and 102°C for the PB72/μglass beads while the Klucel G/$CaCO_3$ creep temperature is around 172°C [18, 19]. A leading factor for the difference between two fills made of PB72 is likely the nature and the proportion of particle volume fraction in the dried material. Indeed there are 25% of μphenolic balls and 10% of μglass beads, respectively, in PB72/μphenolic balls and PB72/μglass beads. The density of the two charges is close according to the data suppliers, that is, 250 ± 20 g·L^{-1} for the μphenolic balls and 230 ± 20·L^{-1} for the μglass beads. As the volume fraction of μglass beads is lower (0.04%) than μphenolic balls (0.11%), it explains the lower modulus curve.

Thermomechanical results thus show that Klucel G/$CaCO_3$ is the material which has properties that are closest to the kuro-nakanuri lacquer reference. However, polyacrylates are also interesting because they can also be applied at temperatures below 100°C.

3.3. Shearing Test. A shearing test was carried out on the 8 wood-fill samples for each filler mixture. Table 2 displays the load at the break. The shearing tests aim to evaluate the mechanical behavior of fill. They also aim to evaluate the adhesion of the fill/wood system. The lacquer kuro-nakanuri reference was not tested because it is only used for more superficial levels.

All the tested fills showed a fragile behavior. Furthermore, all breaks were within the fills, except for one Klucel G/$CaCO_3$ specimen, indicating that they are strongly adhesive.

Concerning the wax/resin fill, no measurement could be obtained, because all the samples were easily fragmented into pieces before the test. It indicates this fill is more brittle than the other ones. This result confirms the DMA result.

Klucel G/$CaCO_3$ breaks at much less shearing load than the other tested fills but only two measurements were successful with this fill. In the other cases, the failure of the fill occurred before the test, indicating a weakness and stiffness.

PVA/$CaCO_3$ fill shows dispersed results with a high standard deviation, parallel to those obtained by DMA, because of the high proportion of carbonate charge. So as $CaCO_3$ is the major component, it influences the mechanical properties of the fill.

The two fills made of Paraloid were consistently strong with an average failure point at 650 N and 754 N, respectively, for PB72/μphenolic balls and PB72/μglass beads.

Previous shearing tests, not described in the present paper, were also carried out on test samples made of beechwood-filler compound-ground coating to the lacquer. The results were the same as the ones with the presented samples made of filler compound-beechwood.

These results show that three of the tested materials, that is, wax/resin, Klucel G/$CaCO_3$, and PVA/$CaCO_3$, are brittle or heterogeneous due to a high proportion of charge. So only the PB72 fills seem to be good candidates. The fills made of Paraloid B72 beads present a good adherence and fail first

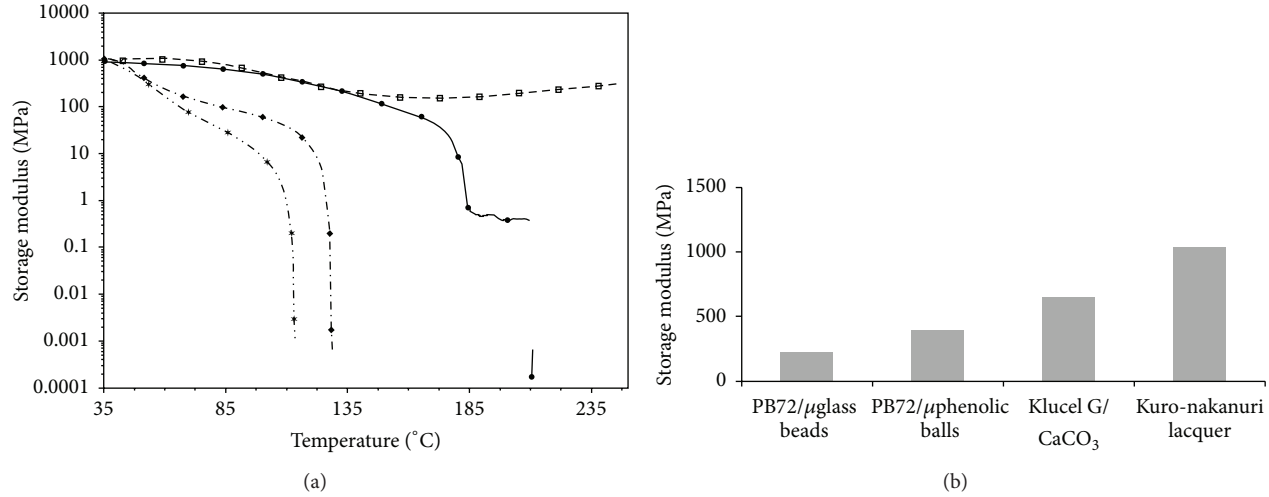

Figure 5: Storage modulus of unaged fills: (●) Klucel G/$CaCO_3$, (◆) PB72/μphenolic balls, (∗) PB72/μglass beads, and (□) kuro-nakanuri lacquer. (b) Storage modulus of fills normalized at 1000 MPa, 35°C, and 1 Hz.

Table 2: Shearing load at break.

Unaged fill	PB72/μphenolic balls	PB72/μglass beads	PVA/$CaCO_3$	Klucel G/$CaCO_3$	Wax/resin
Number of samples broken before the test	1	0	1	6	8
Average load at the failure (N)	650	754	453	153	/
Standard deviation	60	26	107	3	/

Table 3: Contact angle of a water drop on different polymer-composites.

Polymer-composite	Contact angle θ unaged material	Contact angle θ aged material
Wax/resin	99°	98°
PB72/μphenolic balls	73°	72°
PB72/μglass beads	117°	113°
Kuro-nakanuri lacquer	79°	74°
PVA/$CaCO_3$	Not measurable	Not measurable
Klucel G/$CaCO_3$	Not measurable	Not measurable

Table 4: Surface roughness, R_q.

Unaged Fill	R_q (μm)
Wax/resin	0.48
PB72/μphenolic balls	Not measurable
PB72/μglass beads	10.9
PVA/$CaCO_3$	3.9
Klucel G/$CaCO_3$	1.5
Kuro-nakanuri lacquer (aged)	0.9 (3)

before beech. In all tests, no failure occurred in the wood. They also present the highest load at failure among all the fills.

3.4. Contact Angle. To evaluate the influence of the composition of the polymer-composite materials, the wetting properties were investigated by measuring contact angles (Table 3). It is important to have a filler material with the best property of wetting with respect to water, for example. The unaged and aged materials were tested to determine the stability of surface properties.

For PVA/$CaCO_3$ and Klucel G/$CaCO_3$ samples, the contact angle could not be measured as the water drop was instantly absorbed. PVA is a hydrophilic polymer which is dissolved in water [20]. Cellulose derivatives are usually known to be hydrophobic due to the presence of hydroxyl groups. Moreover, no measurement was expected due to the strong presence of inorganic charges in materials [21].

The contact angle values depend on the polymer-composite composition. Conversely, for other materials, the drop did not spread and was still not absorbed after several minutes. The contact angles are between 73° and 117° for the unaged composites. As the unaged kuro-nakanuri lacquer reference (θ = 79°), the unaged PB72/μphenolic balls are slightly hydrophilic (θ = 73°). In contrast, the wax/resin and PB72/μglass beads are hydrophobic with a contact angle of 99° for the former and 117° for the latter. The presence of micro glass beads provides a more pronounced hydrophobic character to the polymer-composite.

Indeed, it has been shown in various studies that the presence of micro glass beads in PMMA polymers increases their hydrophobicity. Thus, Pareo et al. showed that a PMMA-based composite material loaded with hollow glass micro-sized spheres has a hydrophobic behavior [22]. In the study by Chibowski et al., the advancing and receding contact angles of water were measured on PMMA/glass sphere hollows (0.2 g·cm^3) deposited on glass surface by the spin

Table 5: Overall properties of tested fills.

	TGA test	DMA tests	Shearing tests	Contact angle	Roughness
Klucel G/$CaCO_3$	Stable	++++	+	+	++++
PB72/μphenolic balls	Stable	+++	++++	++++	++
PB72/μglass beads	Stable	+++	++++	+++	/
PVA/$CaCO_3$	Stable	+	+++	+	+++
Wax/resin	Stable	+	+	++++	++++

/ indicates the value was not measured.
+ indicates not satisfactory; ++ indicates moderately satisfactory; +++ indicates satisfactory; ++++ indicates highly satisfactory.

coating method [23]. A significant increase of 84° in the measurement of contact angle was observed between PMMA and PMMA/glass sphere hollows with values of the advancing contact angles of 28° for the former and 112° for the latter.

Finally unaged and aged materials have the same behavior. Thus the study of the wettability of the surface shows that two different filler materials Klucel G/$CaCO_3$ and PVA/$CaCO_3$ are not advised in the field of heritage restoration because of their high hydrophilicity. Taking into account the mechanical properties of all materials, at this point of the study, the two materials PB72/μphenolic balls and PB72/μglass beads are susceptible to being able to respond to the expected specifications. PB72/μphenolic balls have a surface wettability similar to kuro-nakanuri lacquer reference while the PB72/μglass beads have markedly improved surface properties.

3.5. Microtopography. The final phase of testing was to measure the surface roughness of the fills. Table 4 presents the value of root-mean-square deviation, R_q.

The filler compounds exhibit different values. But considering the variety of the charges such as glass microspheres, phenolic microballoons, calcium carbonate, and their proportion, these results are not surprising.

Wax/resin and Klucel G/$CaCO_3$ exhibit smooth surfaces. The PB72/μphenolic balls could not be measured due to a diffusion of the light. This fill is usually used for deeper gaps and is covered by another superficial filler compound. So the absence of measurement is not problematic.

The R_q value of the PB72/μglass beads is rather higher when compared to the other fills showing the influence of the granulometry of the micro glass beads.

Nevertheless, on the macroscopic scale, results less than or equal to 10 microns are all satisfactory and differences in R_q among tested filler compounds are negligible. They are also in the same range as the one of lacquer [4]. It means all the tested fills present a R_q value acceptable to be used without disfiguring the restored lacquerware.

4. Discussion

The aim of this research was to study the behavior of filler mixtures that are commonly used in the structural treatment of lacquerware.

In order to compare one fill to another easily, the results from the thermal tests, shearing tests wettability, and roughness are tabulated together (Table 5).

PVA/$CaCO_3$ is brittle and very sensitive to water, like Klucel G/$CaCO_3$, which may be inconsistent with conservation material. The fills made of Paraloid B72 meet basic criteria for conservation materials, that is, stability to humidity and temperature change in terms of stiffness, strength, resistance, and reversibility. Their lower rugosity compared to other fills is nevertheless satisfactory because it is out of the range of visual appreciation. In all tests, no wood damage occurred as failure was in the fill.

5. Conclusion

The aim was to compare the behavior of some representative materials of fillers used in the conservation-restoration of lacquerware. Fills were judged on their thermal, mechanic, and surface properties rather than qualitative factors of appreciation. The study yielded much useful information and revealed the limitations of several gap-filler materials.

All tested fills are stable from a thermal point of view. So they can be used as restoration materials of lacquerware in the cultural heritage. However, wax/resin and PVA/$CaCO_3$ appeared to be very brittle materials and they are not advised. In fact, the lacquerware can be submitted to dimensional variations, especially when the support is porous as wood, paper, bamboo, and so on. In such cases, these fills could not support the subsequent shrinkage or dilation.

Klucel G/$CaCO_3$ presents better mechanical properties, close to the kuro-nakanuri lacquer reference. Nevertheless, its wettability property is poor with a high hydrophilicity. It means the material cannot support ulterior cleaning interventions.

Finally fills made of ethyl methacrylate and methyl acrylate copolymer hold a strong potential. They are stable up to 250°C and easy to spread and are good adhesive. The PB72/μphenolic balls have a wettability similar to the kuro-nakanuri lacquer. The PB72/μglass beads present the advantage of high hydrophobicity. So these two fills show required criteria to be used in conservation-restoration of historical lacquer objects.

Future studies will need to be carried out to follow up the behavior of the treated Asian lacquerware with PB72/μphenolic balls and PB72/μglass beads. They will allow

the full appreciation of the long-term stability of the fills under museum conditions.

Disclosure

This work was conducted as part of a diploma of restorer of heritage, furniture speciality, at the Institut National du patrimoine.

Conflict of Interests

The authors declare that there is no conflict of interests regarding the publication of this paper.

Acknowledgments

Anne Genachte-Le Bail and Sigrid Mirabaud of the Institut National du patrimoine are kindly acknowledged for their support. The authors acknowledge the support from the Laboratoire de Recherche des Monuments Historiques (Champs-sur-Marne) for the shearing tests. The authors thank Mathilde Thienot for helpful discussion.

References

[1] Y. Kamiya, R. Lu, T. Kumamoto, T. Honda, and T. Miyakoshi, "Deterioration of surface structure of lacquer films due to ultraviolet irradiation," *Surface and Interface Analysis*, vol. 38, no. 9, pp. 1311–1315, 2006.

[2] C. Mc Sharry, R. Faulkner, S. Rivers, M. S. P. Shaffer, and T. Welton, "The chemistry of East Asian lacquer: a review of the scientific literature," *Reviews in Conservation*, vol. 8, pp. 29–40, 2007.

[3] T. Ogawa, K. Arai, and S. Osawa, "Light stability of oriental lacquer films irradiated by a fluorescent lamp," *Journal of Environmental Polymer Degradation*, vol. 6, no. 1, pp. 59–65, 1998.

[4] A.-S. Le Hô, C. Duhamel, C. Daher et al., "Alteration of Asian lacquer: in-depth insight using a physico-chemical multiscale approach," *Analyst*, vol. 138, no. 19, pp. 5685–5696, 2013.

[5] Y. Yamashita, "The plan for the conservation of the Mazarin chest," in *Proceedings of the International Course on Conservation of Japanese Lacquer in the Role of Urushi in International Exchange: 27th International Symposium on the Conservation and Restoration of Cultural Property*, pp. 159–170, Tokyo National Research Institute for Cultural Property, Tokyo National Museum, Tokyo, Japan, December 2003.

[6] M. Webb, "Methods and materials for filling losses on lacquer objects," *Journal of the American Institute for Conservation*, vol. 37, no. 1, pp. 117–133, 1998.

[7] M. S. Podmaniczky, "Structural fills for large wood objects: contrasting and complementary approaches," *Journal of the American Institute for Conservation*, vol. 37, no. 1, pp. 111–116, 1998.

[8] J. Thornton, "A brief history and review of the early practice and materials of gap-filling in the west," *Journal of the American Institute for Conservation*, vol. 37, no. 1, pp. 3–22, 1998.

[9] S. Lambooy, "Lacquer on Japanese porcelain: a case study of two Imari vases with urushi lacquer decoration from the collection of the Rijksmuseum Amsterdam," in *Proceedings of the 14th Triennal Meeting*, International Council of Museums Conservation Committee, Ed., vol. 2, pp. 1075–1082, The Hague, The Netherlands, September 2005.

[10] M. H. Carr, "Lacquer loss compensation revisited: more big holes in the top," in *Postprints of the Wooden Artifacts Group, 31st Annual Meeting of the American Institute for Conservation, June 2003*, pp. 59–65, AIC, Arlington, Tex, USA, 2003.

[11] S. Fukuda, "Japanese lacquered albums, an appraisal of their development, construction and repair," *Bookbinder*, no. 23, pp. 35–45, 2009.

[12] V. Horie, "Acrylic polymers," in *Materials for Conservation*, p. 159, Elsevier, Oxford, UK, 2nd edition, 2010.

[13] R. L. Feller, "Standards in the evaluation of thermoplastic resins," in *5th Triennal Meeting: Zagreb, 1-8 October 1978: Preprints*, vol. 3, pp. 78/16/4/1–78/16/4/11, International Council of Museums Conservation Committee, Zagreb, Croatia, 1978.

[14] J. H. Hofenk de Graaff, "Hydroxy propyl cellulose, a multipurpose conservation material," in *Proceedings of the 6th Triennal Meeting*, International Council of Museums Conservation Committee, Ed., vol. 3, pp. 81/14/9-1–81/14/9-7, Ottawa, Canada, September 1981.

[15] K. St. John, "Survey of current methods and materials used for the conservation of leather bookbindings," AIC Book and Paper Group Annual 19, 2000.

[16] J. Brandrup, E. H. Immergut, E. A. Grulke, A. Abe, and D. R. Bloch, *Polymer Handbook*, John Wiley & Sons, New York, NY, USA, 2005.

[17] P. Sakellariou, R. C. Rowe, and E. F. T. White, "The thermomechanical properties and glass transition temperatures of some cellulose derivatives used in film coating," *International Journal of Pharmaceutics*, vol. 27, no. 2-3, pp. 267–277, 1985.

[18] R. F. Landel and L. E. Nielsen, *Mechanical Properties of Polymers and Composites*, CRC Press, Marcel Dekker, New York, NY, USA, 1994.

[19] Klucel hydroxypropylcellulose in hot-melt extrusion applications, Aqualon, Ashland, http://www.ile.com.cn/UpLoad/file/20137231551131402013072303511314O.pdf.

[20] K.-J. Kim, S.-B. Lee, and N.-W. Han, "Effects of the degree of crosslinking on properties of poly(vinyl alcohol) membranes," *Polymer Journal*, vol. 25, no. 12, pp. 1295–1302, 1993.

[21] O. Gordobil, I. Egüés, I. Urruzola, and J. Labidi, "Xylan-cellulose films: improvement of hydrophobicity, thermal and mechanical properties," *Carbohydrate Polymers*, vol. 112, pp. 56–62, 2014.

[22] P. Pareo, G. L. De Gregorio, M. Manca et al., "Ultra lightweight PMMA-based composite plates with robust super-hydrophobic surfaces," *Journal of Colloid and Interface Science*, vol. 363, no. 2, pp. 668–675, 2011.

[23] E. Chibowski, L. Hołysz, K. Terpilowski, and M. Jurak, "Investigation of super-hydrophobic effect of PMMA layers with different fillers deposited on glass support," *Colloids and Surfaces A: Physicochemical and Engineering Aspects*, vol. 291, no. 1–3, pp. 181–190, 2006.

Hindawi Publishing Corporation
International Journal of Polymer Science
Volume 2015, Article ID 782843, 7 pages
http://dx.doi.org/10.1155/2015/782843

Research Article

Polymerization of Oriental Lacquer (Urushi) with Epoxidized Linseed Oil as a New Reactive Diluent

Takahisa Ishimura[1] and Takashi Yoshida[1,2]

[1]*Department of Bio and Environmental Chemistry, Kitami Institute of Technology, 165 Koen-cho, Kitami 090-8507, Japan*
[2]*Research Center for Environmentally Friendly Materials Engineering, Muroran Institute of Technology, 27-1 Mizumoto-cho, Muroran, Hokkaido 050-8585, Japan*

Correspondence should be addressed to Takashi Yoshida; yoshida@chem.kitami-it.ac.jp

Received 24 February 2015; Accepted 31 May 2015

Academic Editor: Wen Shyang Chow

A hybrid lacquer (HBL) paint prepared by combining a natural kurome lacquer (KL) paint and an amino silane reagent, for example, *N*-(2-aminoethyl)-3-aminopropyl triethoxysilane (AATES), produced a polymerized film faster than the KL paint alone. However, the viscosity of the HBL paint was too viscous for easy handling. Addition of 10 wt% of an epoxidized linseed oil, ELO-6, with 6.4 mol% epoxidation as a reactive diluent to the HBL paint decreased the viscosity by 1/2 from 25476 mPa·s to 12841 mPa·s and improved the ease of coatability. The polymerization mechanism was elucidated by NMR measurements of extracts from the resulting polymerization films, suggesting that amino groups in the HBL paint reacted with epoxy groups of ELO-6 in the lacquer matrix, and then the complex reacted with double bonds of the urushiol side-chain by autooxidation and cross-linking reactions to give a hard polymerized film with a high quality of color and gloss. These results indicate that the addition of ELO-6 improved the polymerizability of both KL and HBL paints without decreasing the quality of the resulting films.

1. Introduction

Oriental lacquer (urushi) sap collected from lacquer trees has traditionally been the only natural product that is polymerized by an enzyme, laccase, without any volatile compounds to give a cross-linked polymerized film. Therefore, the lacquer has been used as a natural coating material for containers, tableware, and furniture with high durability and a beautiful glossy surface for more than several thousand years in Japan and other Asian countries [1–3]. Natural lacquer is also expected to be an environment-friendly paint for the next generation.

Lacquer trees are of Asian origin and are known to comprise mainly three species, *Rhus verniciflua* in East Asia (Japan, China, and Korea), *Rhus succedanea* in South Asia (Vietnam and Taiwan), and *Melanorrhoea usitata* in South East Asia (Thailand, Cambodia, and Myanmar) [1, 2]. The lacquer tree sap is a W/O type emulsion and consists of lipids (urushiol, laccol, and thiol) as the main components, acetone-insoluble components (polysaccharides, glycoproteins, and enzymes) as emulsifiers and dispersing agents, and water [4].

In the polymerization of lacquer, urushiol, which is a mixture of 3-alkenylcatechols, is radically polymerized by laccase in the first stage, and then the polymer is autooxidized by air in the second stage to give cross-linked polymers [5–7]. However, the polymerization is affected by temperature and humidity, and the polymerization conditions are limited; that is, 30°C temperature and 70% humidity are necessary over a polymerization time of more than one month. The moisture is necessary for the reoxidation of laccase in the polymerization films with oxygen in the air. Furthermore, the autooxidation in the second-stage polymerization is inhibited by the phenolic hydroxyl groups of the catechol ring. These phenolic hydroxyl groups, which act as an antioxidant, are decreased by the enzymatic oxidation in the first-stage polymerization, and this polymerization obstructs contact

with unsaturated side-chains [8]. Therefore, a long time is necessary to complete polymerization.

Recently, we developed a hybrid lacquer (HBL) paint to improve the polymerizability of kurome lacquer (KL) paint [9]. When an amine-functionalized organic silane compound (amino silane regent), *N*-(2-aminoethyl)-3-aminopropyl trimethoxysilane (AATMS), *N*-(2-aminoethyl)-3-aminopropyl triethoxysilane (AATES), or *N*-(2-aminoethyl)-3-aminopropyl methyl dimethoxysilane (AAMDMS), was added to the KL paint, the polymerization time was shortened to 6 h in humidity below 55% and temperature at 20°C [10, 11]. Therefore, the HBL paint is expected to increase the production of lacquer wear. However, the HBL paint had higher viscosity than the original KL paint due to the increase of polymerized and polycondensed compounds in the first-stage polymerization [12]. Viscosity of lacquer paint, in general, decreases the handling properties compared to that of other coating methods of spraying, dipping, and painting by brush.

Plant oil, linseed oil, has been often used as a diluent to decrease the viscosity of lacquer paint and to increase the gloss of the resulting polymerized lacquer film [13, 14]. After polymerization, however, linseed oil sometimes oozes out of the polymerized film. Thus, improvements in polymerizability are required for the general use of lacquer paints and materials in the future. In this paper, we report a new reactive diluent prepared by the epoxidation of linseed oil [15–21]. We found that the epoxidized linseed oil ELO-6 with 6.4 mol% epoxidation worked effectively in polymerization of both HBL and natural KL paints without any volatile components. The drying properties and hardness after polymerization of the HBL and KL paints with epoxidized linseed oils as reactive diluents are reported. The polymerization mechanism of HBL and KL paints with the epoxidized linseed oil was evaluated by NMR measurements of acetone extracts from the corresponding polymerization films.

2. Materials and Methods

2.1. Materials. Kurome lacquer (KL) paint was purchased from Dohichu Shoten (Osaka, Japan). The KL paint used here was composed of urushiol (89.6%), water (4.1%), and acetone-insoluble compounds (6.3%) such as polysaccharides, glycoprotein, and laccase. *N*-(2-aminoethyl)-3-aminopropyl triethoxysilane (AATES) was obtained from Shin-Etsu Silicone Co. Ltd. (Tokyo, Japan). The linseed oil (LO) used was reagent grade.

2.2. Measurements. The drying of lacquer paints was evaluated by using drying time recorder (Taiyu Equipment, Osaka, Japan) according to the JIS-K-5400 standards. The hardness of polymerized films was determined using mechanical pencil hardness tester (Yoshimitsu Seiki, Tokyo, Japan) according to the JIS-K-5600 standards. Viscosity was measured by Brookfield cone-plate type viscometer DV-II+. The 500 MHz ^{1}H NMR spectrum in $CDCl_3$ as a solvent at 25°C was obtained by using JEOL JNM-ECA500 spectrometer with tetramethylsilane as a reference (0.00 ppm). Color scales of polymerization films were determined by the color standard ($L^*a^*b^*$ system) using BYK-Gardner Gmbh colorimeter (Germany). Spectroguide 45/0 was used. The symbols, L^*, a^*, and b^*, mean brightness and the ratios of red (+) to green (−) and yellow (+) to blue (−), respectively. The gloss of the polymerized films was measured by a gloss meter PG-1M (Nippon Denshoku, Japan). Thermogravimetric analysis (TGA) of the polymerized films was performed using Shimadzu DTG-60 thermoanalyser at the heating rate of 10°C/min under N_2 atmosphere. The glass transition temperature ($\tan\delta$) of polymerization films was recorded using a rigid-body pendulum-testing machine RPT-3000W (A&D Co., Ltd., Japan).

2.3. Synthesis of Epoxidized Linseed Oil [21]. A typical procedure for the epoxidation of linseed oil, ELO-6, with 6.4 mol% epoxidation is as follows. To a solution of linseed oil (44.0 g, 50.0 mmol) in $CHCl_3$ (150 mL) were added 0.6 g of phosphotungstic acid (0.02 mmol) and 0.215 g of cetylpyridinium chloride (0.06 mmol). After 30% hydrogen peroxide solution (5.67 g, 50.0 mmol) was added, the mixture was refluxed for 6 hours with vigorous stirring. After cooling to room temperature, the separated $CHCl_3$ layer was washed by distilled water twice and then dried over anhydrous sodium sulfate. After filtration and evaporation to remove sodium sulfate and $CHCl_3$, respectively, epoxidized linseed oil (ELO-6) (42.0 g) with 6.4 mol% epoxidation was obtained in 95% yield. The epoxidized linseed oil was used without further purification.

2.4. Polymerization of Hybrid Lacquer Paint with ELO-6. To the KL paint (10.0 g) was added 1.0 g of epoxidized linseed oil (ELO-6) as a reactive diluent. The mixture was stirred for 30 min at room temperature and then 0.5 g of hydrolyzed AATES that had been prepared by addition of water was added. The mixture was further stirred for 30 min and then coated at 76 μm thickness on a glass plate by using a film applicator. The lacquer-coated glass plate was maintained at 25°C under 60% humidity for the enzymatic and autooxidative polymerization.

2.5. Extraction of Polymerization Films by Acetone. To investigate the polymerizability of epoxidized linseed oil (ELO-6), the polymerization films of the KL paint with ELO-6 and AATES after polymerization for 2 h, 24 h, and 168 h (7 days), respectively, were extracted by acetone. The extracts were identified by the ^{1}H NMR measurements. The results are shown in Figure 3.

3. Results and Discussion

3.1. Synthesis of Epoxidized Linseed Oils. In general, a small amount of oil of linseed (*Linum usitatissimum*) is used as a diluent of KL paint to decrease the viscosity and improve the gloss of the surface of the polymerized film. However, linseed oil often oozes out of the polymerization film. Therefore, epoxidized linseed oils as a new reactive diluent were synthesized by the epoxidation of linseed oil with hydrogen peroxide (H_2O_2) and heteropoly acid-CPC system as a catalyst. Table 1 shows the viscosity of the KL

Table 1: Viscosity of kurome lacquer paint with epoxidized linseed oil.

Number	Epoxidized linseed oil			Viscosity of mixture[b] mPa·s
		Degree of epoxidation[a] %	Viscosity mPa·s	
1	ELO-6	6.4	51.4	2382
2	ELO-25	24.8	109.9	3866
3	ELO-43	42.6	183.1	4246
4	ELO-100	100	601.7	6904
5	LO	—	51.0	2983[c]
6	None		—	4598

[a]The degree of epoxidation was calculated from ^{1}H NMR spectra.
[b]Epoxidized linseed oils (ELO) were mixed in the kurome lacquer (KL) paint in the weight proportion of 1 : 10 and then viscosity was measured by the DV-II+ viscometer at room temperature.
[c]Phase separation occurred.

Table 2: Polymerization of lacquer paints with epoxidized linseed oil ELO-6.

Number	Paint[a]			Polymerization time[b]		Polymerization film after 7 days[c]							
	ELO-6		Viscosity	TF	HD	Pencil	Color scale			Gloss	T_g	Weight loss at 20%	Residue at 600°C
			mPa·s	h		hardness	L^*	a^*	b^*	60°	°C	°C	%
1	KL	—	4598	4.4	8.6	HB	3.41	13.00	4.41	88.5	90.1	406	0.8
2	KL	◯	2382	2.3	3.8	F	1.39	5.42	1.78	84.3	95.5	377	17.7
3	HBL	—	25476	1.2	2.0	F	0.95	0.61	0.56	76.2	101.8	419	29.6
4	HBL	◯	12841	1.1	2.0	F	0.59	0.38	9.47	86.9	131.8	380	28.7

[a]The KL (kurome lacquer) and HBL (hybrid lacquer) paints with ELO-6 (6.4 mol% epoxidation) were prepared in the weight proportions as follows.
KL: EOL-6 = 10 : 1 for number 2, KL: hydrolyzed AATES = 10 : 1 for number 3, and KL : hydrolyzed AATES : ELO-6 = 10 : 1 : 0.25 for number 4, respectively.
Viscosity was measured by the DV-II+ viscometer at room temperature.
[b]Polymerization time was measured by touch-free (TF) polymerization state and hard (HD) polymerization state under 20–25°C at 55–60% humidity.
[c]Pencil hardness was recorded by the JIS-K 5400 drying recorder. Color scale was measured by the BYK-Gardner according to the spectro-guide 45/0.
L^* means brightness, a^* means +red/−green, and b^* means +yellow/−blue, respectively. The gloss (60°) of polymerized film was obtained by the PG-1M glossmeter.
The glass transition temperature (T_g) measurement was carried out with the RPT-3000W rigid-body pendulum-testing (RPT) machine.
Temperature of weight loss at 20 wt% and residue at 600°C were recorded by the DTG-60 thermoanalyser at the heating rate of 10°C under N_2 atmosphere.

paint with ELOs in the weight proportion of 10 : 1. The viscosity of the KL paint was 4598 mPa·s (number 6). Linseed oil decreased its viscosity to 2983 mPa·s (number 5), but a phase separation occurred at that proportion. When ELO-6 with 6.4 mol% epoxidation was used, the viscosity of the KL paint was found to decrease to 2382 mPa·s (number 1), and no phase separation occurred at that proportion. The viscosity of the KL paint increased gradually as the degree of epoxidation of the added linseed oil increased. ELO-43 (number 1) with 43 mol% epoxidation gave almost the same viscosity (4246 mPa·s) as that of the KL paint (4598 mPa·s), as shown in number 6, and phase separation occurred. With proportions of ELOs higher than 10 wt% being added to the KL paint, a phase separation of the KL paint occurred except with ELO-6. Therefore, ELO-6 was used as a reactive diluent for both KL and HBL paints in this work.

3.2. Polymerization of KL and HBL Paints with ELO-6. Table 2 shows the results of polymerization of the KL and HBL paints with and without ELO-6. The polymerization times of the paints and the color and gloss of the resulting polymerized films were quantitatively compared to those of the polymerized film of the KL paint. The glass transition temperature and thermostability were also compared. The HBL paint that was obtained from the KL paint and hydrolyzed AATES in the weight proportion of 10 : 0.5 had high viscosity of 25476 mPa·s, so that the HBL paint could not be used directly as paint. When 10 wt% of ELO-6 was added to both KL and HBL paints in the proportion of 1 : 10 (numbers 2 and 4), the viscosities decreased by half of the original to 2382 and 12841 mPa·s, respectively, suggesting that ELO-6 worked effectively as a diluent.

The paint was coated on a glass plate at 76 μm thick by using a film applicator and then the polymerization time and pencil hardness were measured after polymerization. The original KL paint (number 1) was polymerized to touch-free (TH) and hard (HD) polymerization states in 4.4 and 8.6 h, respectively, as measured by the drying time recorder. Addition of ELO-6 to the KL paint accelerated the polymerization time to half in both touch-free (TH) and hard (HD) polymerization states (number 2). For the HBL paint (number 4), the polymerization time was the same whether or not ELO-6 was added, because the polymerization rate of the HBL paint was originally fast, but the viscosity of the HBL

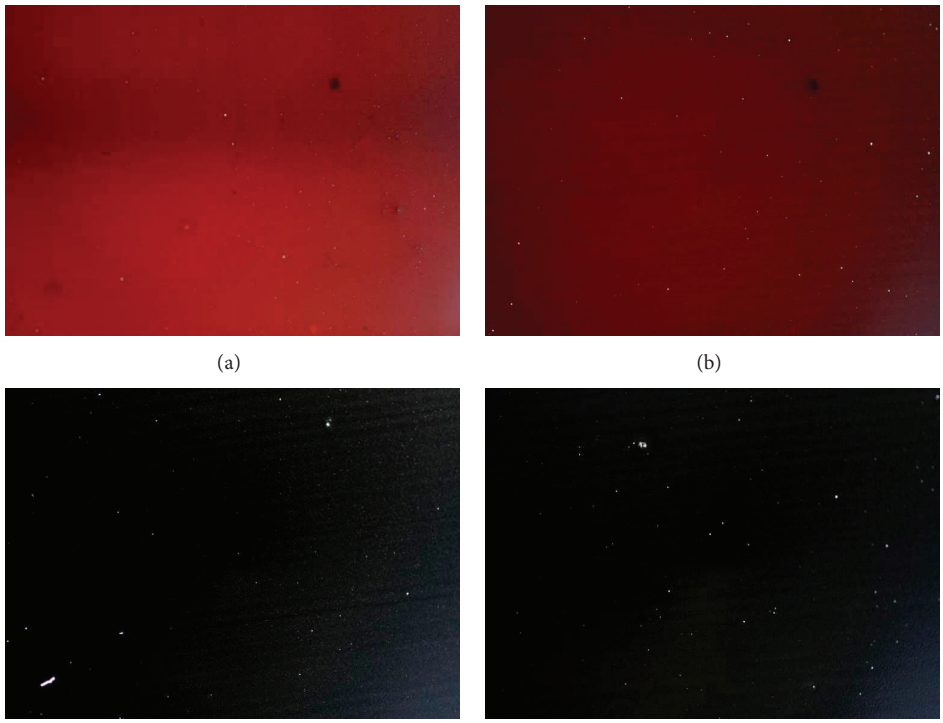

Figure 1: Polymerized films of the KL and HBL paints. (a) KL paint, (b) KL paint with ELO-6 at 10 : 1 by weight, (c) HBL paint, and (d) HBL paint with ELO-6 at 10 : 1 by weight.

paint without ELO-6 was too high (number 3). These results indicate that ELO-6 increased the polymerizability of both KL and HBL paints and decreased the viscosity. After 7 days, the pencil hardness of the polymerized films (numbers 2–4) reached F.

The color scale, gloss, and thermal properties of the polymerized films were also measured and are shown in Table 2. The color scale was evaluated quantitatively by the brightness (L^*), red-green (a^*), and yellow-blue (b^*) proportions, respectively, using the BYK-Gardner apparatus. Larger numbers mean stronger proportions of brightness, red, and yellow, respectively. Figure 1 shows photos of polymerized films of the KL and HBL paints, in which Figure 1(a) is the polymerized film of the KL paint, Figure 1(b) is the KL paint with ELO-6 in the proportion by weight of 10 : 1, Figure 1(c) is the HBL paint, and Figure 1(d) is the HBL paint with ELO-6 in the proportion by weight of 10 : 1. For the KL paint (number 1 in Table 1), the values of color scale were relatively large, and the polymerized film seems to be light brown with a little red, as shown in Figure 1(a). For the HBL paint (number 3), the values were smaller, and the polymerization film showed a black color (Figure 1(c)). Addition of ELO-6 made the color slightly deeper as shown in Figures 1(b) and 1(d), respectively. The surface of the polymerized films (numbers 2–4) remained glossy because they had almost the same gloss values as the film of the KL paint (number 1).

The glass transition temperature (T_g) of the films was measured by the rigid-body pendulum-testing apparatus,

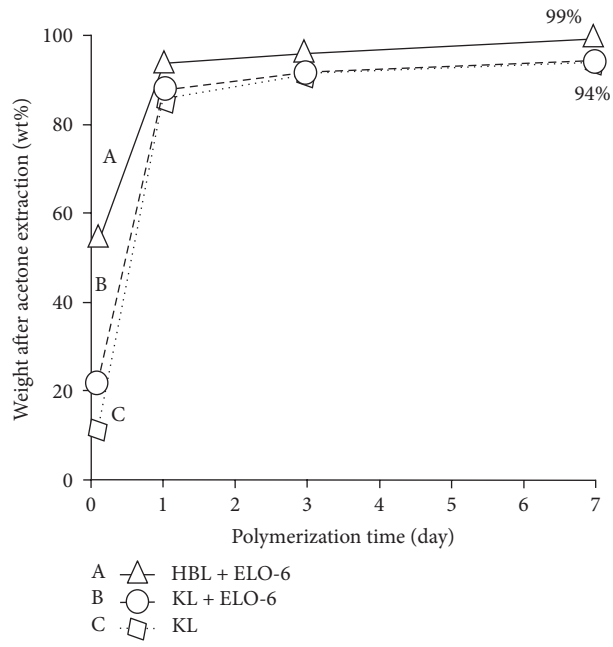

Figure 2: Extraction of polymerized film by acetone. After 7 days of polymerization, the weight of the film of the HBL paint with ELO-6 in the weight proportion of 10 : 1 remained at more than 99 wt% after extraction with acetone, suggesting that the HBL paint with ELO-6 was completely copolymerized.

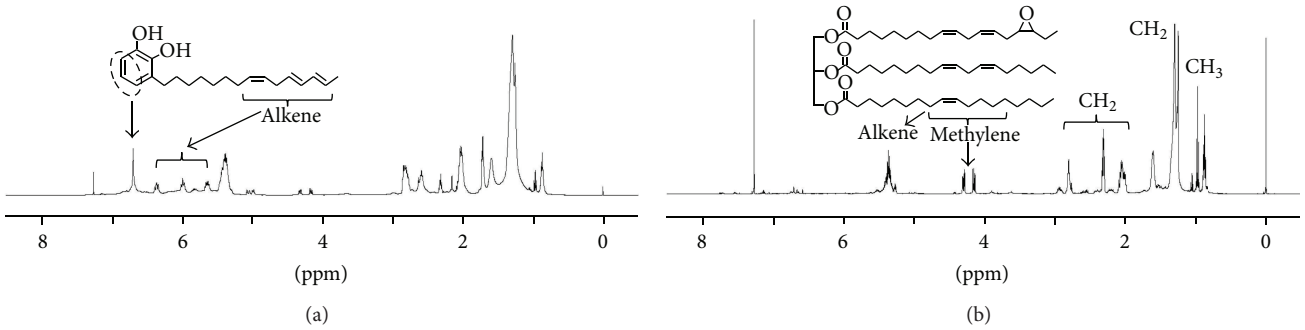

Figure 3: 500 MHz ^{1}H NMR spectra of acetone extracts from polymerization films after (a) 2 h and (b) 24 h polymerization, respectively. The polymerization of the KL paint was carried out with ELO-6 in the weight proportion of 10 : 1. The spectra were obtained in $CDCl_3$ as solvent at 30°C.

and the temperature of the loss of 20% weight and residual weights at 600°C were analyzed by the DTG thermal analyzer. The film of the HBL paint with ELO-6 (number 4) had the highest T_g of 131.8°C and 20% of the weight was lost at 377° (number 2) and 380°C (number 4). We found that the HBL films with and without ELO-6 showed the highest thermal stability and the residues at 600°C still remained at 29.6% and 28.7% of the feed, respectively. One of the reasons why the thermal stability increased was assumed to be that the complex cross-linking which occurred radically between urushiol, the amino silane coupling reagent, epoxy group, and unsaturated double bonds of side-chains in ELO-6 by the autooxidation by air in the second stage of lacquer polymerization. The polymerization films gave no acetone extracts as described below.

3.3. Estimated Polymerization Mechanism. To elucidate the polymerization mechanism of the KL and HBL paints with ELO-6, acetone extraction of the resulting films was performed 2 h and 24 h after coating on the glass plate. Figure 2 shows the weights of polymerization films after acetone extraction. The films of the KL paint with and without ELO-6 had weight loss of 6%. No weight loss of the film of the HBL paint with ELO-6 was observed. The structure of the acetone extracts from the polymerized film of the KL paint with ELO-6 was analyzed by the NMR measurement as shown in Figure 3. After 2 h polymerization, urushiol was the main extract and small signals due to ELO-6 appeared (Figure 3(a)); however, after 24 h, urushiol was completely polymerized and only ELO-6 was detected from the film of the KL paint with ELO-6 (Figure 3(b)). Polymerization of urushiol proceeds by two reaction stages; the first stage is the reaction by laccase to obtain urushiol oligomers and then, in the second stage, autooxidation by air occurred to afford cross-linked polymers. Based on the polymerization time of the KL paint with ELO-6, the double bonds of ELO-6-amino silane reagent-urushiol complex **2**, as shown in Scheme 1, also reacted with urushiol double bonds in the second-stage polymerization to give cross-linked lacquer polymers composed of urushiol, amino silane reagent, and linseed oil. On the other hand, no extracts were obtained from the HBL paint with ELO-6 after 2 h and 24 h polymerization, indicating that ELO-6 reacted with the HBL paint to give a copolymerized film that consisted of HBL and ELO-6 units.

Scheme 1 illustrates the proposed polymerization mechanism of the HBL paint with ELO-6. Based on the recent results on the polymerization of the HBL paint [11], the alcoholysis reaction of the amino silane reagent, *N*-(2-aminoethyl)-3-aminopropyl trialkylsilane, with a hydroxyl group of urushiol occurred rapidly to give hybrid product **1** and then the next urushiol continuously reacted with **1** to give hybrid oligomers. At the same time, enzymatic polymerization of urushiol by laccase and the subsequent autooxidation by air formed cross-linked polymerized film in shorter time than the polymerization of the original KL paint. On the other hand, the amino group of hybrid product **1** also reacted with the epoxy group of ELO-6 to produce product **2** by a covalent bond, which was polymerized in the lacquer emulsion containing urushiol oligomers **2** by the autooxidation by air to give the cross-linked polymerized films. Therefore, no acetone extracts were obtained from the HBL film with ELO-6, as shown in Figure 2.

4. Conclusion

The epoxidized linseed oil ELO-6 with 6.4 mol% epoxidation was found to work effectively as a reactive diluent in the HBL paint matrix. The viscosity and polymerization time of the HBL paint with ELO-6 decreased to half compared to those of the original HBL paint and polymerized films with pencil hardness of F were obtained. The surface was almost as glossy as that of the film polymerized by the original KL paint. The polymerization mechanism was shown by the NMR measurements of the acetone extracts of the polymerized films of the KL and HBL paints with ELO-6 after 2 h and 24 h, suggesting that the HBL paint reacted quickly with ELO-6 to give a polymerized film with hard and glossy surface. On the other hand, the reaction of the KL paint with ELO-6 was slow. These results indicate that the amino group of the HBL paint reacted rapidly with the epoxy group of ELO-6 and then the autooxidation by air occurred to produce the cross-linked polymerized film. Major difference of current and other papers is that our method gave both short polymerization time of urushiol and glossy polymerized surface of oriental

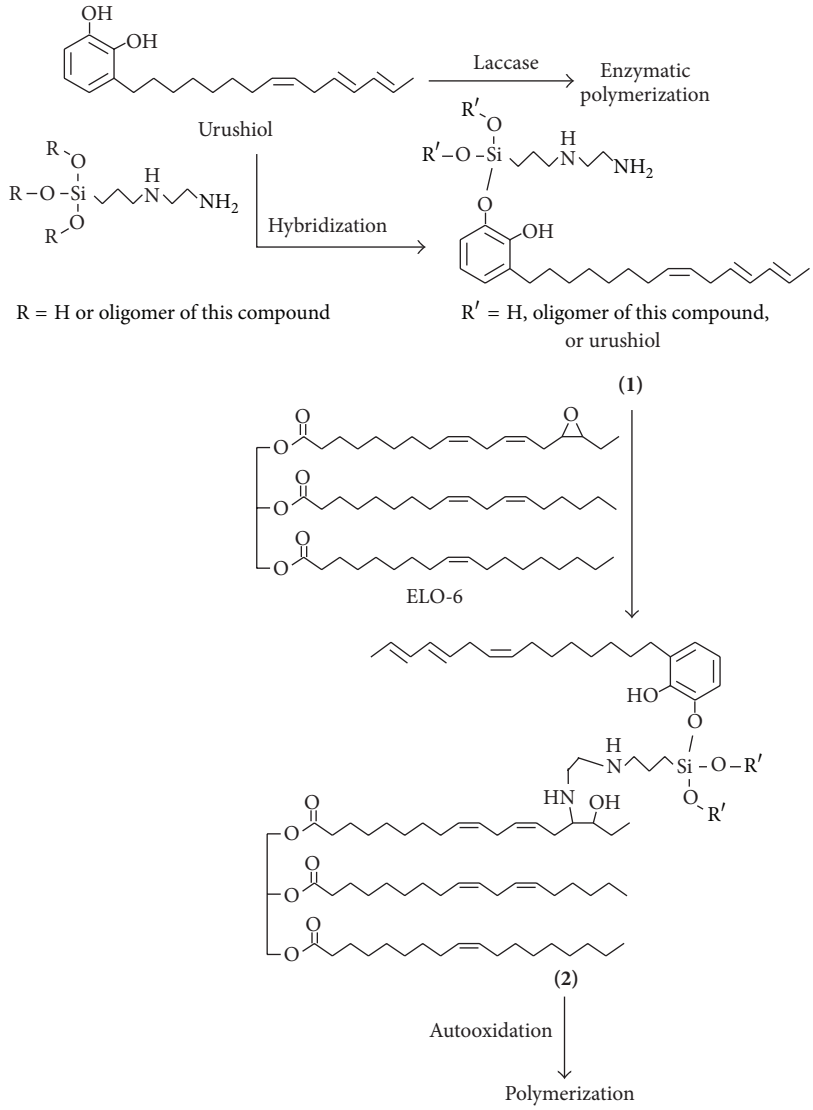

Scheme 1: Proposed polymerization mechanism of HBL paint with the epoxidized linseed oil ELO-6. The proportions of amino silane reagent and ELO-6 were 2.5 and 10 mol% of the KL paint, respectively.

lacquer by addition of alkoxy aminosilane compounds and reactive epoxidized linseed oil. Further studies to elucidate the polymerization mechanism and development of a new lacquer material are now under investigation.

Conflict of Interests

The authors declare that there is no conflict of interests regarding to the publication of this paper.

Acknowledgments

The authors are sincerely grateful to Professor T. Miyakoshi and Dr. R. Lu of Meiji University for many discussions and help in this work. This work was partly supported by the Academic Frontier Project for Private Universities, a matching fund subsidy from MEXT (2007–2011), the New Energy and Industrial Technology Development Organization (NEDO) of Japan, Research Project Grant B by Institute of Science and Technology, Meiji University, and Research Project Grant for Youth, Meiji University.

References

[1] J. Kumanotani, "Urushi (oriental lacquer)—a natural aesthetic durable and future-promising coating," *Progress in Organic Coatings*, vol. 26, no. 2–4, pp. 163–195, 1995.

[2] J. Kumanotani, "Enzyme catalyzed durable and authentic oriental lacquer: a natural microgel-printable coating by polysaccharide-glycoprotein-phenolic lipid complexes," *Progress in Organic Coatings*, vol. 34, no. 1–4, pp. 135–146, 1997.

[3] O. Vogl, "Oriental lacquer, poison ivy, and drying oils," *Journal of Polymer Science Part A: Polymer Chemistry*, vol. 38, no. 24, pp. 4327–4335, 2000.

[4] B. Reinhammar, "Purification and properties of laccase and stellacyanin from *Rhus vernicifera*," *Biochimistry and Biophysics Acta*, vol. 205, no. 1, pp. 35–47, 1970.

[5] R. Oshima, Y. Yamauchi, C. Watanabe, and J. Kumanotani, "Enzymic oxidative coupling of urushiol in sap of the lac tree, *Rhus vernicifera*," *Journal of Organic Chemistry*, vol. 50, no. 15, pp. 2613–2621, 1985.

[6] H. W.-S. Chan, D. T. Coxon, K. E. Peers, and K. R. Price, "Oxidative reactions of unsaturated lipids," *Food Chemistry*, vol. 9, no. 1-2, pp. 21–34, 1982.

[7] N. A. Porter, S. E. Caldwell, and K. A. Mills, "Mechanisms of free radical oxidation of unsaturated lipids," *Lipids*, vol. 30, no. 4, pp. 277–290, 1995.

[8] R. Lu, S. Harigaya, T. Ishimura, K. Nagase, and T. Miyakoshi, "Development of a fast drying lacquer based on raw lacquer sap," *Progress in Organic Coatings*, vol. 51, no. 3, pp. 238–243, 2004.

[9] R. Lu, T. Ishimura, K. Tsutida, T. Honda, and T. Miyakoshi, "Development of a fast drying hybrid lacquer in a low-relative-humidity environment based on kurome lacquer sap," *Journal of Applied Polymer Science*, vol. 98, no. 3, pp. 1055–1061, 2005.

[10] I. Takahisa, L. Rong, and M. Tetsuo, "Studies on the reaction mechanism between urushiol and organic silane," *Progress in Organic Coatings*, vol. 55, no. 1, pp. 66–69, 2006.

[11] T. Ishimura, R. Lu, K. Yamasaki, and T. Miyakoshi, "Effects of hybridization of lacquer sap with organic silane on drying properties," *Progress in Organic Coatings*, vol. 62, no. 2, pp. 193–198, 2008.

[12] T. Ishimura, R. Lu, K. Yamasaki, and T. Miyakoshi, "Development of an eco-friendly hybrid lacquer based on kurome lacquer sap," *Progress in Organic Coatings*, vol. 69, no. 1, pp. 12–15, 2010.

[13] V. Pitthard, S. Wei, S. Miklin-Kniefacz, S. Stanek, M. Griesser, and M. Schreiner, "Scientific investigations of antique lacquers from a 17th-century Japanese ornamental cabinet," *Archaeometry*, vol. 52, no. 6, pp. 1044–1056, 2010.

[14] S. Wei, V. Pintus, V. Pitthard, M. Schreiner, and G. Song, "Analytical characterization of lacquer objects excavated from a Chu tomb in China," *Journal of Archaeological Science*, vol. 38, no. 10, pp. 2667–2674, 2011.

[15] J. T. P. Derksen, F. P. Cuperus, and P. Kolster, "Paints and coatings from renewable resources," *Industrial Crops and Products*, vol. 3, no. 4, pp. 225–236, 1995.

[16] J. T. P. Derksen, F. P. Cuperus, and P. Kolster, "Renewable resources in coatings technology: a review," *Progress in Organic Coatings*, vol. 27, no. 1–4, pp. 45–53, 1996.

[17] W. J. Muizebelt, J. C. Hubert, M. W. F. Nielen, R. P. Klaasen, and K. H. Zabel, "Crosslink mechanisms of high-solids alkyd resins in the presence of reactive diluents," *Progress in Organic Coatings*, vol. 40, no. 1–4, pp. 121–130, 2000.

[18] J. Samuelsson, P.-E. Sundell, and M. Johansson, "Synthesis and polymerization of a radiation curable hyperbranched resin based on epoxy functional fatty acids," *Progress in Organic Coatings*, vol. 50, no. 3, pp. 193–198, 2004.

[19] K. Johansson and M. Johansson, "Fatty acid methyl ester as reactive diluent in thermally cured solvent-borne coil-coatings—the effect of fatty acid pattern on the curing performance and final properties," *Progress in Organic Coatings*, vol. 63, no. 2, pp. 155–159, 2008.

[20] M. A. R. Meier, J. O. Metzger, and U. S. Schubert, "Plant oil renewable resources as green alternatives in polymer science," *Chemical Society Reviews*, vol. 36, no. 11, pp. 1788–1802, 2007.

[21] Y. Ishii, K. Yamawaki, T. Ura, H. Yamada, T. Yoshida, and M. Ogawa, "Hydrogen peroxide oxidation catalyzed by heteropoly acids combined with cetylpyridinium chloride: epoxidation of olefins and allylic alcohols, ketonization of alcohols and diols, and oxidative cleavage of 1,2-diols and olefins," *Journal of Organic Chemistry*, vol. 53, no. 15, pp. 3587–3593, 1988.

Hindawi Publishing Corporation
International Journal of Polymer Science
Volume 2015, Article ID 517202, 8 pages
http://dx.doi.org/10.1155/2015/517202

Research Article

Prepolymerization of Lacquer Sap under Pure Oxygen Atmosphere and Its Effects on the Properties of Lacquer Film

Jianhong Yang, Jianfeng Zhu, Wanghui Liu, Jianping Deng, and Yuanyuan Ding

Department of Environmental Engineering, School of Environmental and Safety Engineering, Changzhou University, Changzhou, Jiangsu 213164, China

Correspondence should be addressed to Jianhong Yang; yangjianhong@cczu.edu.cn

Received 10 February 2015; Revised 20 May 2015; Accepted 25 May 2015

Academic Editor: T. Yoshida

A series of lacquer saps were prepared by prepolymerization under oxygen atmosphere. The prepolymerization process was investigated by GPC, UV-Vis, FT-IR, NMR, and microscope. The results showed that the polymerization of urushiol monomer was accelerated. The content of monomer in the lacquer sap swiftly decreased from 82.68% to 47.75% in 0.5 h. The mechanism of polymerization was complex and was involved in the coupling reaction of phenyl ring, the addition reaction of the unsaturated carbon-carbon double bond groups with urushiol hydroxyl groups, and other reactions that occurred on the side chains. In addition, the prepolymerization also improved significantly the drying property of lacquer film, especially at low relative humidity. At the same time, the sizes of the water drops in the lacquer saps significantly decreased with increasing the stirring time and the surface of lacquer film became smoother, which resulted in its excellent gloss (109–125). Due to the prepolymerization, the pencil hardness and the thermal stability of lacquer film were slightly improved as well.

1. Introduction

Lacquer sap, a kind of water-in-oil (W/O) type emulsion, is collected from lac trees grown mainly in China and Japan (*Rhus vernicifera*), Vietnam and Chinese Taiwan (*Rhus succedanea*), and Burma and Thailand (*Melanorrhoea usitata*) [1, 2]. The sap of lac tree *R. vernicifera* consists of complex components including urushiol (60~65%), laccase (~0.2%), gummy substance (5~7%), glycoprotein (~2%), and water (20~30%) [3]. The lacquer sap has been used as coatings in China and Japan for thousands of years [4]. A red wooden bowl is the known earliest lacquer ware, which was found at Hemudu site in Zhejiang Province of China. It was made more than 7000 years ago [3, 5]. Today, lacquer sap is still interesting due to its natural ecofriendly feature and the excellent physicochemical properties of its film such as anticorrosiveness, high thermal stability, good brilliance, and superhigh durability [6–9]. However, lacquer sap dries by the oxidative polymerization of urushiol catalyzed by laccase under a specific condition (about 70~90% relative humidity at 20~30°C), which is followed by an autoxidation reaction on the long aliphatic unsaturated side chain as well [2, 4, 10–14]. This strict drying condition has prevented its use as an industrial paint [1].

Recently, many methods have been developed to improve the drying property of lacquer sap. A UV irradiation method had been used to promote the drying of lacquer sap, but it severely damaged some properties of lacquer film such as gloss and durability [15]. A lacquer with a decrease of the urushiol monomer had also been prepared using a repeated *kurome* process by stirring with additional moisture in the reaction vessel. The *kurome* lacquer dried quickly in a natural environment due to prepolymerization of urushiol [10]. Some hybrid lacquers were also developed based on the *kurome* lacquer, such as lacquer/polyurethane-hybrid lacquer and lacquer/organic silane-hybrid lacquer [3, 16–18], but the process of repeated *kurome* needs to take a long time and only very small amount of fast drying lacquer could be obtained. In addition, it is well known that O_2 is essential for the oxidation polymerization of urushiol [19–21]. Thus, the fast drying lacquer should also be able to be prepared under oxygen atmosphere. Li et al. prepared some refined lacquers under oxygen atmosphere at 20°C. However, it was surprising that these lacquers did not dry

[22]. So far, further study has not been done to investigate the polymerization of lacquer sap under pure oxygen atmosphere and the properties of the polymerized lacquer. In this paper, we aim to accelerate the drying of lacquer film through the prepolymerization of lacquer sap under pure oxygen atmosphere. The polymerization mechanism of lacquer sap was studied by GPC, UV-Vis, FT-IR, and NMR methods. Some properties of the prepolymerized lacquer films were investigated as well.

2. Materials and Methods

2.1. Materials. The raw lacquer sap collected from lac tree *R. vernicifera* in China was purchased from Lichuan Delong Co., Ltd. (Enshi, China). The lacquer, a neat filtered sap, has naturally high moisture content of 26.9%. All other chemicals were of analytical grade and were used as received.

2.2. Prepolymerization of Lacquer Sap. Raw lacquer sap (100 g) was polymerized in a closed four-neck reaction flask (250 mL) equipped with a mechanic stirrer, reflux condenser, thermometer, and oxygen inlet. The lacquer sap was stirred with the rate of 240 rmp at 30°C under 1 atm oxygen atmosphere. A series of samples were prepared by controlling the prepolymerization time from 0.5 h to 3.0 h. Similarly, under the condition of air instead of pure oxygen, a series of samples were also prepared.

2.3. Drying Property. The raw and prepolymerized lacquer saps were applied on glass plate using 50 μm film applicators (Tianjin Jingke Material Equipment Co., Ltd., China) and dried at different relative humidity (RH) in a 302 A temperature damp-heat regulation chamber (Shanghai Laboratory Instrument Works Co., Ltd., China) and their drying time was evaluated by QGZ-24 automatic drying time recorder (Tianjin Jingke Material Equipment Co., Ltd., China). The process of lacquer drying can be divided into two steps: touch-free dryness (TD) and hardened dryness (HD). The time until the marks of needle appear on the film surface is equivalent to TD, and the time until the marks of needle disappear completely on the lacquer film surface is equivalent to HD [10].

2.4. Pencil Hardness Test. The pencil hardness was checked on previously degreased tinplate with a dry film (thickness of the wet coating 50 μm). Panels were subjected to property evaluation after two weeks of cure at 30°C and 80% RH. Pencil hardness was determined according to current national standard of GB/T6739-2006.

2.5. Characterization. The molecular weight of sample was measured by a gel permeation chromatography (GPC) on a LC-20AD instrument (Shimadzu, Japan) equipped with a TSK G3000-H_{XL} column (TOSOH, Japan). The eluent was THF. The flow rate was 1.0 mL/min. The temperature of the column was maintained at 30°C. The eluate was monitored with RID-10A refractive index detector (Shimadzu, Japan). The standards used for calibration the column were polystyrene. All data provided by the GPC system were collected and analyzed with the aid of the LCsolution Workstation software package.

The UV-Vis spectra were recorded on a SPECORD 50 spectrophotometer (Analytik Jena AG, Germany). The sample was thinly spread on the quartz plate.

FT-IR spectra were recorded on a Nicolet Avatar 370 FT-IR spectrometer (Thermo, Madison, USA). The samples were thinly applied on the KBr pellets. 32 scans at a resolution of 2 cm^{-1} were averaged and referenced against air.

^{1}H NMR spectra were recorded on a Bruker AVANCE III 400 MHz NMR spectrometer (Switzerland) with tetramethylsilane (TMS) as the internal standard. The samples were dissolved in $CDCl_3$.

The micrographs of lacquer saps were observed by a BX43 microscope (Olympus, Japan) and obtained using a digital camera (ToupCam, China).

The surface morphologies of lacquer films were examined using a scanning electron microscope (SEM) Zeiss SUPRA55 (Germany).

The thermal behavior of lacquer film was estimated using a NETZSCH TG 209 F3 apparatus (Germany). The TG oven was programmed from 48°C to 647°C under N_2 atmosphere, a rise of 10°C/min. The lacquer film (thickness of the wet coating 50 μm) was dried at 30°C and 80% RH for one week.

The gloss of lacquer film was tested with an XGP20°-60°-85° specular gloss meter (Tianjin Xintongguangda Technology Co., Ltd., China). Lacquer films were prepared with 50 μm thickness of the wet coating on tinplate panels and evaluated after two weeks of cure at 30°C and 80% RH.

3. Results and Discussion

3.1. Prepolymerization of Lacquer Sap

3.1.1. Molecular Weight Change in the Polymerization Process. The molecular weight distribution of the lacquer saps was monitored by GPC in the polymerization process under oxygen atmosphere and air atmosphere, respectively. The results are summarized in Table 1. It can be seen from Table 1 that the contents of urushiol monomer, oligomer, and polymer were 82.68%, 17.23%, and 0.09% in the raw lacquer, respectively. Under oxygen atmosphere, the urushiol monomer decreased rapidly to 47.75% in the prepolymerized lacquers and the oligomer increased quickly to 48.61% in the initial half an hour, indicating that the oxidation polymerization of urushiol was very fast. With increasing the reaction time from 0.5 h to 3.0 h, the content of urushiol monomer only decreased slowly from 47.75% to 23.28%. The polymerization of urushiol monomer became slow, which could mainly be due to the increase of the viscosity of prepolymerized lacquers. At the same time, a prominent feature was also observed in which the polymer increased swiftly from 3.64% to 20.48%, while the oligomer changed within the scope of 48.61–58.62%. Compared with the polymerization of urushiol under oxygen atmosphere, the conversion of urushiol monomer was very slow under air atmosphere. The contents of urushiol monomer, oligomer, and polymer were

Table 1: The molecular weight distribution of the raw and the prepolymerized lacquer saps under different atmospheres.

Sample	Prepolymerization time	Oxygen atmosphere[b]			Air atmosphere		
		Polymer/%	Oligomer/%	Monomer/%	Polymer/%	Oligomer/%	Monomer/%
RL[a]	0 h	0.09	17.23	82.68	0.09	17.23	82.68
1	0.5 h	3.64	48.61	47.75	0.50	28.29	71.21
2	1.0 h	4.66	58.32	37.02	0.63	31.44	67.93
3	1.5 h	7.10	55.35	37.55	0.88	32.87	66.25
4	2.0 h	10.95	58.62	30.43	1.08	33.34	65.58
5	2.5 h	15.84	54.38	29.78	1.10	34.17	64.73
6	3.0 h	20.48	56.24	23.28	1.51	37.85	60.64

[a]Raw lacquer; [b]polymer: $M_w \geq 3000$; oligomer: $3000 > M_w \geq 640$; monomer: $M_w < 640$.

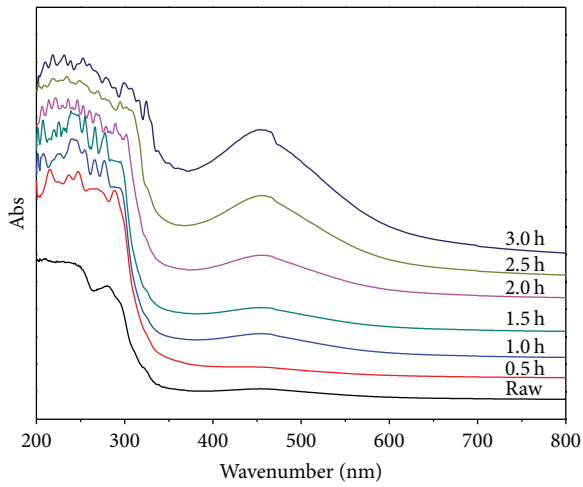

Figure 1: UV-Vis spectra of the raw lacquer sap and the prepolymerized lacquer saps.

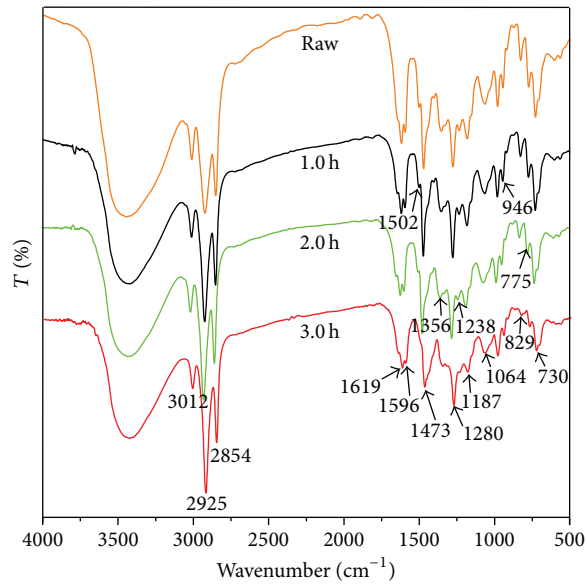

Figure 2: FT-IR spectra of the raw lacquer sap and the prepolymerized lacquer saps.

only 60.64%, 37.85%, and 1.51% until 3.0 h, respectively. All the results suggested that the condition with pure oxygen atmosphere was advantageous to accelerate the polymerization of urushiol monomer. It is well known that the oxidation polymerization of urushiol is mainly catalyzed by laccase. The laccase contains four copper atoms and catalyzes the reduction of O_2 at a trinuclear copper cluster. O_2 is essential for the oxidation polymerization of urushiol [19–21]. Under pure oxygen atmosphere, the fully reduced form of laccase could adequately contact O_2 and quickly react with O_2 to produce the intermediate with an oxygen-radical bound to the trinuclear copper cluster and oxidized the substrates into the products [19]. Thus, the laccase catalyzed polymerization of urushiol was accelerated under pure oxygen condition.

3.1.2. UV-Vis Spectra. The prepolymerization process of the lacquer sap under oxygen atmosphere was monitored with a UV-Vis spectrophotometer. Figure 1 shows the UV-Vis spectra of the raw lacquer sap and prepolymerized lacquer saps. In the UV-Vis spectrum of raw lacquer, the broad peak at 200–265 nm was due to the π-π^* of conjugated alkadiene (K band), and the peak at 280 nm was due to the π-π^* of phenyl of urushiol (B band) [23]. In the oxidation polymerization process of lacquer sap, the K band became broad and overlapped the B band. In the meantime, the B band also shifted toward the red end of the spectrum. These indicated that the polymerization of urushiol occurred to form a bigger conjugated structure. In addition, a new band at about 450 nm was also observed, which also resulted from the absorption of the molecules with large conjugated structure. The intensity of the band increased gradually in the polymerization process, indicating that the extent of conjugation increased.

3.1.3. FT-IR and NMR Spectra. The prepolymerization process of the lacquer sap under oxygen atmosphere was also analyzed with FT-IR and NMR spectrophotometers. Figure 2 shows the FT-IR spectra of the raw and the prepolymerized lacquer saps. The peaks at 1356, 1280, and 1187 cm^{-1} were due to βO-H, γO-H, and C-O vibration of C-O-H group [24], respectively. In the spectra of the prepolymerized lacquer saps, their intensities decreased gradually with the increase of prepolymerization time, suggesting that the O-H groups on the phenyl ring participated in the polymerization reaction. A peak at 3012 cm^{-1} was related to C-H vibration of the phenyl ring [9]. Its intensity decreased with increasing

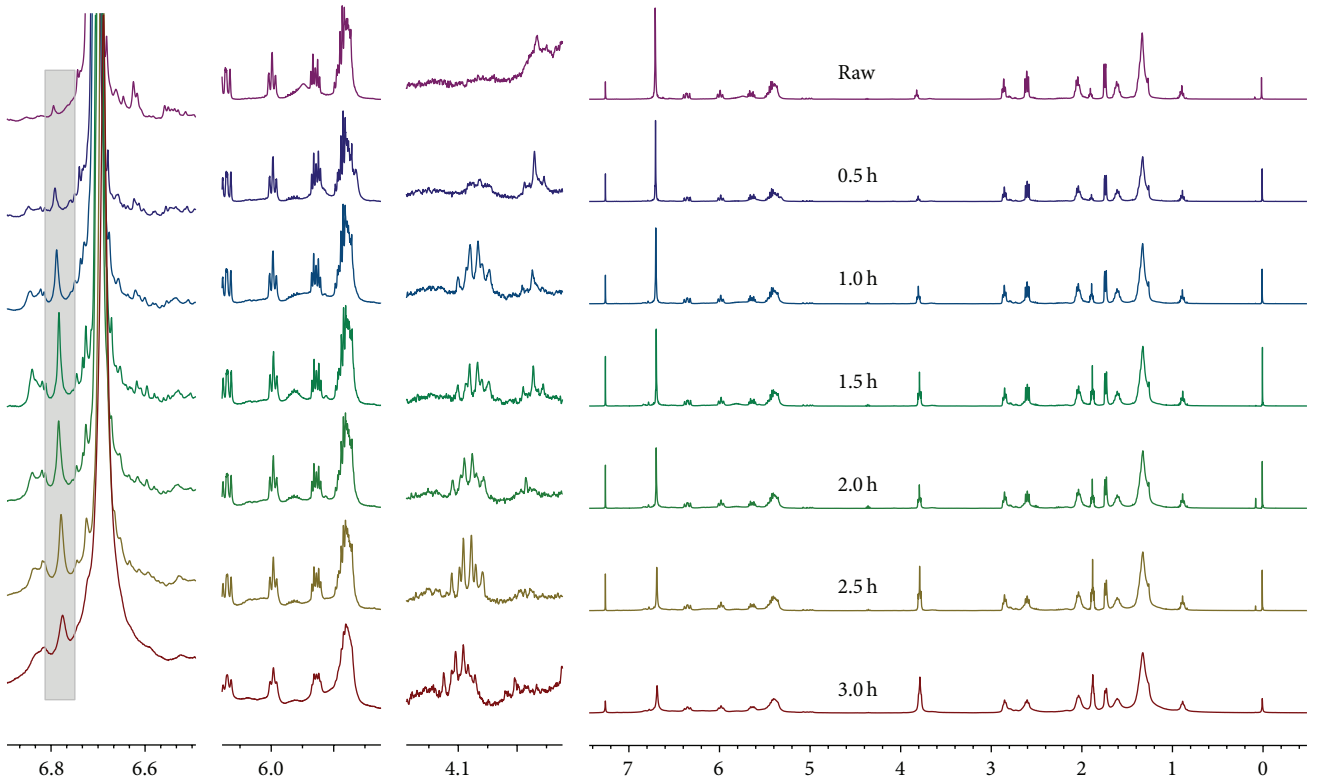

Figure 3: ^{1}H NMR spectra of the raw lacquer saps and the prepolymerization lacquer saps in $CDCl_3$.

the prepolymerization time, and the peaks at 775 cm^{-1} also became weak, suggesting that more substitution occurred on the phenol ring [14]. Furthermore, the peaks at 946 and 983 cm^{-1} due to the conjugated dienes obviously decreased [15], and the peak at 983 cm^{-1} shifted to 987 cm^{-1} in 3 h of prepolymerized lacquer sap as well [24], indicating that some reactions occurred not only on the phenol rings, but also in the side chains.

^{1}H NMR spectra of the raw and prepolymerized lacquer saps are shown in Figure 3. The peak at about 6.71 ppm is assigned to the ^{1}H signal on the phenyl ring, and the peak at 6.78 ppm is due to the ^{1}H signal of the biphenyl [25, 26]. The integral value of the former gradually decreased with increasing the reaction time from 0 to 3.0 h, but the value of the latter increased, suggesting that more substitutions occurred on the phenyl rings, and the polymerization is involved in the oxidative coupling reaction of urushiol molecules as well. The peaks at 5.15–5.55 ppm were assigned to the protons of the –C–CH=CH-C– in the side chain [10]. Their integral values gradually decreased, suggesting that some reactions also occurred on the side chain. In addition, some new peaks that appeared at 4.05–4.20 ppm could be assigned to the proton of the –C=C–C–CH–O–Ph [10], indicating that the addition reaction of the unsaturated carbon-carbon double bond groups in the side chain with urushiol hydroxyl groups had occurred in the polymerization process too.

3.1.4. Micrograph. Figure 4 shows the micrographs of the raw and the prepolymerized lacquer saps. Raw lacquer sap is a kind of natural water-in-oil (W/O) type emulsion. It can be seen from the micrographs of raw lacquer sap that the water was dispersed in the oil phase and the diameter of water drops was in the scope of 0.5–10 μm. The distribution of the size of water drops was broad. In the prepolymerization process, as the lacquer sap was continuously stirred, the sizes of water drops gradually decreased and their distribution was also more homogeneous as shown in Figure 4. The sizes of water drops were 0.5–3.0 μm after 3 h. In the meantime, the color of lacquer saps also changed gradually. For the raw lacquer sap, the color of its oil was gray and the color of its water drops was light blue-purple in the microscope. After 3 h of prepolymerization, the color of the water drops was still maintained basically, but the color of the oil became deep yellow. It could be related to the polymerization extent of urushiol. The intensity of the band of the prepolymerized lacquer sap at about 450 nm increased gradually in the polymerization process as mentioned in the UV-Vis spectra, which led to the change of its color [27].

3.2. Properties and Characterization of Lacquer Film

3.2.1. Drying and Coating Properties. The drying time and the coating properties such as gloss and pencil hardness of the raw lacquer sap and the prepolymerized lacquer saps are shown in Table 2. It can be seen from Table 2 that the drying time of the raw lacquer to reach touch-free dryness and hardened dryness was 3 h 20 min and 5 h 50 min at a high relative humidity of 78%. Compared with the raw lacquer, the prepolymerized lacquers dried faster and the drying time

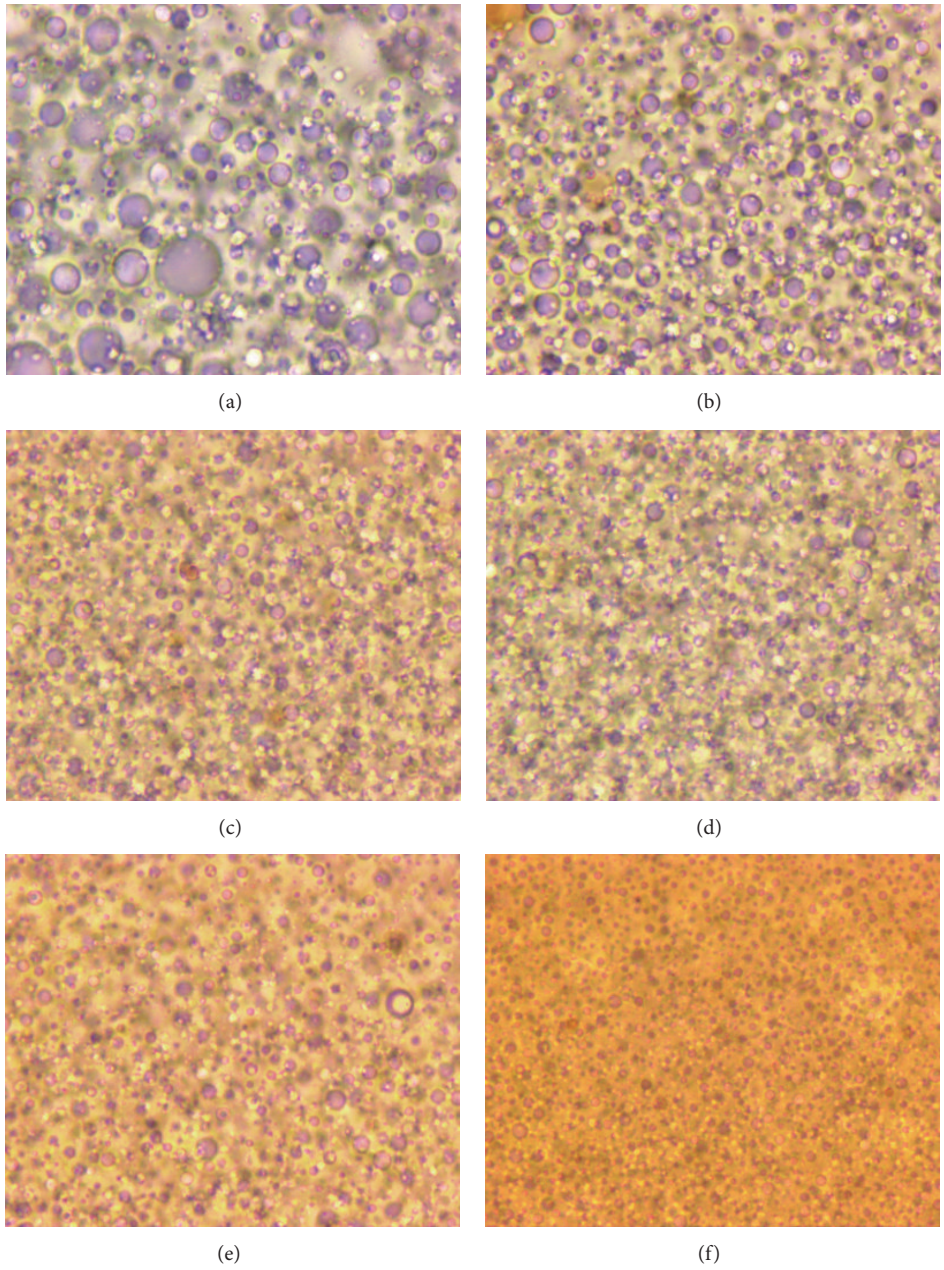

Figure 4: Micrographs (1000x magnification) of raw lacquer saps in different prepolymerization time. (a) 0 h; (b) 0.5 h; (c) 1.0 h; (d) 1.5 h; (e) 2.5 h; (f) 3.0 h.

Table 2: Drying time (h:min) of lacquer films and coating properties of cured films.

Sample	Prepolymerization time (h)	30°C, 78% RH		30°C, 65% RH		Pencil hardness[b]	Gloss[b]
		TD	HD	TD	HD		
RL[a]	0	3:20	5:50	23:30	30:20	3H	81
1	0.5 h	2:30	4:30	18:10	26:20	4H	119
2	1.0 h	2:30	4:00	11:20	18:40	4H	118
3	1.5 h	2:20	3:30	9:50	17:10	4H	115
4	2.0 h	1:30	2:50	8:50	15:10	4H	125
5	2.5 h	0:30	2:30	6:40	13:20	4H	109
6	3.0 h	0:40	2:20	5:40	12:30	4H	110

[a]RL: raw lacquer; [b]the lacquer films were tested after drying at 30°C and 80% RH for two weeks.

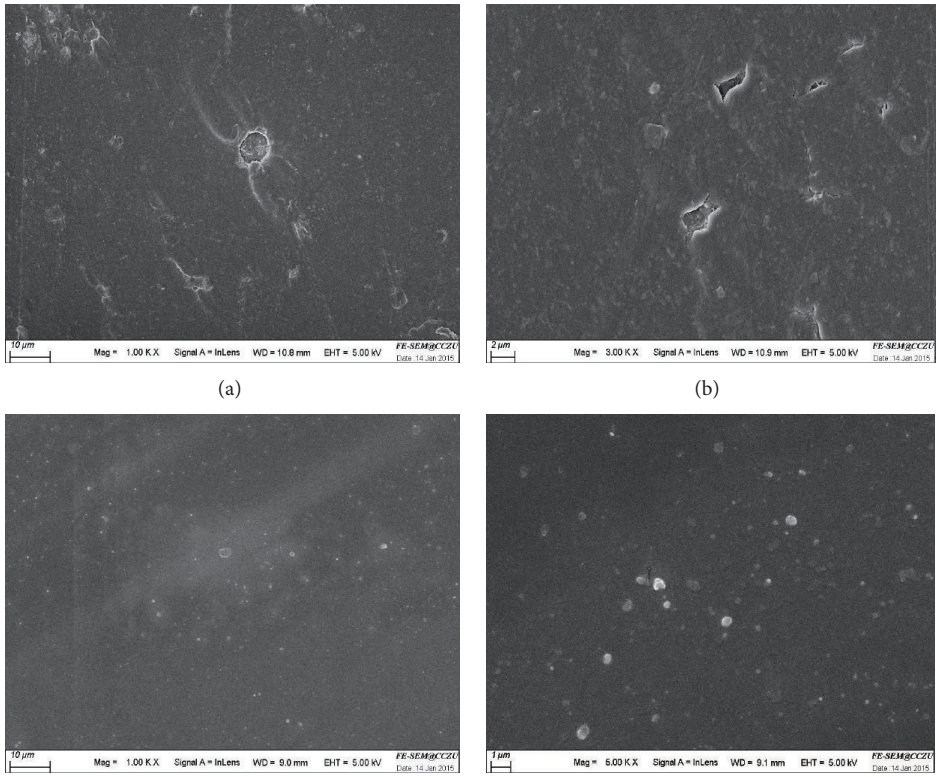

Figure 5: SEM photographs of the raw lacquer film ((a) magnification: 1.00 Kx; (b) magnification: 3.00 Kx) and the prepolymerization lacquer film after 3.0 h ((c) magnification: 1.00 Kx; (d) magnification: 5.00 Kx).

gradually decreased with the increase of prepolymerization time. When the prepolymerization time was 3.0 h, the drying time of sample's film to reach TD and HD was 40 min and 2 h 20 min, respectively. Moreover, the drying time of the raw lacquer to reach TD and HD greatly increased at low relative humidity of 65% and was 23 h 30 min and 30 h 20 min, respectively. However, for the prepolymerized lacquer saps, their drying time was much shorter than that of lacquer sap. After the lacquer sap was prepolymerized for 3.0 h, its drying time of TD and HD was only 5 h 40 min and 12 h 30 min correspondingly. Obviously, the prepolymerization of lacquer sap could improve significantly the drying property, especially at low relative humidity. Furthermore, from the data shown in Table 2, it was also observed that the pencil hardness of the prepolymerized lacquer films slightly increased from 3H to 4H. However, the gloss of lacquer films was markedly improved by the prepolymerization of lacquer sap. The gloss of the raw lacquer film was 81, but that of all prepolymerized lacquer films was higher and within the scope of 109–125. It could be because the prepolymerization of lacquer sap resulted in the decrease of the water drops' sizes as mentioned previously in the micrographs.

3.2.2. SEM. The surface morphologies of the raw lacquer and its prepolymerized lacquer films were analyzed with a SEM, and their SEM images are shown in Figure 5. It was observed that there were some "caves" in the raw lacquer film, which resulted from the evaporation of water in the drying process [10, 24]. The diameters of the "caves" were about 0.2–5 μm (Figures 5(a) and 5(b)). Due to the caves, the surface of the raw lacquer film was not very smooth. For the prepolymerized lacquer film, some "caves" were also observed. But their sizes were smaller (<0.5 μm), which was due to the smaller diameters of water drops in the lacquer sap (Figures 5(c) and 5(d)). Compared with the raw lacquer film, the surface of the prepolymerized lacquer film was smoother as well. The gloss of the lacquer films was closely related to their surface smoothness [24]. Obviously, the excellent gloss of the prepolymerized lacquer films resulted from their good surface smoothness.

3.2.3. Thermal Analysis. The TG curves of the raw and prepolymerized lacquer films are shown in Figure 6. The degradation of the raw lacquer film could be divided into three stages. The first stage of raw lacquer film at 48–220°C with the weight loss of 3.28% was due to the loss of water and other small molecules. Its second degradation stage started at 220°C till 420°C with weight loss of 28.62%, which stemmed from the decomposition of lacquer polysaccharide, glycoprotein, and urushiol monomer [13]. The third stage began at 420°C till 647°C with weight loss of 52.58% that was attributed to the degradation of urushiol oligomer and polymer. Compared with the raw lacquer film, the prepolymerized lacquer films had similar TG curves. However, their weight loss was less

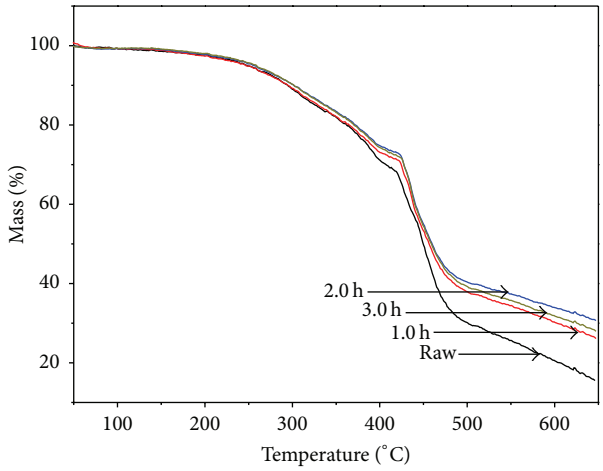

Figure 6: TG and DTG curves of the raw and the prepolymerized lacquer films.

after 200°C. At 647°C, the weight loss of raw lacquer film was 84.48% while that of the prepolymerized lacquer films was in the range from 69.38% to 75.07%. It indicated that the prepolymerized lacquer films possessed higher thermal stability, which could be because the extent of polymerization of lacquer films was improved after the prepolymerization of lacquer sap.

4. Conclusion

In this study, the raw lacquer sap was prepolymerized under oxygen atmosphere. The polymerization rate was quicker than that under air atmosphere. 59.4% of urushiol monomer was converted into the oligomer and polymer in 3.0 h. The polymerization of urushiol was complex, which was involved in the coupling reaction of phenyl ring, the addition reaction of the unsaturated carbon-carbon double bonds with urushiol hydroxyl groups, and other reactions that occurred on the side chains. Due to the prepolymerization, the drying time of lacquer sap was shortened greatly, especially at the low relative humidity. In addition, the thermal stability of lacquer film was improved, and its gloss also became very excellent. Thus, the prepolymerization of lacquer sap under oxygen atmosphere is to hopefully be used to prepare a fast drying lacquer on a large scale and promote the applications of lacquer sap as an industrial paint.

Conflict of Interests

The authors declare that there is no conflict of interests regarding the publication of this paper.

Acknowledgment

This work was supported by the National Natural Science Foundation of China Grant no. 31270616.

References

[1] J. Kumanotani, "Urushi (oriental lacquer)—a natural aesthetic durable and future-promising coating," *Progress in Organic Coatings*, vol. 26, no. 2-4, pp. 163–195, 1995.

[2] R. Lu, T. Yoshida, and T. Miyakoshi, "Oriental lacquer: a natural polymer," *Polymer Reviews*, vol. 53, no. 2, pp. 153–191, 2013.

[3] R. Lu, Y.-Y. Wan, T. Honda, T. Ishimura, Y. Kamiya, and T. Miyakoshi, "Design and characterization of modified urethane lacquer coating," *Progress in Organic Coatings*, vol. 57, no. 3, pp. 215–222, 2006.

[4] J. Kumanotani, "Enzyme catalyzed durable and authentic oriental lacquer: a natural microgelprintable coating by polysaccharide–glycoprotein–phenolic lipid complexes," *Progress in Organic Coatings*, vol. 34, no. 1–4, pp. 135–146, 1997.

[5] W. Bai, L. Cai, D. Zhou et al., "Resurrection of dead lacquer-Cupric potassium chloride dihydrate ($K_2CuCl_4 \cdot 2H_2O$) used as the mimic laccase," *Progress in Organic Coatings*, vol. 77, no. 2, pp. 431–438, 2014.

[6] H. Langhals and D. Bathelt, "The restoration of the largest archaelogical discovery—a chemical problem: conservation of the polychromy of the Chinese Terracotta Army in Lintong," *Angewandte Chemie International Edition*, vol. 42, no. 46, pp. 5676–5681, 2003.

[7] N. Niimura and T. Miyakoshi, "Structural study of oriental lacquer films during the hardening process," *Talanta*, vol. 70, no. 1, pp. 146–152, 2006.

[8] H. S. Kim, J. H. Yeum, S. W. Choi, J. Y. Lee, and I. W. Cheong, "Urushiol/polyurethane-urea dispersions and their film properties," *Progress in Organic Coatings*, vol. 65, no. 3, pp. 341–347, 2009.

[9] J. Xia, J. Lin, Y. Xu, and Q. Chen, "On the UV-induced polymeric behavior of chinese lacquer," *ACS Applied Materials and Interfaces*, vol. 3, no. 2, pp. 482–489, 2011.

[10] R. Lu, S. Harigaya, T. Ishimura, K. Nagase, and T. Miyakoshi, "Development of a fast drying lacquer based on raw lacquer sap," *Progress in Organic Coatings*, vol. 51, no. 3, pp. 238–243, 2004.

[11] J. K. Agbenyega, M. Claybourn, and G. Ellis, "A study of the autoxidation of some unsaturated fatty acid methyl esters using Fourier transform Raman spectroscopy," *Spectrochimica Acta Part A: Molecular Spectroscopy*, vol. 47, no. 9-10, pp. 1375–1388, 1991.

[12] A. I. Yaropolov, O. V. Skorobogat'ko, S. S. Vartanov, and S. D. Varfolomeyev, "Laccase properties, catalytic mechanism, and applicability," *Applied Biochemistry and Biotechnology*, vol. 49, no. 3, pp. 257–280, 1994.

[13] A. M. Mayer and R. C. Staples, "Laccase: new functions for an old enzyme," *Phytochemistry*, vol. 60, no. 6, pp. 551–565, 2002.

[14] J. Kumanotani, K. Inoue, M. Achiwa, and L. W. Chen, "Behavior of water in oriental lacquers," *Polymer Science and Technology*, vol. 33, pp. 163–176, 1986.

[15] J. Xia, Y. Xu, J. Lin, and B. Hu, "UV-induced polymerization of urushiol without photoinitiator," *Progress in Organic Coatings*, vol. 61, no. 1, pp. 7–10, 2008.

[16] R. Lu, T. Ishimura, K. Tsutida, T. Honda, and T. Miyakoshi, "Development of a fast drying hybrid lacquer in a low-relative-humidity environment based on *kurome*lacquer sap," *Journal of Applied Polymer Science*, vol. 98, no. 3, pp. 1055–1061, 2005.

[17] R. Lu, T. Moteki, and T. Miyakoshi, "Development and characterization of micro-dispersed lacquer," *Journal of Chinese Lacquer*, vol. 29, no. 1, pp. 1–5, 2010.

[18] T. Ishimura, R. Lu, K. Yamasaki, and T. Miyakoshi, "Effects of hybridization of lacquer sap with organic silane on drying properties," *Progress in Organic Coatings*, vol. 62, no. 2, pp. 193–198, 2008.

[19] S.-K. Lee, S. D. George, W. E. Antholine, B. Hedman, K. O. Hodgson, and E. I. Solomon, "Nature of the intermediate formed in the reduction of O_2 to H_2O at the trinuclear copper cluster active site in native laccase," *Journal of the American Chemical Society*, vol. 124, no. 21, pp. 6180–6193, 2002.

[20] N. Hakulinen, L.-L. Kiiskinen, K. Kruus et al., "Crystal structure of a laccase from *Melanocarpus albomyces* with an intact trinuclear copper site," *Nature Structural Biology*, vol. 9, no. 8, pp. 601–605, 2002.

[21] N. Aktaş, H. Çiçek, A. Taşpnar Ünal, G. Kibarer, N. Kolankaya, and A. Tanyolaç, "Reaction kinetics for laccase-catalyzed polymerization of 1-naphthol," *Bioresource Technology*, vol. 80, no. 1, pp. 29–36, 2001.

[22] X. Li, Y. Shi, and F. Zhang, "Research on the influencing factors of lacquer refining process," *Journal of Chinese Lacquer*, vol. 25, no. 2, pp. 6–10, 2006.

[23] X. Zheng, J. Weng, Q. Huang, B. Hu, T. Qiao, and P. Deng, "Fabrication of a stable poly(vinylpyrrolidone)/poly(urushiol) multilayer ultrathin film through layer-by-layer assembly and photo-induced polymerization," *Colloids and Surfaces A: Physicochemical and Engineering Aspects*, vol. 337, no. 1–3, pp. 15–20, 2009.

[24] J. Yang, J. Deng, Q. Zhang, Q. Shen, D. Li, and Z. Xiao, "Effects of polysaccharides on the properties of Chinese lacquer sap," *Progress in Organic Coatings*, vol. 78, pp. 176–182, 2015.

[25] S. Harigaya, T. Honda, L. Rong, T. Miyakoshi, and C.-L. Chen, "Enzymatic dehydrogenative polymerization of urushiols in fresh exudates from the lacquer tree, *Rhus vernicifera* DC," *Journal of Agricultural and Food Chemistry*, vol. 55, no. 6, pp. 2201–2208, 2007.

[26] M. Takada, R. Oshima, Y. Yamauchi, J. Kumanotani, and M. Seno, "Coupling reactions of 4-tert-butyl-*o*-benzoquinone with olefinic compounds," *The Journal of Organic Chemistry*, vol. 53, no. 13, pp. 3073–3080, 1988.

[27] D. L. Pavia, G. M. Lamoman, G. S. Kriz, and J. R. Vyvyan, *Introduction to Spectroscopy*, Brooks/Cole Cengage Learning, Belmont, Tenn, USA, 4th edition, 2009.

Hindawi Publishing Corporation
International Journal of Polymer Science
Volume 2015, Article ID 719328, 6 pages
http://dx.doi.org/10.1155/2015/719328

Research Article

Characterization of Vietnamese Lacquer Collected in Different Seasons

Rong Lu,[1] Kenichiro Anzai,[1] Bach Trong Phuc,[2] and Tetsuo Miyakoshi[1]

[1]*Department of Applied Chemistry, School of Science and Technology, Meiji University, 1-1-1 Higashi-mita, Tama-ku, Kawasaki-shi 214-8571, Japan*
[2]*Research Center for Polymer Materials, Hanoi University of Science and Technology, Hai Ba Trung District, Hanoi, Vietnam*

Correspondence should be addressed to Rong Lu; lurong@meiji.ac.jp

Received 20 January 2015; Revised 12 March 2015; Accepted 12 March 2015

Academic Editor: S. M. Sapuan

Vietnamese lacquers collected every month from June to March of next year were characterized. Composition analysis showed that lacquer collected in rainy season contained much water, while those collected in dry season contained more lipid component. Although hardness of lacquer films is not very hard, lacquers tapped in all seasons can reach hard dry (HD) within 48 hours. Refining lacquer can accelerate drying time but the water concentration should be maintained around 10 wt% for laccase activity.

1. Introduction

Lacquer is sap collected from lacquer tree, which belongs to Anacardiaceae and *Toxicodendron* families growing in Asia. It has been used as coating material for thousands of years in Asian countries due to durability and beauty [1–4]. Lacquer from *Toxicodendron vernicifluum* lacquer tree, which grows in China, Japan, and Korea, is usually collected from June to October, and the characters are somewhat different according to the collection month [5]. For example, lacquer tapped from June to July (rainy season in East Asia) contains much water and dries faster than another season. Lacquer tapped in August has better gloss and transparency due to the higher lipid component compared with other seasons. These characters of lacquer depend on the climate during the collection season. Therefore, in lacquer market, the price differs according to collection season and lacquer collected in August with high lipid content fetches the highest price.

In South Asia, especially in Vietnam, lacquer is collected from *Toxicodendron succedaneum* lacquer trees from January to December because of tropical climate [6]. Vietnamese people have used *T. succedaneum* lacquer sap as adhesive and coating material in their long lacquer culture history [7–11]. Composition and characterization of laccol [12] and synthesis of epoxy resin derivative from laccol [13] also have been reported. However, how to improve the quality of Vietnamese lacquer is rarely reported.

In the lacquer market, Vietnamese lacquer has relatively poor reputation because of its slow drying and soft film. It has been said that Vietnamese lacquer collected throughout the year is combined in one barrel. This practice may be one reason it has a reputation for low quality in international lacquer market. In order to better understand the real quality and characteristics of Vietnamese lacquer, Vietnamese lacquer saps collected every month from June of 2012 to March of 2013 were analyzed. The composition, drying time, laccase activity, and infrared absorption of lacquer film collected during those months were determined; the characteristics of Vietnamese lacquer are discussed. In addition, development of fast drying lacquer was also carried out by refining (*kurome*) process, and the results are also discussed.

2. Experimental

2.1. Materials. Lacquer sap was tapped from *Toxicodendron succedanea* lacquer tree growing in Tho Van (T6–T3 series) and Di Nau (D6–D3 series) communes of Tam Nong, Pho Tho, Vietnam, every month from June 2012 to March 2013. Because the quantity collected was inadequate for use in the *kurome* study, lacquer sap collected in September 2012 in Tho Van commune which was provided by United Nations Industrial Development Organization (UNIDO) of Vietnam was used in the *kurome* process.

2.2. Method. Lacquer viscosity was determined at room temperature using a Brookfield Engineering Laboratories programmable DV-II viscometer with a CPE-51 spindle. The rotation speed was 5–20 rpm, and the measurement volume was 0.5 mL.

Drying time was carried out using an automatic drying time recorder (Tai Yu Equipment, Osaka, Japan), and the thickness of the tested lacquer films on the glass plate was 76 μm when wet as we previously reported [14].

The hardness and color change of lacquer film were measured by pencil hardness tester (Yoshimituseiki, Japan) and Color-Guide instrument (BYK-Gardner, Germany), respectively. ATR-IR spectra of lacquer films were measured using JASCO FT-IR410 spectrophotometer.

Laccase activity was determined using 0.216 mmol/L syringaldazine/methanol as substrate in 0.1 mmol/L sodium phosphate buffer (pH 6.5) and measured by monitoring the increase in UV absorbance at 525 nm at 30°C. One unit of enzyme was equal to an increase of 0.001 absorbance unit per min per mg of acetone powder (AP).

The *kurome* process is microdispersal of water molecules and dehydration of lacquer sap by mixing. In this study, the *kurome* process was carried out by changing rotating speed and mixing time, as described in our previous report [15].

Molecular weight distribution and average molecular weight were determined at 40°C by gel permeation chromatography (GPC, TSK-gel columns α-3000, α-4000, and α-M, φ7.8 mm × 300 mm × 3, Tosoh). Dimethylformamide (DMF) with 0.01 mol of LiBr was used as an eluent on a high-performance liquid chromatography system (HPLC). A refractive-index detector was used and polystyrene having molecular weights of 1.90×10^5, 4.39×10^4, 5.40×10^3, and 5.00×10^2 g/mol was used as standards. The elution rate and pressure of the DMF eluent were 0.8 mL/min and 48 kg/cm^2, respectively.

3. Result and Discussion

3.1. Composition Analysis of Season Lacquers. After measuring the viscosities, lacquer samples were separated with acetone to obtain lipid component and acetone powder (AP). The separation results and viscosities are summarized in Table 1.

The lacquers collected from June to September (T6–T9, D6–D9) had higher water concentration compared with those collected from October to January (T10–T1, D10–D1). May to October is rainy and November to March is dry season in Vietnam. Obviously, the water concentration in lacquer is related to climate, and this phenomenon affected lacquer collected from *Toxicodendron vernicifluum* lacquer tree growing in China, Japan, and Korea. Although February and March are not a rainy season, lacquer collected in both months had a high water concentration, which can be considered due to high humidity in this season in Vietnam. However, we found that the ratio of AP increased with increasing concentration of water, and the water concentration to AP ratio was constant as shown in Figure 1. This phenomenon means that the higher water concentration in lacquer sap is not simply matter of rain or humidity when collected in rainy season or the very humid months of February and March. A lacquer tree is a higher plant, its life activity is very complex, and there is much that we humans do not understand. It can also be seen that seasonal lacquer viscosities increased with increasing water concentration, as shown in Figure 2. That is, the energy of emulsification is increased with increasing percentage of water in lipid.

The drying time and hardness of lacquer films are summarized in Table 2. The drying time does not differ much by collecting season, because the drying time is related to

Table 1: Compositions of season Vietnamese lacquer.

Samples	Area	Month	Lipid (%)	AP (%)	Water (%)	Viscosity (mPas)
T6	Tho Van	6	43.22	21.38	35.39	4447
T7		7	43.85	21.23	34.92	3113
T8		8	62.40	14.17	23.43	549
T9		9	55.56	15.74	28.70	1088
T10		10	61.32	13.11	25.57	726
T11		11	62.17	13.15	24.68	778
T12		12	59.35	13.91	26.74	713
T1		1	62.26	13.58	24.16	818
T2		2	29.43	24.71	45.86	8865
T3		3	29.84	24.22	45.94	7525
D6	Di Nau	6	70.42	11.12	18.47	1012
D7		7	39.23	23.43	37.34	3659
D8		8	37.42	25.20	37.38	7387
D9		9	46.49	20.21	33.30	1779
D10		10	61.34	13.84	24.82	811
D11		11	66.13	13.85	20.02	713
D12		12	38.87	24.49	36.64	2195
D1		1	59.03	16.87	24.10	726
D2		2	49.73	20.30	29.97	1300
D3		3	44.52	21.37	34.10	1884

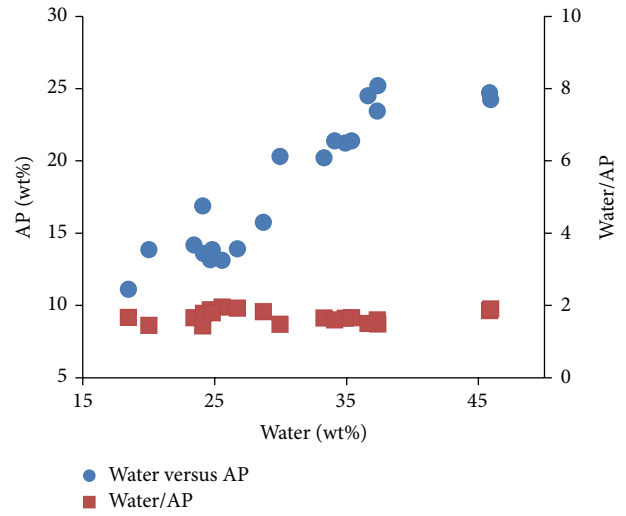

Figure 1: Ratio of water to AP.

Table 2: Compositions of season Vietnamese lacquer.

Samples	Drying time[1] (h)			Hardness[2] for drying days								
	DF	TF	HD	1	2	3	4	5	6	7	14	21
T6	4.3	5.4	8.0	<6B	<6B	<6B	<6B	<6B	<6B	<6B	<6B	4B
T7	3.8	4.8	8.8	<6B	<6B	<6B	<6B	<6B	<6B	<6B	<6B	5B
T8	2.6	3.2	6.0	<6B	<6B	<6B	<6B	<6B	<6B	<6B	<6B	4B
T9	6.5	7.5	15.0	<6B	<6B	<6B	<6B	<6B	<6B	<6B	5B	5B
T10	2.8	3.5	6.5	<6B	<6B	5B	5B	5B	5B	5B	3B	3B
T11	4.0	5.0	8.5	<6B	<6B	<6B	6B	5B	5B	5B	3B	3B
T12	4.0	4.7	8.5	<6B	<6B	<6B	6B	5B	5B	5B	3B	3B
T1	7.8	8.5	16.0	<6B	<6B	<6B	<6B	<6B	<6B	<6B	4B	4B
T2	2.8	3.5	6.0	<6B	<6B	<6B	<6B	<6B	<6B	4B	4B	4B
T3	2.0	3.0	4.5	<6B	<6B	<6B	<6B	<6B	<6B	4B	4B	3B
D6	14.0	15.5	<48	—	<6B	<6B	<6B	<6B	<6B	<6B	<6B	<6B
D7	6.0	8.2	<48	—	<6B	<6B	<6B	<6B	<6B	<6B	<6B	4B
D8	3.8	5.5	<48	—	<6B	<6B	<6B	<6B	<6B	<6B	<6B	<6B
D9	2.7	3.2	4.5	<6B	<6B	6B	5B	5B	5B	5B	3B	3B
D10	2.5	3.0	5.0	<6B	<6B	<6B	5B	5B	5B	5B	4B	4B
D11	6.7	7.0	15.0	<6B	<6B	<6B	5B	5B	5B	5B	4B	4B
D12	3.0	4.0	5.5	<6B	<6B	<6B	<6B	<6B	<6B	<6B	4B	4B
D1	3.8	4.3	8.0	<6B	<6B	<6B	<6B	<6B	<6B	<6B	4B	4B
D2	1.5	2.0	3.5	<6B	<6B	<6B	<6B	<6B	<6B	<6B	4B	3B
D3	1.5	2.0	3.0	<6B	<6B	<6B	<6B	<6B	<6B	4B	4B	3B

[1]Drying condition: 25°C, 80%RH, and wet thickness 76 μm. DF: dust-free dry; TF: touch-free dry; HD: hard dry.
[2]Based on pencil hardness test method.

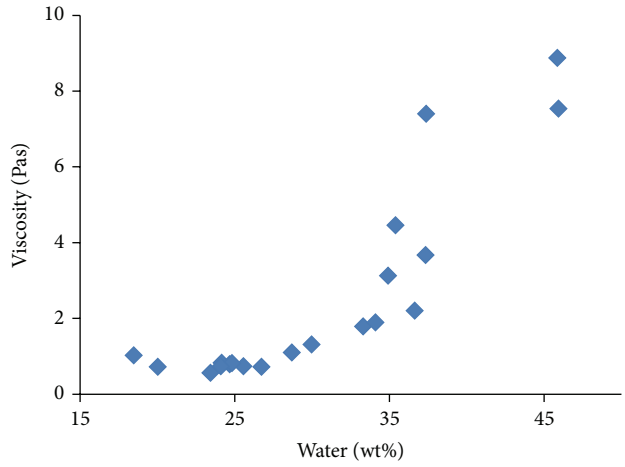

Figure 2: Viscosity of lacquer sap.

laccase concentration and activity, and almost all collecting season samples have similar laccase concentration and activity (Table 3). On the other hand, the film hardness is relative to the percentage of lipids in the lacquer sap. Hardness is strongly influenced by the lipid concentration because autoxidation of lipid side chain causes film hardness.

The laccase activity contained in AP was measured using syringaldazine as substrate, and the results are summarized in Table 3. Like drying time, no significant difference was found in the laccase activity by collecting season, and this results in almost the same drying time (Table 2).

Table 3: Lacquer laccase activities.

Samples	Activities (unit/mg AP)	Samples	Activities (unit/mg AP)
T6	555	D6	693
T7	556	D7	416
T8	750	D8	538
T9	552	D9	455
T10	669	D10	710
T11	645	D11	528
T12	697	D12	329
T1	614	D1	746
T2	570	D2	534
T3	617	D3	447

Table 4: Composition percentage, lipid/AP, and contact angle of lacquer films.

Samples	Composition percentage (wt%)			Lipid/AP	Contact angle (degree)
	Lipid	AP	Water		
T3	29.8	24.2	45.9	1.23	67.0
T7	43.8	21.2	34.9	2.07	72.5
T11	62.2	13.2	24.7	4.73	77.0

Because components are rather different depending on the collection season and lacquer dries by evaporation of water, we hypothesized that dry lacquer films have different properties. In order to reveal the reason, we analyzed the contact angle of drying lacquer films, T3, T7, and T11, and the results are summarized in Table 4. It can be seen that

Table 5: Data results of kneaded lacquers.

Kneading speed (rpm)	Kneading time (min)	Water (%)	Viscosities (mPas)	MW distribution (%)[1]			Drying time[2] (h)		
				Monomer	Oligomer	Polymer	DF	TF	HD
—	—	35.4	1203	86.8	13.0	0.2	7.8	8.1	12.5
60	15	26.4	1400	73.8	25.6	0.6	12.2	13.8	31.5
60	30	20.4	2442	56.5	41.8	1.7	6.6	7.2	11.8
60	45	13.6	2694	50.1	48.1	1.8	2.8	3.3	5.5
60	60	12.5	4639	44.8	52.8	2.4	2.2	2.7	5.2
120	15	27.1	3192	66.9	32.6	0.5	15.8	19.0	96
120	30	16.6	2747	54.1	45.0	1.0	3.8	4.5	7.5
120	45	8.1	3558	51.3	45.3	1.6	3.0	3.4	4.5
120	60	5.2	3625	50.2	47.4	2.4	3.4	3.8	6.0
180	15	21.5	1936	67.4	32.0	0.6	16.2	18.5	72
180	30	9.0	2250	56.1	42.7	1.1	1.7	2.8	6.0
180	45	5.2	2389	55.7	42.7	1.6	3.3	3.6	7.0
180	60	4.3	3322	52.3	45.8	1.9	3.1	3.7	6.0

[1]Determined by GPC. Monomer: MW = 320; oligomer: 10000 > MW > 600; polymer: MW > 10000.
[2]Drying condition: 25°C, 80%RH, and wet thickness 76 μm. DF: dust-free dry; TF: touch-free dry; HD: hard dry.

Table 6: Lightness, gloss, and coloration of kneaded lacquer films[1].

Kneading speed (rpm)	Kneading time (min)	Lightness and coloration[2]			Gloss
		L^*	a^*	b^*	
—	—	22.66	33.27	22.78	8.9
60	15	31.42	40.09	49.75	72.8
60	30	20.57	38.84	33.33	76.6
60	45	9.40	27.52	12.50	85.8
60	60	6.08	25.27	9.05	98.2
120	15	35.87	37.43	58.74	98.3
120	30	11.78	30.72	16.53	92.2
120	45	6.22	25.32	9.26	96.1
120	60	5.03	21.42	7.18	96.6
180	15	40.24	37.22	65.49	99.0
180	30	6.32	25.99	9.57	96.7
180	45	5.05	21.21	7.16	97.0
180	60	6.47	21.91	7.23	95.2

[1]Drying condition: 25°C, 80%RH, and wet thickness 76 μm.
[2]L^*: lightness; a^*: +red/−green; b^*: +yellow/−blue.

the contact angle increased with decreasing percentage of AP. Figure 3 shows ATR-IR spectra of T3, T7, and T11 lacquer films. Increasing stretch vibrations of hydroxyl group (O–H) at 3330 cm^{-1} and ether (C–O) or alcohol (C–OH) at 1037 cm^{-1} were discernible with increasing percentage of AP. The major component of AP is polysaccharide, and polysaccharides dissolve in water micelles that are dispersed in the W/O emulsion of lacquer sap to form a film after drying, when the polysaccharide usually appears at the surface of lacquer film. It was suggested that increasing polysaccharides made lacquer film more hydrophilic.

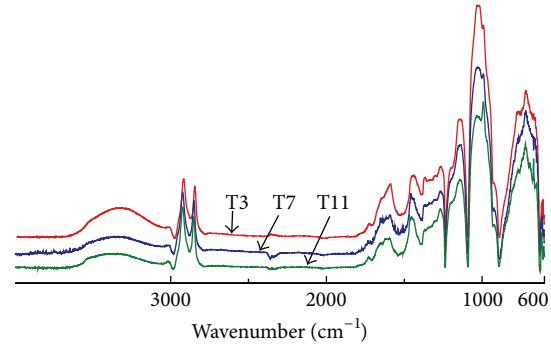

Figure 3: ATR-IR spectra of lacquer film.

From the above analyses, it can be concluded that although selecting the best season to collect high quality Vietnamese lacquer sap is difficult, sap collected in dry season (from September to December) has a higher percentage of lipid that gives the film high hardness, and the sap collected in other seasons has a higher percentage of water and AP that makes the film more hydrophilic.

3.2. Development of Fast Drying Lacquer. In order to improve the performance of Vietnamese lacquer, we performed differential *kurome* process with kneading speed of 60, 120, and 180 rpm and kneading time of 15, 30, 45, and 60 min, as summarized in Table 5. During the *kurome* process, the water concentration decreased with increasing kneading speed, and enzymatic polymerization of the lacquer sap was promoted. The polymerization of lacquer sap is catalyzed by the laccase contained in water micelles and requires oxygen. A high kneading speed beats in more oxygen and promotes polymerization. On the other hand, a high kneading speed also quickly evaporates water, which then decreases laccase

Table 7: Data results of repeated *kurome* lacquers.

Water addition	Kneading time (min)	Water (%)	Viscosities (Pas)	MW distribution (%)[1]			Drying time[2] (h)		
				Monomer	Oligomer	Polymer	DF	TF	HD
None	0	33.6	1.2	86.8	13.0	0.2	7.8	8.1	12.5
	60	5.2	6.6	50.2	47.5	2.3	3.0	3.6	8.3
	90	4.3	9.0	45.9	51.2	2.8	4.4	7.4	8.6
	120	4.1	10.8	45.3	51.7	3.0	4.4	5.3	8.6
	180	4.4	10.6	45.0	51.6	3.3			
5%/30 min	60	7.1	6.1	49.3	48.0	2.7	2.9	3.3	8.3
	90	4.5	7.8	44.6	52.4	3.1	3.4	3.8	5.3
	120	5.1	8.4	43.5	53.2	3.3	3.5	3.9	7.7
	180	3.7	12.6	39.5	56.3	4.1			
10%/30 min	60	7.8	4.2	56.1	41.2	2.7	3.4	4.2	8.6
	90	5.9	6.3	47.1	49.3	3.6	3.8	4.3	8.3
	120	4.1	10.9	40.6	54.6	4.7	3.3	3.6	7.5
	180	3.8	22.4	35.9	58.2	5.9			
20%/30 min	60	7.3	5.8	48.2	47.5	4.2	3.2	4.5	8.3
	90	5.5	11.2	39.6	54.8	5.6	5.5	6.4	9.0
	120	9.5	23.4	33.1	58.2	8.7	2.6	3.4	6.0
	150	12.3	43.5	30.5	59.4	10.1			

[1]Determined by GPC. Monomer: MW = 320; oligomer: 10000 > MW > 600; polymer: MW > 10000.
[2]Drying condition: 25°C, 80%RH, and wet thickness 76 μm. DF: dust-free dry; TF: touch-free dry; HD: hard dry.

activity. In our previous work [16, 17], it was found that lacquer sap collected from *T. vernicifluum* lacquer trees can be polymerized to form a film even if the water concentration is just over 3 wt%. However, in this study, we found that the lacquer sap collected from *T. succedanea* lacquer trees was not polymerized when the water concentration was lower than 10 wt%. Because the AP concentration in *T. succedanea* lacquer sap is higher than that in *T. vernicifluum* lacquer sap, this difference suggested that *T. succedanea* sap requires more water to dissolve the laccase and become polymerized. In general, viscosity of lacquer sap decreases with increasing water concentration. Therefore, the viscosity of kneaded lacquer increased with progression of polymerization due to decrease of water concentration during the kneading process, and the drying time of kneaded lacquer was also substantially shortened with the progress of polymerization.

Gloss, L^*, a^*, and b^* are summarized in Table 6. Gloss reached 100 for lacquer saps kneaded for 15 min at 120 and 180 rpm. Kneading at a speed of 60 rpm which needed 60 min made gloss reach 100. Because water micelles contained in lacquer sap can be microdispersed by kneading and stirring, the film surface becomes smooth and the gloss increases. Water micelles can be miniaturized quickly when the kneading speed is high. At all kneading speeds, L^*, a^*, and b^* all decrease as the kneading time increased suggesting that the lacquer film become transparent and color change from red/yellow to green/blue.

In this study, we found that if the water concentration in Vietnamese lacquer is lower than 10 wt%, which was kneaded at 120 rpm for 45 and 60 min and 180 rpm for 30, 45, and 60 min (Table 5), the polymerization of laccol catalyzed by laccase should not occur. In order to prevent a decrease in the water concentration, repeated *kurome*, which is the addition of water every 30 min during the kneading, was carried out. The results are summarized in Table 7. *Kurome* can accelerate laccase polymerization of lacquer because as kneading time increases and is repeated, monomer decreases and oligomer increases, and polymer also slightly increases. This phenomenon is consistent with the results from *kurome* lacquer sap collected from *T. vernicifluum* lacquer tree [18].

4. Conclusions

Lacquer saps collected from *Toxicodendron succedanea* lacquer tree growing in Vietnam during the rainy season contained a relatively high concentration of water and during the dry season contained a relatively high concentration of lipid component. The compositions of Vietnamese lacquer are affected by collecting season like the lacquer sap collected from *Toxicodendron vernicifluum* lacquer tree growing in China, Japan, and Korea. The increasing ratio of AP makes the film hydrophilic, and the increasing ratio of lipids increases the film hardness. After being refined by the *kurome* process, the lacquer polymerizes faster than in its raw state. The polymerization stopped when the amount of water fell below 10 wt%, but the polymerization can be promoted further by adding water during the kneading process, and this is called the repeat-*kurome* process.

Conflict of Interests

The authors declare that there is no conflict of interests regarding the publication of this paper.

Acknowledgments

The authors thank United Nations Industrial Development Organization (UNIDO) of Vietnam for *Toxicodendron succedanea* lacquer sample. This work was supported financially in part by a Grant-in-Aid for Scientific Research on Innovative Areas from the Ministry of Education, Culture, Sports, Science and Technology (MEXT) of Japan and by the cooperative research program of the MEXT-Supported Program for the Strategic Research Foundation at Private Universities.

References

[1] E. J. Kidder, *Japan Before Buddhism*, Ancient Peoples and Places, Thames & Hudson, London, UK, 1959.

[2] J. Hu, "Conservation of water-logged lacquerwares unearthed in China," in *Conservation and Restoration of Cultural Property: Conservation of Far Eastern Objects*, pp. 89–112, Tokyo National Research Institute of Cultural Property, Tokyo, Japan, 1980.

[3] Y. Kuraku, "Origins of the use of urushi in Japan and its development," in *Urushi*, N. S. Brommelle and P. Smith, Eds., p. 45, Getty Conservation Institute, Los Angeles, Calif, USA, 1988.

[4] Y. M. Du, "The production and use of Chinese raw urushi and the present state of research," in *Urushi*, N. S. Brommelle and P. Smith, Eds., p. 194, Getty Conservation Institute, Los Angeles, Calif, USA, 1988.

[5] T. Terada, K. Oda, H. Oyabu, and T. Asami, *Lacquer—the Science and Practice*, Rikou Publisher, Tokyo, Japan, 1999.

[6] T. Miyakoshi, K. Nagase, and T. Yoshida, *Progress of Lacquer Chemistry*, IPC, Tokyo, Japan, 1999.

[7] D. van Luyen, T. Vinh Dieu, and N. T. Thin, "Synthesis epoxy resin from Vietnamese lacquer sap," *Vietnam Journal of Chemistry*, vol. 4, p. 31, 1972.

[8] T. V. Dieu, L. T. Phai, and N. T. Cuc, "Study of curing process of epoxy-laccol collected from Vietnamese lacquer sap," *Vietnam Journal of Chemistry*, vol. 1, p. 26, 1976.

[9] T. V. Dieu and L. T. Phai, "New composite of epoxy from epoxydian cured by laccol," *Vietnam Journal of Chemistry*, vol. 1, p. 18, 1980.

[10] T. V. Dieu, L. T. Phai, N. H. Yen, and P. H. Quynh, "The factors influence on curing reaction of oligomer epoxy by laccol," *Vietnam Journal of Chemistry*, vol. 4, p. 24, 1978.

[11] T. V. Dieu, L. T. Phai, and B. T. Phuc, "About resin adhesive from synthetic rubber with metal based on epoxydian resin ED-6, ED-20 and technical laccol collected from Vietnamese lacquer sap," *Vietnam Journal of Chemistry*, vol. 4, p. 1, 1994.

[12] T. V. Dieu and L. T. Phai, "New hardeners for epoxy resin based on Vietnam natural phenolic lacs, polyamine and formaldehyde," *Vietnam Journal of Chemistry*, vol. 2, p. 47, 1979.

[13] D. V. Luyen, T. V. Dieu, H. T. Mui, N. T. Cuc, and N. T. Thin, "Composition and characterization of laccol collected from Vietnamese lacquer sap," *Vietnam Journal of Chemistry*, vol. 2, p. 45, 1972.

[14] R. Lu, T. Ishimura, K. Tsutida, T. Honda, and T. Miyakoshi, "Development of a fast drying hybrid lacquer in a low-relative-humidity environment based on kurome lacquer sap," *Journal of Applied Polymer Science*, vol. 98, no. 3, pp. 1055–1061, 2005.

[15] K. Nagase, R. Lu, and T. Miyakoshi, "Studies on the fast drying hybrid urushi in low humidity environment," *Chemistry Letters*, vol. 33, no. 2, pp. 90–91, 2004.

[16] K. Nagase, Y. Kamiya, T. Kimura, K. Hozumi, and T. Miyakoshi, "The relationship between the change of progress time in the urushi liquid by the enzymic polymerization and the natural drying property occurring under a low humidity environment," *Nippon Kagaku Kaishi*, vol. 2001, no. 10, pp. 587–593, 2001.

[17] K. Nagase, Y. Kamiya, K. Hodumi, and T. Miyakoshi, "The relationship between the change in urushiol by repetitive 'KUROME' of the urushi liquid and natural drying property occurring in a low humidity environment," *Nippon Kagaku Kaishi*, vol. 3, pp. 377–384, 2002.

[18] R. Lu, S. Harigaya, T. Ishimura, K. Nagase, and T. Miyakoshi, "Development of a fast drying lacquer based on raw lacquer sap," *Progress in Organic Coatings*, vol. 51, no. 3, pp. 238–243, 2004.